UNIVERSIDADE ESTADUAL DE CAMPINAS
Faculdade de Engenharia Mecânica

RODRIGO BATISTA TOMMASINI

Nonlinear dynamic models for deep water subsea lifting operations

Modelos dinâmicos não lineares para operações de içamentos submarinos em águas profundas

CAMPINAS
2021

RODRIGO BATISTA TOMMASINI

Nonlinear dynamic models for deep water subsea lifting operations

Modelos dinâmicos não lineares para operações de içamentos submarinos em águas profundas

Thesis presented to the Faculty of Mechanical Engineering of the University of Campinas in partial fulfilment of the requirements for the degree of Doctor in Mechanical Engineering, in the area of Solid Mechanics and Mechanical Design.

Tese apresentada à Faculdade de Engenharia Mecânica da Universidade Estadual de Campinas como parte dos requisitos exigidos para obtenção do título de Doutor em Engenharia Mecânica, na área de Mecânica dos Sólidos e Projeto Mecânico.

Orientador: Prof. Dr. Renato Pavanello

ESTE EXEMPLAR CORRESPONDE À VERSÃO FINAL DA TESE DEFENDIDA PELO ALUNO RODRIGO BATISTA TOMMASINI E ORIENTADO PELO PROF. DR. RENATO PAVANELLO.

CAMPINAS
2021

Ficha catalográfica
Universidade Estadual de Campinas
Biblioteca da Área de Engenharia e Arquitetura
Rose Meire da Silva - CRB 8/5974

Tommasini, Rodrigo Batista, 1989-
T598n Nonlinear dynamic models for deep water subsea lifting operations / Rodrigo Batista Tommasini. – Campinas, SP : [s.n.], 2021.

Orientador: Renato Pavanello.
Tese (doutorado) – Universidade Estadual de Campinas, Faculdade de Engenharia Mecânica.

1. Dinâmica não-linear. 2. Hidrodinâmica. 3. Cabos submarinos. 4. Estruturas offshore. 5. Vibração. I. Pavanello, Renato, 1959-. II. Universidade Estadual de Campinas. Faculdade de Engenharia Mecânica. III. Título.

Informações para Biblioteca Digital

Título em outro idioma: Modelos dinâmicos não lineares para operações de içamentos submarinos em águas profundas
Palavras-chave em inglês:
Nonlinear dynamics
Hydrodynamics
Subsea cables
Offshore structures
Vibrations
Área de concentração: Mecânica dos Sólidos e Projeto Mecânico
Titulação: Doutor em Engenharia Mecânica
Banca examinadora:
Renato Pavanello [Orientador]
Celso Kazuyuki Morooka
Antonio Carlos Fernandes
Clóvis de Arruda Martins
Juan Pablo Julca Avila
Data de defesa: 29-07-2021
Programa de Pós-Graduação: Engenharia Mecânica

Identificação e informações acadêmicas do(a) aluno(a)
- ORCID do autor: https://orcid.org/0000-0002-1392-4937
- Currículo Lattes do autor: http://lattes.cnpq.br/4585434417622335

UNIVERSIDADE ESTADUAL DE CAMPINAS
FACULDADE DE ENGENHARIA MECÂNICA

TESE DE DOUTORADO

Nonlinear dynamic models for deep water subsea lifting operations

Modelos dinâmicos não lineares para operações de içamentos submarinos em águas profundas

Autor: Rodrigo Batista Tommasini
Orientador: Prof. Dr. Renato Pavanello

A Banca Examinadora composta pelos membros abaixo aprovou esta Tese:

Prof. Dr. Renato Pavanello, Presidente
Universidade Estadual de Campinas – UNICAMP

Prof. Dr. Celso Kazuyuki Morooka
Universidade Estadual de Campinas – UNICAMP

Prof. Dr. Antonio Carlos Fernandes
Universidade Federal do Rio de Janeiro – UFRJ

Prof. Dr. Clóvis de Arruda Martins
Universidade de São Paulo – USP

Prof. Dr. Juan Pablo Julca Avila
Universidade Federal do ABC – UFABC

A Ata da defesa com as respectivas assinaturas dos membros encontra-se no SIGA/Sistema de Fluxo de Tese e na Secretaria do Programa da Unidade.

Campinas, 29 de julho de 2021.

Acknowledgments

Firstly, I would like to thank my supervisor Prof. Renato Pavanello for his guidance, support and motivation throughout my research and academic life. I am particularly thankful for his help on the management of the research contract with Petrobras and for the support during my visit to the University of Bristol. After all these years working together, I have you as a good friend.

I would like to thank Prof. John Macdonald and Dr. Tom Hill for receiving me in the University of Bristol, for supervising my research and for the support, especially during the pandemic. I am deeply grateful for the fruitful discussions we had about nonlinear dynamics and hydrodynamics.

I would also like to thank Petrobras for the financial support (process n. 2017/00591-0). Particularly, I would like to thank Dr. Leonardo Carvalho for the many discussions on the practical aspects of subsea lifting operations.

I would like to thank all my friends in Alegre, Rio de Janeiro, Campinas and Bristol for the pleasant moments we spent together.

I would like to thank my family for the unconditional support during this doctoral degree. Specially, my beloved wife, Leah, for being my strength and foundation; and my sons, Benjamin and Giuseppe, for the joy and love that you bring to my life.

Above all, I would like to thank God for my life and health.

To all other people who directly or indirectly helped me to conclude this thesis, my deepest thank you.

Resumo

Esta tese apresenta novos modelos para análise da dinâmica não linear de operações de içamentos submarinos. Foco é dado ao desenvolvimento de novos modelos e suas implicações no planejamento e análise de operações de içamento submarino em águas profundas. Dentre os pontos abordados na tese, os mais relevantes são a modelagem de cabos de comprimento variável, a análise estatística de séries temporais não estacionárias, a dinâmica do sistema em ressonâncias super-harmônicas e a modelagem de coeficientes hidrodinâmicos dependentes de amplitude. Verifica-se que a velocidade de lançamento ou içamento tem impacto direto nas forças estáticas e dinâmicas que atuam no sistema e também no tempo de exposição do sistema a condições de ondas aleatórias. A seleção de uma velocidade adequada para o guincho pode, portanto, ser usada para otimizar a operação. Dois métodos também são apresentados para a previsão das cargas de projeto quando o sistema é modelado assumindo um cabo de comprimento variável. Um desses métodos permite uma representação precisa das estatísticas da resposta por meio de um número reduzido de simulações aleatórias independentes em comparação aos métodos tradicionais da literatura. Além disso, soluções semi-analíticas são apresentadas para analisar a dinâmica do sistema em ressonância super-harmônica e quando os coeficientes hidrodinâmicos são dependentes da amplitude. O método é considerado preciso em comparação à integração no domínio do tempo, mas significativamente mais rápido. É mostrado os impactos que as ressonâncias super-harmônicas podem ter na dinâmica do sistema, já que em alguns cenários as zonas onde essas ressonâncias ocorrem podem ser o caso limite de projeto em operações reais. Finalmente, o uso de coeficientes hidrodinâmicos dependentes da amplitude é considerado chave para a análise de operações em águas profundas, pois esta formulação prevê variações nas cargas extremas e nas profundidades onde ocorrem, devido à variação da frequência natural e amortecimento do sistema.

Abstract

This thesis presents new models for the analysis of the nonlinear dynamics of subsea lifting operations. Focus in given on the development of new models and their implications on the planning and analysing of deep water subsea lifting operations. Among the points addressed in the thesis, the most relevant are the modelling of variable length cables, the statistical analysis of non-stationary time series, the dynamics of the system in super-harmonic resonances and the modelling of amplitude-dependent hydrodynamic coefficients. It is found that the lowering or lifting velocity has a direct impact on the static and dynamic forces acting on the system and also on the time of exposure of the system to random wave conditions. The selection of a suitable velocity for the winch might be therefore used to optimize the operation. Two methods are also presented for the prediction of the design loads on the system when the system is modelled assuming a variable length cable. One of these methods, enables an accurate representation of the statistics of the response via a reduced number of independent random simulations in comparison to traditional methods in the literature. Furthermore, semi-analytical solutions are presented to analyse the dynamics of the system in super-harmonic resonance and when the hydrodynamic coefficients are amplitude-dependent. The procedure is considered accurate in comparison to time domain integration, but significantly faster. It is shown the impacts that super-harmonic resonances can have on the dynamics of the system, as in some scenarios the zones where these resonances occur might be the limiting design case in real operations. Finally, the use of amplitude-dependent hydrodynamic coefficients is found to be key for the analysis of deep water operations, as this formulation predicts variations in the extreme loads and on the depths where they occur, due to the variation of the natural frequency and damping of the system.

List of Figures

List of Tables

List of Publications

Indexed journal articles:

- Tommasini, R. B.; Carvalho, L. O.; Pavanello, R. A dynamic model to evaluate the influence of the laying or retrieval speed on the installation and recovery of subsea equipment. *Applied Ocean Research*, v. 77, p. 34-44, 2018.
- Tommasini, R. B.; Pavanello, R.; Carvalho, L. O., Prediction of design loads for deep water subsea lifting operations based on non-stationary time response. *Marine Structures*, v. 74, n. 102818, 2020.
- Tommasini, R. B.; Hill, T. L.; Macdonald, J. H. G.; Pavanello, R.; Carvalho, L. O. The dynamics of deep water subsea lifting operations in super-harmonic resonance via the harmonic balance method. Accepted for publication in *Marine Structures*
- Tommasini, R. B.; Hill, T. L.; Macdonald, J. H. G.; Pavanello, R.; Carvalho, L. O. Nonlinear dynamics of deep water subsea lifting operations considering KC-dependent hydrodynamic coefficients. *Ocean Engineering*, v. 233, n. 109172, 2021.

Conference proceedings articles:

- Tommasini, R. B.; Carvalho, L. O.; Pavanello, R. Subsea equipment installation considering the influence of the laying speed. *Proceedings of the Rio Oil and Gas Expo and Conference 2018*, IBP1087_18. 2018.
- Tommasini, R. B.; Carvalho, L. O.; Pavanello, R. A Study on the Validity of a One Degree of Freedom Model for Deepwater Subsea Lifts. *Proceedings of the ASME 2019 38th International Conference on Offshore Mechanics and Arctic Engineering*, OMAE2019-96047. 2019.
- Carobino, E. S.; Pavanello, R.; Tommasini, R. B.; Fonseca, D. J.; Carvalho, L. O. A nonlinear finite element model to analyse the dynamics of subsea lifting operations using synthetic cables. *Proceedings of the ASME 2020 39th International Conference on Offshore Mechanics and Arctic Engineering*, OMAE2020-18225. 2020.
- Ribeiro L. H. M. S.; Sales L. P. A.; Tommasini R. B. Uncertainty Quantification in Subsea Lifting Operations. *Proceedings of the 5th International Symposium on Uncertainty Quantification and Stochastic Modelling, Uncertainties 2020*, p. 139-149. 2020.

Table of Contents

1. INTRODUCTION

This thesis is organized as a collection of scientific papers reproduced in specific chapters. A general introduction is presented in this first chapter, where the motivation and objectives of this study are stated. Further, a comprehensive literature review is presented in the second chapter, detailing the historical background and the dynamic models used to analyse offshore lifting operations. Finally, a general conclusion is presented in the last chapter, where the contributions of this thesis are presented as well as the suggestions for future work.

1.1 Motivation

Offshore oil and gas exploration is one of the main sources of energy in the world. Particularly in Brazil, the beginning of the production dates back to the 1960s, progressing continuously to deeper waters as new fields were discovered. In contrast to this consolidated activity, exploration of renewable sources of energy has grown significantly in recent decades, driven especially by the raising concerns with climate changes. Among several available technologies, the exploration of offshore wind energy is increasing steadily and already accounts for a significant part of the energy mix in Europe. Other significant exploration frontier that starts to get significance is the deep sea mining. As reserves on land reduces, the extraction of marine minerals are likely to get importance in the future. Therefore, exploration of offshore resources plays a key role in the world economy, whether through already consolidated activities such as oil and gas extraction or through emerging areas related to renewable energy or mining.

A critical aspect of any offshore exploration system is the capital expenditure necessary to implement the infrastructure required to start the production of the field. Particularly, the installation of equipment, via offshore lifting operations, accounts for a major part of these costs. This is because these operations are weather restricted and depend on complex vessels, with high daily rates and low availability. In addition, when the production field reaches the end of its life, decommissioning activities are required. Depending on the current legislation, the removal of part of the infrastructure may be required. Once more, the cost of these operations are preponderant in an overall analysis of the economic viability of the field.

Based on this context, the improvement of the technologies for offshore lifting operations is a key point to be considered, as this activity is present in every offshore exploration scenario and

is directly linked to their economic viability.

1.2 Objectives

In general, the challenge regarding offshore lifting operations is to reduce their costs preserving the safety requirements. This can be achieved by two means: (1) development of new lifting procedures or (2) improvement of the methodologies to analyse these operations.

The development of new lifting procedures allows for faster operations or for the use of cheaper vessels to install a given piece of equipment. Substantial effort has been made towards this end in recent years, leading to the development of the pendulous method and of synthetic rope lifting systems, among others. On the other hand, offshore lifting operations are classified as weather restricted according to the standard DNVGL-ST-N001, so that assessment of the environmental conditions that lead to safe operations is required during the planning phase. Thus, the improvement of the dynamic models to analyse these operations can result in reduced weather restrictions and, consequently, faster and cheaper operations.

Based on this scenario, the main objective of this work is the development of new models to analyse offshore lifting operations, aiming to obtain more accurate representation of the dynamics of the system in comparison to real conditions. The focus in this context is the inclusion of nonlinear features of deep water subsea operations that have not been entirely addressed so far in the literature.

During the deep water lowering phase of the subsea lifting operation, two typical conditions are possible: either the payload is lowered with a given speed or kept stationary at a certain depth. Last scenario occurs when inspections or operational tasks are necessary to be performed, which can be more or less frequent depending on the operational procedure. Different models are necessary to predict the dynamics of each scenario. The main difference in this case is that for the lowering scenario, the length of the cable must be considered variable throughout the simulation, while in the fixed depth scenario, it is considered constant.

This thesis is thus divided in two parts, the first one accounts for the variable length models and the second one deals with the constant length models. The objectives of each part is detailed in the rest of this Section.

1.2.1 Variable length models

The use of variable length models to analyse subsea lifting operations is more recent compared to the fixed length models. In this case, the majority of studies focus on the validation of the proposed method, instead of on the consequences that this formulation has in the operation. Also, the formulations found in the literature consider a discretized cable. No simplified model that takes into account the variable length condition has been yet considered to the best knowledge of the author. Therefore, the first objective of this thesis is to develop a simple model that accounts for a variable length cable, aiming to study the influence of the winch speed on the dynamics of the system.

Furthermore, when the system is modelled using a variable length cable and the input of the system is stochastic, the response of the system presents a nonstationary behaviour. This is due to the fact that the resonance frequency of the system changes as the length of the cable varies throughout the operation. The prediction of the extreme loads in nonstationary time series is challenging and has not being covered in the literature in the specific scenario of deep water subsea lifting operations. The second objective of this thesis is then to develop a methodology to predict the extreme loads on the system under stochastic excitation when the system is modelled by a variable length cable.

1.2.2 Constant length models

The use of constant length models to analyse deep water subsea lifting operations is recurrent in the literature. An important feature of this problem is the hydrodynamic forces that are introduced in the payload. These forces are typically modelled via Morison's equation, which introduces a quadratic velocity term in the equation of motion. The presence of this nonlinear term can lead to super-harmonic resonances in the system. This phenomenon, although well described in the nonlinear dynamics literature, has not been covered in detail for the scenario of deep water subsea lifting. Therefore, the third objective of this thesis is to use analytical and numerical procedures to solve the nonlinear equation of motion for the system and to study the effects that super-harmonic resonance can introduce in real operations.

Another significant feature of the hydrodynamic forces is the dependence of the hydrodynamic coefficients on the amplitude of oscillation, which is typically represented by the Keulegan-Carpenter number (KC). Although several studies have been published recently addressing this

dependence, the majority of papers dealing with the dynamics of the operation consider constant hydrodynamic coefficients. Thus, the fourth objective of this thesis is to develop a model that considers KC-dependent hydrodynamic coefficients and study the impacts that this formulation has on the dynamics of the system.

1.2.3 Summary of objectives

1. Development of a dynamic model that accounts for a variable length cable, aiming to study the influence of the winch speed on the dynamics of the system;
2. Development of a methodology to predict extreme loads on the system under stochastic excitation when the system is modelled considering a variable length cable;
3. Study the dynamics of the system in super-harmonic resonances, aiming to understand their features and influence in the operational weather window;
4. Development of a dynamic model that accounts for KC-dependent hydrodynamic forces, aiming to understand the nonlinear phenomena that arise in the response of the system.

1.3 Thesis structure

In addition to this introduction chapter, where the motivation and objectives of this thesis have been stated, a comprehensive literature review on offshore lifting operations is presented in Chapter 2. Firstly, an historical overview is presented, describing the development of new procedures to conduct the operations. Then, specific studies detailing dynamic models to analyse the lifting in air, the lowering through the wave zone, the lowering through deep waters and the landing on the seabed are presented. Particular attention is also given to studies dealing with control strategies and hydrodynamic modelling of oscillating bodies.

Chapter 3 describes the study published in Applied Ocean Research (v. 77, p. 34-44, 2018) by R. B. Tommasini, L. O. Carvalho and R. Pavanello addressing the objective n. 1 of this thesis (as per Section 1.2.3). In this study, a single degree-of-freedom model, taking into account a variable length cable, has been presented to explore the influence of the winch speed on the dynamics of deep water subsea lifting operations.

Chapter 4 describes the study published in Marine Structures (v. 74, n. 102818, 2020) by R. B. Tommasini, R. Pavanello and L. O. Carvalho addressing the objective n. 2 of this thesis (as per Section 1.2.3). In this study, two methodologies are presented to estimate the extreme loads on

the system when the cable is modelled using a variable length approach and random inputs, which leads to a non-stationary signal.

Chapter 5 is a pre-print of the study by R. B. Tommasini, T. L. Hill, J. H. G. Macdonald, R. Pavanello and L. O. Carvalho, accepted for publication in Marine Structures, addressing the objective n. 3 of this thesis (as per Section 1.2.3). In this study, an analytical method is used to solve the nonlinear equation of motion of the system, aiming to study the influence of super-harmonic resonances in the dynamics of the system.

Chapter 6 describes the study published in Ocean Engineering (v. 233, n. 109172, 2021) by R. B. Tommasini, T. L. Hill, J. H. G. Macdonald, R. Pavanello and L. O. Carvalho addressing the objective n. 4 of this thesis (as per Section 1.2.3). In this study, amplitude-dependent hydrodynamic coefficients are considered in the modelling of the problem. Numerical and analytical solutions for the problem are presented, focusing on the impacts that this formulation has on the dynamics and planning of the operation.

Finally, the conclusion of this thesis is presented in Chapter 7, where a summary of the outcomes of this thesis is presented. In addition, suggestions of future studies are also included aiming to inspire future progress on the modelling of offshore lifting operations.

2. LITTERATURE REVIEW

This Section presents a literature review on offshore lifting operations. Firstly, it is presented an historical overview about this topic, illustrating the early methods considered for the operation and how they evolved throughout time. Then, studies describing methodologies to predict the dynamics of the system are presented, particular attention has been given to the lifting in air, lowering through the wave zone, lowering through deep waters and landing on the seabed phases of the operation. Works detailing control strategies to alleviate the dynamic loads or reduce motions on the system are also included. Finally, attention has been given to papers describing the hydrodynamic forces acting on oscillating bodies, as these forces are a major concern on the correct prediction of the dynamics of the system in subsea operations.

2.1 Historical overview

Early subsea lifting operations considered the use of drilling rigs or sling-over-sling methods to install structures on the seabed. Examples of some operations based on these methodologies, along with their description, advantages and limitations were presented in the study by Rowan and Ahilan [1] in 1989. In addition, Roveri *et al.* [2] described the installation of a 420 tonnes manifold at 620 m depth in 1996 by the sling-over-sling method. They also presented the frequency and time domain analysis to plan the operation and experimental tests that were conducted to predict the hydrodynamic coefficients of the manifold.

In 1997, Nelson *et al.* [3] proposed a simple heave compensation landing system based on the use of a chain and a buoy connected in series with the payload. The system was tested in the Gordon Banks field (Gulf of Mexico), which confirmed the effectiveness of the system to enable the use of simpler vessels to perform the operations.

During the beginning of the 21st century, offshore oil fields started to reach water depths on the order of 2000 m. This fact raised concerns in the industry regarding the technical and economic viability of extending the traditional installation methods to this deeper scenario. Aiming to address this challenge, the DISH (Deepwater Installation of Subsea Hardware) JIP (Joint Industry Project) was created [4,5]. Among the findings of the JIP, it was concluded that there was a limitation on the installation systems using steel wire ropes to install equipment at 2000 m depth, since the increased weight of the suspended cable in deep waters limited the operation.

The solution proposed was the development of an installation system based on synthetic cables, since this construction would benefit from their neutral weight inside the water to reduce the loads on the system.

According to Beckman [6] and Torben *et al.* [7], during the second phase of the DISH JIP, laboratory experiments were conducted to assess the performance of several synthetic cables regarding the fatigue life, wear and heating due to bending over sheave, and creep, among others. Based on the results, a blend of High Modulus Polyethylene (HMPE) fibres and Liquid Crystal Polymer (LCP), known as BOB (Braid Optimized for Bending), was considered the most appropriate construction.

Another JIP was created in 2002 to address the development of an installation system based on synthetic ropes, which was known as FRDS (Fibre Rope Deployment System). According to Ingeberg *et al.* [8], the first system developed could work at 3000 m depth and withstand 50 tonnes. The system consisted of a BOB cable passing through several sheaves before entering the drum. It could operate on heaving compensation mode or constant tension and had automatic landing/retrieving options. A field test considering the installation of a 35 tonnes piece of equipment demonstrated the functionality of the system.

Further details of the efficiency of the system and integrity of the synthetic rope of the FRDS were presented by Torben *et al.* [9] in 2007. In their work, they described the installation of 60 equipment, showing a reduction on the global operational times compared to traditional lifting procedures. In 2008, Torben *et al.* [7] presented updated results about the synthetic rope integrity. They showed that, after 6 months of operation and the installation of 140 pieces of equipment, no fibre had been damaged and external layers were in good conditions.

An improved system, capable of working with 250 tonnes in double fall configuration, was developed and tested as presented by Torben *et al.* [10] in 2011. The system was assembled in the Skandi Santos vessel and the tests were conducted in the North Sea with a load of 100 tonnes at 940 m depth. The results were satisfactory, indicating no torsion of the cable in the double fall configuration. Another vessel that uses the FRDS is the Aker Wayfarer, as presented by Job *et al.* [11] in 2018. This system has a capacity to withstand 290 tonnes in the double fall configuration and has been used for the installation of subsea manifold in the Pre-Salt fields, in Brazil.

An alternative solution developed to install heavy equipment in deep water fields was the Pen-

dulous Installation Method. In this method, the equipment is dropped from the sea surface connected by a polyester rope and falls on an overdamped pendulous motion, avoiding high dynamic loads in the resonance zone. According to Cerqueira *et al.* [12] and Costa and Lima [13], the method was patented in 2003. Scale models (1:35 and 1:70) and a dummy manifold (in the scale 1:1) were used to assess the viability of the operation. Following this preliminary phase, two manifolds, weighting up to 280 tonnes, were installed at 1900 m depth using this method in 2006 and 2007, attesting its effectiveness to install heavy equipment in deep waters.

A study on the use of the pendulous installation method for the deployment of a 195 tonnes manifold at 1500 m depth in China was also presented by Wang *et al.* [14]. They described the operational procedure and the numerical study conducted, showing the economic viability of the method compared to traditional lifting procedures.

Alternative solutions based on towing operations, via submerged buoys, were proposed by several authors [15–18] to install heavy equipment in deep water fields. The studies detail the possibility to install and recover equipment using low costs vessels with increased operational weather windows in comparison to traditional procedures. A drawback of this procedure is the need for a proper harbour to connect the equipment to the buoy.

In 2011, another innovative method was proposed for the installation of heavy equipment in deep waters [19,20]. This method is known as Y-method and it consists of two vessels supporting the payload using a Y rigging configuration. Dynamic amplifications at the resonance zone can be reduced in this method by controlling the distance between the two vessels. The authors presented experimental and numerical analysis to support the effectiveness of this method.

Other illustrative examples of non-conventional installation procedures to install subsea equipment can be found in the literature. The experimental and numerical evaluation of the installation of a support structure for risers was presented by Fujarra *et al.* [21] and the installation of a 60,000 tonnes oil storage tank at 135 m depth was presented by Velema and Bokhorst [22] in 2015.

During the past decade, the installation of offshore wind turbines grew considerably and several studies were also published regarding the installation of these structures. In 2013, Sarkar and Gudmestad [23] presented a preliminary technical feasibility study for a new methodology to install monopile based wind turbines. They showed that the method had the potential to be more robust than traditional alternatives at the time.

In 2017, Acero *et al.* [24] described a novel procedure for the installation of the tower and Rotor Nacelle Assemblies on bottom fixed foundations. The procedure was based on an inverted pendulum principle that could eliminate the use of huge heavy lifting vessel for the operation. Following a numerical study, they showed the procedure was viable for the example scenario.

A novel concept for replacement or installation of offshore wind turbine blades was proposed by Acero *et al.* [25] in 2020. Their system consisted of a medium-sized jack-up crane vessel and a tower climbing mechanism, that provided a stable platform for clamping, lowering and lifting the blades. A case study of a 5 MW offshore wind turbine was studied, demonstrating the technical feasibility of the concept.

A comparative assessment of the vessels to install offshore wind turbines, including cost predictions, was presented by Ahn *et al.* [26] for an application in the Korean sea and by Paterson *et al.* [27] for the United Kingdom scenario. In addition, Lacal-Arantegui *et al.* [28] studied the evidence for the reduction of installation times of offshore wind turbines by analysing the data for the installation of 87 wind farms from 2000 to 2017.

Finally, the works of Frazer *et al.* [29], Wang *et al.* [30] and McPherson [31] presented a review of the methods available for the installation of subsea equipment by the time they were written. Particularly, Wang *et al.* [30] also describe a list of the vessels capable of performing the lifting operations. Reviews on the methods to install offshore wind turbines were presented by Esteban *et al.* [32], Haselsteiner *et al.* [33] and Jiang [34].

2.2 Dynamics of offshore lifting operations

Offshore lifting operations are typically classified in four different phases: lifting in air, lowering through the wave zone, lowering through deep waters and landing on the seabed. Each of these phases must be analysed in order to predict the loads on the system and check if these loads are within safe limits. The main outcome of the analysis is an operational weather window, which details the sea states (combination of wave height and period) that lead to a safe operation. Specific models found in the literature to analyse each of these phases are presented in this Section.

2.2.1 Phase 1 – Lifting in air

During the lifting in air phase (Figure 2.1), the payload is released from its sea-fastening, lifted off the deck and then lowered into the ocean waves or transferred to the desired location. The

main concern during this phase is the large motions of the payload induced by the vessel movement or wind, which can lead to impacts and damages in adjacent structures or in the payload itself.

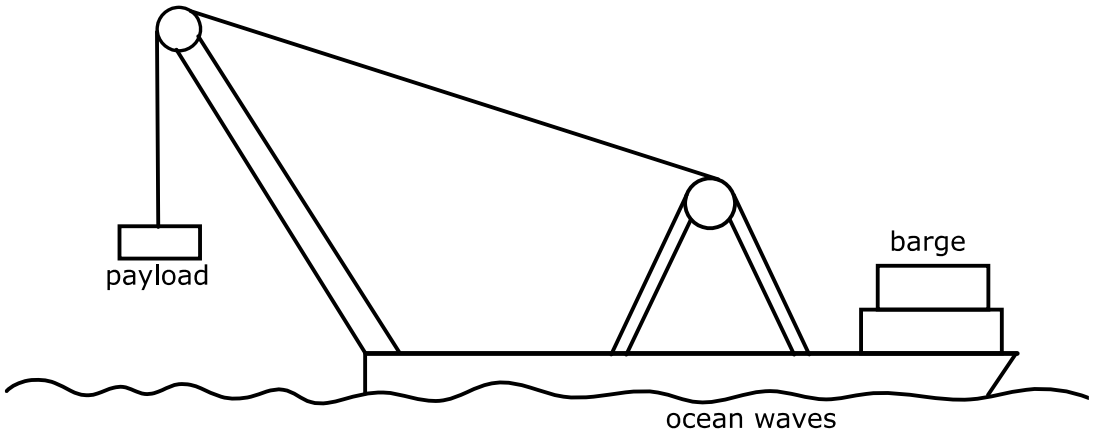

Figure 2.1: Representation of the lifting in air phase of the operation.

Early works on the dynamics of floating cranes started to be published during the end of the 20th century. A 9-DOF model was developed by Schellin [35] in 1991 to evaluate the response of a shear-leg crane ship in waves. The model included the coupled dynamics of the vessel (translation and rotation) and payload (translation), nonlinear mooring forces and hydrodynamic forces on the vessel. It was found that wave groups with period near the resonance of swing motion of the payload were relevant for defining the limits of the operation, in contrast to slowly varying motions which did not affect the hook load response.

Parametric resonances due to time-varying stiffness of the lifting line was studied by Witz [36] in 1995. Once more, a 9-DOF model was considered and time domain integration was used to obtain the response of the payload in random seas. It was concluded that the effects of parametric excitation were less significant for random seas compared with regular seas, but were still sufficient to influence the operability limits of the vessel.

The influence of the nonlinear mooring forces on the dynamics of floating cranes was experimentally assessed by Clauss and Vannahme [37] in 1999. The study showed that when motion amplitudes were large, the nonlinear term of the mooring forces governed the response of the system. This led to 2:1 and 3:1 sub-harmonic resonance, causing an increase of motion and load amplitudes.

Experimental, numerical and analytical studies on the nonlinear dynamics of moored floating cranes were conducted by Ellerman *et al.* [38,39] in the beginning of the 2000s. The model

considered 4-DOF (surge, heave and pitch for the vessel and the swing angle of the payload); only head seas were considered acting on the vessel; the moored forces were modelled as a cubic polynomial; and hydrodynamic forces, including quadratic viscous terms, were included. They showed that nonlinear phenomena, such as sub-harmonic resonances and bifurcations, could occur and affect the operating limits of the floating vessel.

The analysis of the installation of the Gas Modules for the Njord FPU (Floating Production Unit) was experimentally and numerically studied by Van der Wal *et al.* [40]. The experimental tests were conducted using 1:50 scale models of the crane vessel, the FPU and the Gas Modules. The results from the experiments were considered an input to calibrate the data for a numerical model. Next, the computational model was used to assess the weather window of the real operation.

Multibody system dynamics were used to study the response of a heavy payload suspended by a floating crane in the work of Cha *et al.* [41] in 2010. In this study, the equation of motion was obtained by considering a 12-DOF system, including all the three translational and three rotational degrees-of-freedom of both the vessel and the payload. The motion of the system and the tension in the lifting rope were calculated, which could be used as a guide for the planning of the operation. Following this study, similar methodology was used to model the dynamics of the floating crane by considering: the nonlinear effects of the hydrostatic force [42] and crane stiffness [43]. More recently, direct application of the methods presented in [41–43] to the lifting in air of a subsea manifold was presented by Hong *et al.* [44] in 2016.

The dynamical model presented by Cha *et al.* [41] led to numerical instability when the stiffness of the rope was large. In order to avoid this problem, Ham *et al.* [45] used the Discrete-Euler-Lagrange equation to formulate the problem and they considered the rope as a constrain for the motion of the vessel and the payload. The results presented confirmed the stability of the proposed method.

A numerical and experimental study on the dynamics of a mating operation of a topside module by a floating crane was presented by Ha *et al.* [46] in 2018. The model considered the coupled motions of the crane barge, the payload and the vessel where the topside module should be connected. The forces due to the waves, mooring lines and thrusters were included; the connection of the crane barge to the payload was modelled by a bi-linear elastic cable; and a soft landing system was included to represent the mating of the payload. Regular and irregular waves were analysed and the results demonstrated a good agreement between the numerical

model and the experiments.

During the 2010s the installation of offshore wind turbines grew considerably and many studies focused their attention on the dynamics of these operations. Graczyk and Sandvik [47] analysed the performance of two different vessels during lift-off and landing operations of offshore wind turbine components. The acceleration and impact loads on the deck were assessed and, after comparison to limiting criteria, the operational weather window was presented for both vessels.

Ku and Roh [48] used the model presented in [41] to study the dynamics of the installation of a fully assembled offshore wind turbine by a floating vessel. They considered a system with 14-DOF, including the 6-DOF of both the vessel and turbine plus the roll and yaw of the nacelle. The results illustrated the dynamic amplification of forces on the lifting lines during the lifting off, translating to desired position and landing on its foundation.

The modelling of the landing of an offshore wind turbine onto its supporting structure was presented by Ming *et al.* [49]. The authors considered a 11-DOF coupled model, an elastic cable, the possibility of slack conditions for the cable and the impact loads when the turbine hits the supporting structure. The influence of the wave and landing velocity on the dynamics of the system was assessed, providing a tool to estimate the optimal conditions to perform the operation.

Recently, several studies have been conducted at NTNU (Norwegian University of Science and Technology) on the dynamics of the installation of offshore wind turbines. Acero *et al.* [50] presented a methodology to predict the operational weather window for the installation of offshore wind turbine transition pieces onto a monopile foundation. Ren *et al.* [51] presented the development of a modularized blade installation simulation toolbox for the purpose of control design; and Zhao *et al.* [52] developed a fully coupled model for the installation of single blades by jack-up vessels considering the hydrodynamic and aerodynamic loads, soil-structure interaction and flexibility of crane and jack-up legs. Jiang *et al.* [53] presented a parametric study on the installation of single blades by jack-up vessels onto monopiles, where the influence of water depth, mean wind speed, turbulence intensity, and wind-wave misalignment on the dynamics of the system was stressed. An assessment of the impact loads during a single blade installation by a jack-up vessel was presented by Verma *et al.* [54], illustrating that bending and plastic deformations of the guide pin could occur in certain scenarios. The dynamics of single blade installation by floating cranes, and its comparison with jack-up vessels, was presented by Zhao *et al.* [55], where it was shown that the operation with the floating vessel is possible as

long as slowly varying motion of the vessel could be mitigated by the dynamic position system. Finally, the use of passive tuned mass dampers attached at the tower top during the installation of single blades was assessed by Jiang *et al.* [56] and Verma *et al.* [57], highlighting the potential to increase the operability of the vessel for the mating phase by using these devices.

2.2.2 Phase 2 – Lowering through the wave zone

The lowering through the wave zone (Figure 2.2) starts when the payload crosses the surface of the sea and lasts until it reaches depths where the kinematics of the sea waves are not relevant (i.e. typically around 50 m depth). During this phase, hydrodynamic forces due to the relative motion of the payload inside the waves, slamming loads and varying buoyance forces are crucial to the dynamics of the system. Dynamic amplifications due to these loads can lead the violation of the structural limits of the lifting system or induce slack conditions in the cable. Therefore, careful assessment of the dynamics of the system during this phase is necessary to guarantee the safety of the operation.

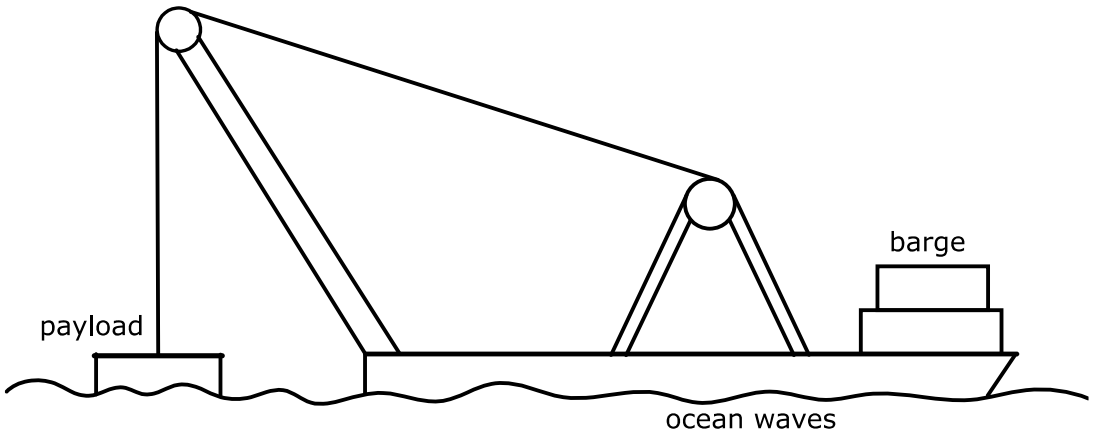

Figure 2.2: Representation of the lifting through the wave zone phase of the subsea lifting operation.

An early work on the dynamics of subsea lifting operations in the wave zone is due to Kopsov and Sandvik [58] in 1995. They analysed the installation of a pre-drilling template using a non-linear time domain program. Close to the water surface, the hydrodynamic coefficients were considered dependent on the distance from the payload to the surface. Results showed that, in the wave zone, the forces were dominated by the direct action of the waves on the structure; the motion of the vessel was found to be secondary.

Several studies were conducted by Li *et al.* [59–61] on the installation of monopiles for offshore wind turbines. In [59], their model considered the coupled dynamics of the monopile and the

crane vessel, variable length cable and the effects of the vessel shielding on the wave field. The results showed that wave shielding could reduce extreme loads on the system depending on the vessel heading and wave length. In [60], they analysed the non-stationary response of the lowering operation by assuming stepwise steady-state conditions. Further, the hydrodynamic forces on the monopile were modelled by a modified Morison's equation, which included potential damping terms. It was found that the inclusion of the potential damping reduced the response of the structure at the monopile rotational natural frequency, which could lead to wider operational weather windows. In [61], the installation of a rigid large subsea spool was considered by using the methodologies presented in [59,60]. It was shown that sufficient wave seeds were necessary to account for transient effects during the lowering process; shielding effects actually decreased the allowable significant wave heights for the operation due to unbalanced wave loads in the spool; and increased operability could be obtained by controlling the heading of the vessel.

A study on slamming loads on suction anchors was presented by Naess *et al.* [62] in 2014. They conducted experimental and numerical (i.e. Computational Fluid Dynamics - CFD) studies to calibrate the slamming coefficients of the suction cans, which were used as input for time domain simulation software (i.e. SIMO from Marintek). The outcomes obtained showed correlation between model tests and CFD; and the results from SIMO agreed well with experience from real operations.

The dynamics of a fully submerged cylindrical payload suspended by a crane barge was analysed by Hannan and Bai [63,64]. They modelled the system via a three-dimensional numerical wave tank using a fully nonlinear potential flow model in the time domain based on the boundary element method. Different wave directions, cable lengths and lowering velocities were considered. The results showed the presence of a large mean drift force at high frequencies due to shielding effects and various nonlinear effects, such as sub-harmonic motion and period doubling.

Jeong *et al.* [65] considered a multibody system model to analyse the lifting operation of a subsea equipment. They included the effects due to the lowering speed, snap loads, collisions with the vessel, slamming and varying buoyance forces. Several environmental and operational conditions were simulated, illustrating the influence of each factor on the dynamics of the system.

Kane's formalism was used by Raman-Nair *et al.* [66] to develop a fully coupled model of the

deployment or retrieval of a cylinder from a rectangular barge. The model approximated the first order wave forces via simplified analytical equations, considered an elastic cable connecting the barge to the cylinder and included forces due to the mooring of the barge. The motion of the system and tension on the lifting line was presented for different operational conditions, illustrating the effectiveness of the model to predict the dynamics of the system.

2.2.3 Phase 3 – Lowering into deep waters

The lowering into deep waters phase of the subsea lifting operation (Figure 2.3) starts when the payload finishes to cross the wave zone (i.e. typically around 50 m depth) and lasts until the payload is positioned some meters above the sea floor. During this phase, large dynamic loads can occur in the system due to the wave induced motion of the crane tip, especially when the natural frequency of the cable-payload system matches any of the excitation frequencies. Further, horizontal offsets due to the current are expected to occur; and the static tension on the top of the cable increases due to its weight as the payload reaches deeper waters. To guarantee the safety of the operation, it is necessary to assure that the loads in the system are always bellow the structural limits. Also, slack conditions are typically to be avoided as they can lead to large snap loads in the cable and unpredictable motions of the payload.

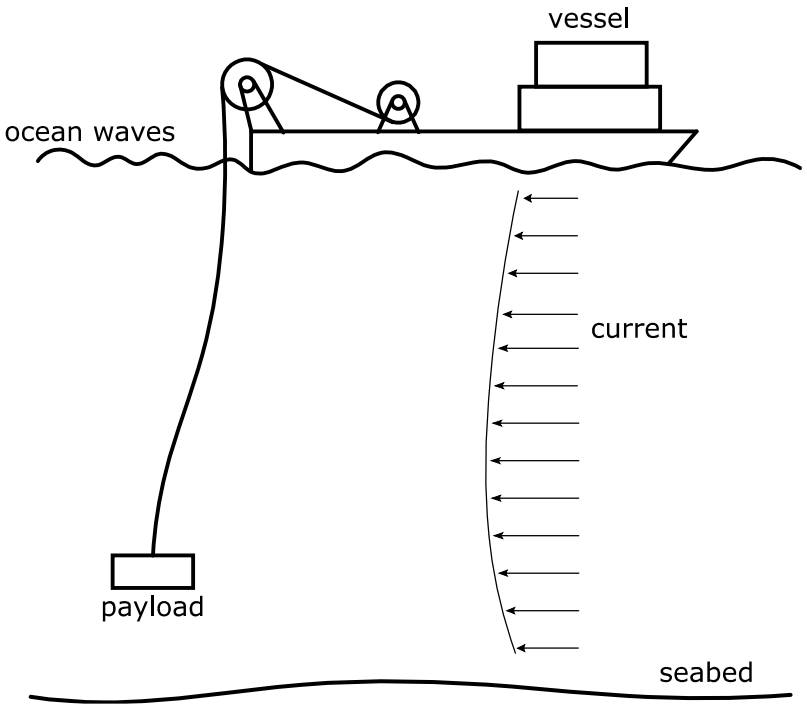

Figure 2.3: Representation of the lowering into deep waters phase of the subsea lifting operation.

The possible first study regarding the dynamics of deep water lifting operations is due to the consulting company Arthur D. Little [67] in a report for the USA Navy Department in 1963. In

this study, the subsea lifting system was modelled as a continuum bar element subjected to a sinusoidal displacement at the top of the cable. The drag force acting on the payload was linearized and the forces on the cable were obtained analytically. It was shown that effects of ocean currents were negligible, provided that the vertical forces due to gravity minus buoyancy were much larger than the horizontal drag forces due to the currents. Vertical friction along the cable was also found to be minor in comparison to the drag acting on the payload, and it was argued that the velocity of sound in the cable should be as high as possible, making the resonant frequencies large so that they would lie on the cut-off edge of the spectrum of a given sea state.

Another report for the USA Navy Department was published by Holmes [68] in 1966, as a continuation of the work by Arthur D. Little Co. [67]. In this case, the dynamic model for the system was equal to that presented in [67] and a wider range of parameters were considered to evaluate the forces on the system, which were presented as non-dimensional charts. Further, a design procedure was provided, where the maximum allowable input amplitude for the lifting operation, as a function of the input frequency, could be obtained by direct analysing the non-dimensional charts provided. This procedure was verified against a real subsea lifting operations, but, in some depths, the measured stresses on the cable exceed by a factor of 2 the calculated stresses. It was argued that these deviances were due to uncertainties in the hydrodynamic coefficients and in the input.

A study considering the stochastic aspects of the operations was presented by Iwan [69] in 1972. In this paper, the author considered a suspended cable-payload system connected to a buoy at the top. The nonlinear discretized equation of motion was replaced by a pseudo-linear system, that was obtained via an equation difference minimization technique. Then, the steady-state and stationary random response was obtained via an iterative procedure considering different parameters. Some general conclusions regarding the response of the system were presented. Particularly, the nonlinear drag force was found to have a significant contribution to the dynamics of the system.

An early application regarding deep sea mining was presented by Chung and Whitney [70] in 1983, where the axial vibration of a pipe attached to an equipment in its lower end was studied. In their work, the pipe was modelled as a continuum bar element and the drag at the equipment was linearized. They showed that resonance amplifications could occur depending on the mass of the payload, geometric properties and length of the pipe.

An important paper on the field was published by Niedzwecki and Thampi [71] in 1991, where

a simplified single degree-of-freedom model was considered to predict the occurrence of snap loads in the cable based on three dimensionless groups: the frequency, the displacement and the damping ratios. Through the use of this model, the analyst could infer if snap conditions would occur and, if so, use a multi degree-of-freedom model to predict the forces in the cable in the time domain.

A study presented by Huang [72] in 1999 detailed the stability of the taut-slack response of a submerged cable-body system through a single degree-of-freedom system. It was shown that the system could become unstable, especially at low damping conditions, and chaotic motion could occur.

A series of studies were published by Driscoll, Lueck and Nahon in 2000 [73–76] addressing the dynamics of tethered cage mounted ROV (Remotely Operated Vehicle) systems. They presented measurements of the motion of the ship and the cage in real operations [73], showing that the vessel and the payload were only coupled vertically, so that unidimensional models could be sufficient to represent the dynamics of the system. They also indicated that the system could be in resonance conditions at certain depths; and snap loads could occur, leading to propagation of waves inside the tether. The third and fifth harmonics, generated due to the quadratic drag term, were also reported in the response of the system, but for moderate ship displacements, were not preponderant in the total response. Further, the author presented analytical and numerical models to represent the dynamics of the system. The analytical models [74,75] considered a continuum bar element and a linearized drag force that were used to calculate the displacement and tension transfer functions of the system and to infer the possibility of snap loads. The numerical model [76] was based on a finite element representation of the cable and included the drag force in its nonlinear quadratic form. This model was integrated in the time domain and led to more accurate representation of the dynamics of the system. It was argued that deviations between the model and measure data were due to deficiencies in the representation of the hydrodynamic forces by constant hydrodynamic coefficients; in this context, the authors showed that the use a simplified wake model, simulating the influence of the history of the flow, could increase the accuracy of the finite element model in comparison to measured data.

The possibility of heave induced pitch resonance during the installation of suction piles was presented both experimentally and numerically by Huang *et al.* [77] in 2011. In this study, an equivalent damped Mathieu equation was used to interpret this phenomenon. It was found that

the heave induced pitch resonance could occur if both (a) the pitch natural frequency was roughly one half of the heave natural frequency, and (b) the heave excitation frequency was approximately equal to the heave natural frequency.

An experimental and numerical study on the lifting of a subsea manifold in deep waters was conducted by Nam *et al.* [78] in 2017. The coupled dynamics of the crane barge and the payload was analysed using a linearized frequency domain approach. It was found that the suspended payload increased the roll motions of the vessel even in head seas. Also, the vertical motion of the payload under stochastic input presented significant components at the natural frequency of the cable-manifold system and at the natural frequencies of the vessel. Finally, Passive Heave Compensation (PHC) could reduce the dynamic response of the system by shifting its natural frequency.

Other studies considering the use of passive heave compensation were presented by Driscoll *et al.* [79] in 2000, where the effectiveness of ship-mounted and cage mounted PHC system were assessed; and by Quan *et al.* [80] in 2016, where the influence of subsea currents was considered. Both these studies reported the capacity of the PHC system to reduce the dynamic loads during the operation.

The use of synthetic ropes in combination with steel wire cables was covered by Neto *et al.* [81] in 2019. They showed that axial resonance amplifications could occur at shallow depths for the synthetic cable and at deeper waters for the steel wire cable, due to the difference of stiffness of these materials. Therefore, the correct selection of the length of polyester cable and the depth where it is attached to the steel wire cable could reduce the total axial dynamic forces on the system and increase the operational weather window.

The studies presented above considered a constant length cable in their models, so no influence of the winch speed on the dynamics of the system was presented. The assumption of variable length cables is also recurrent in the literature. An early study on this topic was presented by Wang *et al.* [82] in 1998, where a finite element model for an underwater cable with time-dependent length was considered. More recent studies were presented by Hu and Liu [83] in 2015, studying the installation of deep sea mining structures; Hu *et al.* [84] in 2017, considering the lifting of subsea trees by marine risers; Gao *et al.* [85] in 2020, considering the lowering of medium size manifold; and Quan and Chang [86] in 2020, assessing the response of a drill rig suspended by a tether. All these works highlighted the influence of the winch speed on the

dynamic loads in the cable, reinforcing the importance of considering this variable when planning subsea lifting operations. Theoretical aspects of variable mass systems, which can be directly applied to the scenario of subsea lifting operations considering variable length cables, can be found in the works by Pesce *et al.* [87,88] and Cveticanin [89].

Other representative examples of studies addressing the dynamics of deep water subsea lifting operations can also be found in the literature. Morrison and Cermelli [90] studied the installation of suction piles via a simplified single degree-of-freedom model. The installation of a suction can was considered by Ireland *et al.* [91]. Jacobsen and Leira [92] considered the dynamics of suspended payload during a towing operation. A comparison of the natural frequencies of the system calculated by using an analytical continuous model and a lumped mass model was presented by Richter *et al.* [93]. Parametric transversal resonances due to axial tension variations were studied via Mathieu equation by Kang *et al.* [94,95]. Time domain analysis was used to study the complete installation of a manifold in the South China Sea by Chen *et al.* [96]. The pendulous vibration due to current excitation using a single degree-of-freedom model by the method of averaging was presented by Li *et al.* [97]. A virtual reality software for the simulation of subsea lifting operations was presented by Zhang *et al.* [98]. An Orcaflex model for the installation of subsea manifold by using drilling pipes was considered by Wang *et al.* [99]. The installation of a subsea manifold by the sheave method considering the software Orcaflex was analysed by Zhao *et al.* [100]. The quasi-static analysis of a drill pipe during the installation of subsea trees was presented by Qin *et al.* [101] and natural frequencies of this system was considered by Xiao *et al.* [102].

2.2.4 Phase 4 – Landing on the seabed

The final phase of the subsea lifting operation is the landing on the seabed or onto a hosting structure. During this phase, it is important to guarantee the correct positioning of the payload and to avoid high impact loads on the system in order to avoid damages on the structures.

The dynamic models presented to model the lowering into deep water phase (Section 2.2.3) can typically be used to model the landing phase. In this context, the displacement, velocity and acceleration of the payload can be evaluated and the operational weather window can be constructed by checking if these variables are within specified limits.

Specific studies on this phase consider active control strategies to guarantee the correct positioning of the payload. For example, How *et al.* [103,104] designed a control strategy based on

the use of thrusters on the payload, while Simoes *et al.* [105] based their modelling on the control of the motions of the lifting platform.

2.3 Control Systems

Control strategies to alleviate dynamic loads and increase the operational weather window of offshore lifting operation can be typically classified in passive or active systems. Besides the studies presented in the above Sections describing passive strategies, a great review on the use of passive heave compensation systems was presented by Woodacre *et al.* [106] in 2015.

Active control strategies to reduce the pendulum motion of the payload during lifting on air has been covered by several authors. Henry *et al.* [107] controlled the motion via actuation on the boom-luff angle, while Masoud *et al.* [108] controlled the slew and luff angles. A tagline proportional-derivative control method was used by Ku *et al.* [109]. The installation of offshore wind turbine components was considered in the study by Ren *et al.* [110], where an active control scheme was proposed to control the tugger line forces acting on the blade during the final installation phase before mating.

Controlling the dynamics of the system in moonpool operations has also been considered in several studies. Johansen *et al.* [111] used a wave synchronization approach in their work. Skaare and Egeland [112] considered a parallel force/position method, showing improved results in comparison with active heave compensation and wave synchronization methods. Messineo *et al.* [113,114] considered a control strategy to reduce slamming loads, keeping the tension on the wire within acceptable bounds.

Regarding the deep water lifting scenario, Bohm *et al.* [115] presented the boundary control for the displacement of a payload hanging by a cable under the action of a steady current. A semi-active heave-compensation system was designed and experimentally evaluated by Quan *et al.* [116], showing an increased efficiency in comparison to the passive counterpart. Another study considering a semi-active system was presented by Li *et al.* [117].

2.4 Hydrodynamics of oscillating bodies

During the lowering through the wave zone or into deeper waters, the payload is subjected to hydrodynamic forces due to its oscillatory motion inside the water or due to the direct action of

the ocean waves on the structure. The correct prediction of these forces is essential for an accurate determination of the global dynamics of the lifting system. Due to the high complexity of this time-dependent flow, which may account for viscous effects, oscillation of the payload inside its own wake and transition from laminar to turbulent regimes, no closed solution exists to represent the hydrodynamic forces acting on the payload. Approximate solutions are then typically used to estimate these forces.

A recurrent approach found in the literature and in commercial software is the use of Morison's equation [118] to estimate the hydrodynamic forces. This formulation was originally developed for the analysis of surface wave loads on piles back in 1950 and it accounts for a term that is proportional to the acceleration and a term proportional to the square of the velocity. These two terms require the knowledge of two coefficients: the added mass and drag coefficients, which depend on the shape of the structure and flow conditions.

Another relevant early work on this field is due to Keulegan and Carpenter [119] in 1958. This study presented the added mass and drag coefficients of cylinders and plates on oscillating flows for various conditions. The authors showed that the hydrodynamic coefficients were dependent on a non-dimensional number given by the amplitude of the velocity multiplied by the period of oscillation and divided by the characteristic length of the body. This non-dimensional number was lately named as Keulegan-Carpenter number (KC).

Building on these two classical works ([118,119]), a great variety of studies have been published on the determination of the hydrodynamic coefficients for different geometries and flow conditions. The rest of this Section presents a review on the studies addressing the determination of these coefficients for relevant structures on the context of subsea lifting operations.

2.4.1 Simplified geometries

The prediction of the hydrodynamic coefficients for simplified geometries such as cylinders and plates is recurrent in the literature. These simplified geometries are often used as structural components of subsea structures, justifying their relevance. An important reference on the hydrodynamics of cylinders was presented by Sarpkaya [120] in 2010. This work included a review of the state-of-art on this topic, stressing the influence of the number of Reynolds (Re) and Keulegan-Carpenter (KC) in time-dependent flows. Another important aspect highlighted by Sarpkaya is the difficulty in finding an accurate and general representation of the hydrodynamic forces on offshore applications. This is due to the random nature of turbulence and the

large parameter space in any real application.

Recent studies on the hydrodynamic of cylinders are also frequent on the literature. Hu *et al.* [121] presented in 2017 an experimental study on the nonlinear hydrodynamics of a floating cylinder in oscillatory flow alone and combined with a current. The hydrodynamic damping of circular cylinders was experimentally obtained for KC numbers lower than 5 and Reynolds between 10^3 to 10^5 with and without background current by Gao *et al.* [122] in 2020. Direct numerical simulation was used by Ren *et al.* [123] in 2021 to analyse the oscillatory flow around a cylinder for various Keulegan-Carpenter and Stokes numbers.

A relevant reference on the hydrodynamics of flat plates is the review presented by Molin [124] in 2011. In this study, Molin presented a summary of his studies on the hydrodynamic of perforated plates. Particularly, a theoretical model was presented by Molin for the calculation of the added mass and damping coefficients of the perforated plates, which were dependent on a non-dimensional number referred as porous Keulegan-Carpenter number ($\widetilde{KC}$). The results obtained were in agreement with experimental data for several geometries in both forced motion or subjected to incoming waves.

An experimental and numerical study on the hydrodynamics of rectangular plates was presented by An and Faltinsen [125] in 2013. The numerical model combined potential flow theory with nonlinear viscous pressure loss. A domain decomposition technique was used combining a boundary element method in the inner domain and an analytical representation of the velocity potential in the outer domain. The results obtained showed the dependence of the hydrodynamic coefficients with KC and agreed with experimental data, especially in the deep submerged cases.

Li *et al.* [126] presented an experimental investigation of the hydrodynamic coefficients of heave plates in forced oscillation. Results considering the influence of the amplitude and frequency of oscillation, plate depth, thickness-to-width ratio, shape of the edge, perforation ratio and hole size were presented. Among other findings, it was argued that the added mass increased with KC, while the frequency of oscillation had little influence.

The influence of the proximity to the seabed and amplitude of oscillation of heave plates was investigated by Garrido-Mendoza *et al.* [127] in 2015. Numerical simulations via a finite volume solver showed that, for low KC numbers, increasing the seabed proximity resulted in an increased added mass and damping coefficients.

An experimental investigation on the hydrodynamics of flat plates for the KC ranging from 0.15

to 3.15 was conducted by Tian *et al.* [128] in 2016. The influence of the thickness ratio, shape, edge corner radius, perforation ratio and hole size were analysed for single plate configuration, and spacing effects was considered also in the double and triple plates configuration.

A series of studies were published by Mentzoni and Kristiansen [129–131] in 2020 and 2021 on the numerical and experimental investigation of the hydrodynamics of perforated plates. The numerical solver was based on the solution of the Navier-Stokes equations in two dimensions. It was found that the hydrodynamic coefficients were highly dependent on the amplitude of the oscillation. Influence of the period of oscillation was found to be minor. The authors also showed that separation at the edges of the plate were important on the calculation of the damping coefficient.

2.4.2 Complex structures

Subsea lifting operations are typically conducted for the installation or recovery of complex structures on the seabed, such as manifolds, X-trees, protection structures, etc. Direct correlation to simplified geometries (as those presented in the above Section) when evaluating their hydrodynamic coefficients is not straightforward and, most of the times, not possible. Therefore, it is necessary to study the hydrodynamic of these complex structures in detail in order to obtain an accurate representation of the dynamic of the subsea lifting operations.

Fernandes and Mineiro [132] published a study describing the translational and rotational added mass coefficients of a manifold in 2007. They used the panel method and an experimental setup based on a constant acceleration towing. The results showed coherence between the models, which were argued to be directly applicable to the pendulum installation scenario, where rotational motions are expected.

An experimental evaluation of the hydrodynamics of an ROV (Remotely Operated Vehicle) was presented by Avila and Adamowski [133] in 2011. They conducted forced oscillation tests in a full-scale open-frame ROV. The results showed a large influence of the KC number and a low influence of the period of oscillation (particularly for $KC > 3$) on the hydrodynamic coefficients.

A detailed study on the hydrodynamics of suction anchors was published by Solaas and Sandvik [134] in 2017. Different perforation ratios of the top plate and different height to diameter ratios were considered in their study. Influence of these variables and the amplitude of oscillation were highlighted and showed agreement with previous data on the literature.

Another study on the determination of the hydrodynamic coefficients of subsea manifolds was presented by Du *et al.* [135] in 2020. Experimental and numerical studies (via Computational Fluid Dynamics) were conducted and it was found that the added mass increased nearly linearly with the KC number and was not significantly affected by the period of oscillation.

Finally, Pestana *et al.* [136] studied the variation of the added mass and drag coefficients with the KC number for three subsea manifold geometries. They considered an experimental setup to perform oscillatory tests with 1:35 scale models representing the different geometries. The results showed a linear increase of the added mass with KC and a reciprocal relation of the drag coefficient with KC.

2.5 Discussion

Based on the references presented in this Chapter, some key aspects of offshore lifting operations can be highlighted. Analysing the historical perspective, it is clear the presence of some periods of time when attention has been given to particular aspects of the operation. During the end of the 20th century, early models were studied, focusing on oil and gas applications. During the 2000s, attention was given to deep water operations due to the new frontier for the exploration of hydrocarbons at that time. Finally, the past decade was marked by the increase on the studies regarding the installation of offshore wind turbines. This trend to focus on renewable energy is expected to get even larger importance on the future, as new renewable technologies, such as floating wind and wave energy convertors, achieve a more mature level.

Regarding the design methodologies, great attention has been given to the development of general numerical tools to predict the dynamics of the lifting system and, therefore, enable the analysts to estimate a safe weather window for real operations. In addition, the development of control methods to alleviate the dynamic loads on the system has been considered by several authors, while the study of the hydrodynamics of oscillation bodies has been focused by many others.

However, few studies have actually been published on the impact that intrinsic nonlinearities of the system can have on the dynamics of the system and how this can affect the planning of the operation. This thesis aims to address this issue, focusing on the deep water lowering phase of the operation. As presented in Section 1.2, the emphasis is to model the system assuming a variable length cable and include the nonlinear aspects introduced by the hydrodynamic forces on the system due to the oscillatory motion of the payload inside the water. Finally, the models

to be developed in this thesis are general in the sense that they can be used on any type of application, both on the oil and gas or renewable energy perspective.

3. A DYNAMIC MODEL TO EVALUATE THE INFLUENCE OF THE LAYING OR RETRIEVAL SPEED ON THE INSTALLATION AND RECOVERY OF SUBSEA EQUIPMENT

The original version of this paper has been published in Applied Ocean Research (v. 77, p. 34-44, 2018) by R. B. Tommasini, L. O. Carvalho and R. Pavanello [137] addressing the objective n. 1 of this thesis (as per Section 1.2.3). In this study, a single degree-of-freedom model, taking into account a variable length cable, has been presented to explore the influence of the winch speed on the dynamics of deep water subsea lifting operations.

Abstract

A new model for the dynamics of a cable-mass system representing the installation or retrieval of subsea equipment is analysed. It considers a one-degree of freedom system, which is able to account for the variation of the cable's length during the time, simulating the equipment laying or recovering process. Also, the cable's mass is included in the analysis and the hydrodynamic forces are modelled by the Morison's equation. The resulting nonlinear equation of motion is integrated over the time domain via a predictor-corrector Newmark-β method. Firstly, the proposed model is compared with an Orcaflex model on fixed and variable length scenarios. The results show that the proposed model gives accurate solutions in comparison with the finite element model through all the depths evaluated, even at zones where super-harmonic response occurs. Secondly, the influence of payout speed on the dynamics of the system is assessed. Here, the system presents a variation on the static and dynamic forces, especially at the resonance zone. Finally, an operational weather window is generated for a specific case, which shows that the acceptable sea states change depending on the laying or retrieval speed considered. This highlights the importance of using models that account for the payout speed when analysing subsea equipment installation and retrieval operations.

Nomenclature

A	Cross-section area of the cable
A_p	Vertical projected area of the equipment
C_d	Drag coefficient of the equipment
E	Elastic modulus of the cable
F_{static}	Static force on the cable
g	Gravity acceleration
H_s	Significant height
$h(t)$	Function for the movement of the vessel at the lifting point
ℓ	Length of the cable from the equipment to a given point
L	Full suspended length of the cable
M_{add}	Added mass
M_{eq}	Mass of the equipment
m'	Linear mass of the cable
w	Displacement of the equipment
w_0	Displacement of the top of the cable
w_ℓ	Displacement of a material point within the cable
ρ	Specific mass of the water
$\mathbb{Q}$	Nonconservative generalized forces
SWL	Safe Working Load
T_p	Peak period
$\mathbb{T}$	Kinetic energy
t	Time
$\mathbb{V}$	Potential energy
V	Volume of the equipment
$V_c(t)$	Function for the payout/retrieval speed
$\dot{(\ )}$	First derivative over the time domain
$\ddot{(\ )}$	Second derivative over the time domain
$\lvert\ \rvert$	Absolute value of a variable

3.1 Introduction

Subsea production systems have been used in offshore oil production for the past fifty years. One of the most costing activities to implement a subsea layout is the installation of equipment on the seafloor, mainly due to the high daily costs of dedicated vessels used on these operations.

The two main approaches considered to reduce these costs, preserving the safety requirements, are the development of new installation methods, and the improvement of the methodologies to analyse these operations.

Regarding the development of new installation methods, the first ones considered the use of a drilling rig to deploy the equipment on the seafloor. This procedure is usually expensive and subjected to tight schedule restrictions since the main task of these rigs is the drilling of subsea wells. To overcome this challenge some new installation procedures have been proposed. Roveri, de Oliveira and Moretti [2] described the installation of a manifold by a multiple slings technique. They showed that this method was efficient and cheaper than the traditional ones on their application. Further, Nelson *et al.* [3] proposed the use of buoy-chain device in-line with the hardware to be deployed to reduce the dynamic loads on the system. Another innovative solution is known as the pendulous installation method [14,138,139]. This procedure enables the use of low-cost support vessels to install heavy equipment in ultra-deep water. Great effort [5,7,9,10] was also made to qualify and provide an installation system based on synthetic cables. This system is of huge value as the increase of the cable's mass tends to lead to prohibitive weather windows on ultra-deep water. More recently, some authors [16–18] described a method in which the equipment is assembled to a submerged floating device in sheltered waters and then transported in a towing operation until the installation location. Since the equipment is not directly connected to the vessel in this scenario, the operation presents lower weather restrictions. Lastly, a review of the available methods to install subsea equipment is described by [29–31].

On the other hand, the improvement of the analysis methodologies is useful since it allows the industry to have more accurate solutions regarding the system's dynamics, which leads to wider installation windows preserving the safety requirements. The firsts studies [1,67,71] about the deployment of subsea loads considered analytical approaches, linearizing the drag force acting on the equipment and solving the resulting equations in the frequency domain. Later, some authors [71,140–142] considered systems which were solved in the time domain, accounting for the nonlinear drag forces and the possibility of predicting snap loads on the cable. While these works were focused only on the dynamics of a suspended cable, Kopsov e Sandvik [58] detailed all the steps that should be addressed in an installation analysis: liting from the deck, lowering through the splash zone, lowering into deep water and landing on the seabed. More recently, fluid-structure interaction models have been used [76,143–145] to predict the dynamics of the equipment in the wave zone. Although this tends to lead to more realist results, the

computational cost is somewhat prohibitive. Finally, as a general guide, the recommended practice DNV-RP-H103 [146] provides simplified models for all the installation analysis steps, guidance for choosing hydrodynamic coefficients, and recommendations on how to use nonlinear dynamic models.

The lowering into deep water is one of the critical steps to be analysed when the final installation depth is high. In this case, the cable-equipment system may achieve a resonance regime due to the motion induced by the ocean waves. The common feature of the traditionally used models to analyse this step [1,58,67,71,140–142,146] is that the equipment is considered to be placed at a given depth and the cable has fixed suspended length. Therefore, to perform a full installation analysis, it is necessary to run several simulations with the equipment positioned at different depths. This procedure is considered valid according to the recommended practice DNV-RP-H103 [146]; however, it does not take into account the influence that the laying or retrieval speed might have on the dynamics of the system and on the operational weather window.

Even though these models do not consider the influence of the payout speed on the dynamics of the system, some works have already been presented dealing with this effect. The models proposed by [147–150] focused their efforts on the installation of submarine cables (such as communication or control cables); Wang, Fung and Lee [82] considered a finite element model to analyse an underwater cable with time-dependent length, while Hu *et al.* [84] modelled the dynamics of a rigid riser with variable length during the installation of a subsea production tree. Outside the subsea area, Terumichi *et al.* [151] presented a model for the analysis of a string with variable length representing an elevator system; Moustafa *et al.* [152] dealt with the dynamics of overhead cranes during the load hoisting or lowering; and Du *et al.* [153] presented a model for the analysis of variable length cables to be used on large scale radio telescopes. Further, the version 10.2 of the commercial software Orcaflex [154], which was released in 2017, introduced the possibility of line feeding, enabling the users to analyse cables being laid or hauled.

Based on the works presented above, two main gaps may be pointed out regarding the methodologies to analyse the installation and recovery of subsea equipment. The first one is the lack of a simple model that is able to account for the influence of the payout speed on the dynamics of the system during the laying or recovery process. The existents models that deal with the payout speed [82,84,147–154] consider discretized systems, which take longer times to run the

required simulations to construct a complete operational weather window. This is a crucial point, especially if an analysis is needed to be run aboard the vessel during the operation. The second one is the absence of studies presenting results of how the dynamics of the installation or recovery operation is affected by the payout speed, since the aforementioned works focused their results on the validation of the method or on different applications.

Consequently, this paper presents two main objectives: (1) to propose a simple model suitable to analyse subsea equipment installation and retrieval operations, which is able to account for the variation of the cable's length during the time, simulating the equipment laying or recovering process, and (2) to present results regarding the influence of the payout speed on the dynamics of the system and on the operational weather window.

The proposed model is based on a one-degree of freedom system, in a similar manner as described by Niedzwecki and Thampi [71]. However, it includes the possibility of varying the suspended length of the cable throughout time, and it considers the drag force on its nonlinear form. This model is then compared with the results presented by Orcaflex, in order to assess its accuracy on fixed and variable cable's length scenarios. Finally, the model is used to predict the influence of the payout speed on the dynamics of the system, and on the operational weather window for installation and retrieval operations.

3.2 Variable length cable-equipment model

Previous work has shown that in the absence of time-varying currents or large horizontal excursions of the vessel, the ship and the equipment are only coupled vertically. Therefore, a one-dimensional model is sufficient to represent the system [76]. Further, the system is considered to have one degree of freedom, which is the vertical displacement of the equipment.

It is also considered that the dynamics of the vessel is uncoupled from the dynamics of the cable-mass system. This assumption is normally acceptable and will give conservative results, as the object in most cases tends to reduce the vertical crane tip motion [146].

The mass of the cable is included in the analysis, and its suspended length is modeled as variable throughout time. Besides, a linear stress-strain relation and an elastic behavior are considered for the cable. Consequently, snap loads are not possible to be predicted by the proposed model, and only positive values for the efforts on the cable should be considered as valid results.

Figure 3.1 represents the proposed model. The displacement of the top of the cable and the

displacement of the equipment are respectively denoted by w_0 and w. As a simplification, it is considered that the cable is fully submerged, and the hydrodynamics forces act only at the equipment. These assumptions are usually taken for one-degree of freedom systems [1,71].

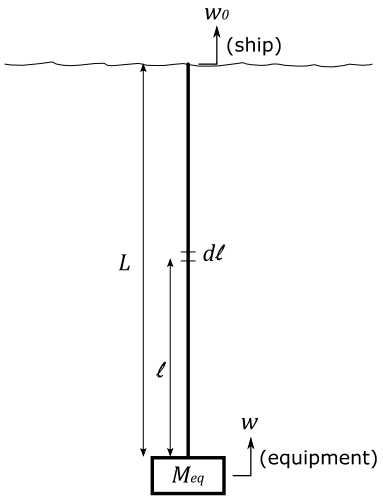

Figure 3.1: Proposed model for the evaluation of subsea equipment installation and retrieval operations.

The resulting equation of motion for this system may be obtained via Lagrange's equation, which can be stated as [155]:

$$\frac{d}{dt}\left(\frac{\partial \mathbb{T}}{\partial \dot{w}}\right) - \frac{\partial \mathbb{T}}{\partial w} + \frac{\partial \mathbb{V}}{\partial w} = \mathbb{Q} \tag{3.1}$$

It is then necessary to evaluate the kinetic ($\mathbb{T}$) and potential energies ($\mathbb{V}$), and the non-conservative generalized forces ($\mathbb{Q}$) acting on the system as a function of the generalized coordinate w. The kinetic energy of a differential cable element ($d\ell$) is given by:

$$d\mathbb{T}_{cable} = \frac{1}{2} m' d\ell \dot{w}_\ell{}^2 \tag{3.2}$$

Since a one-degree of freedom system is used, the velocity of a material point within the cable ($\dot{w}_\ell$) is considered to be the linear interpolation between the velocity of the top of the cable ($\dot{w}_0$) and of the equipment ($\dot{w}$):

$$\dot{w}_\ell = \dot{w} + \frac{\ell}{L}(\dot{w}_0 - \dot{w}) \tag{3.3}$$

Therefore, integration along the cable's length and the addition of the kinetic energy of the equipment lead to the total kinetic energy of the system:

$$\mathbb{T} = \frac{m'L}{6}(\dot{w}_0^2 + \dot{w}_0\dot{w} + \dot{w}^2) + \frac{1}{2}M_{eq}\dot{w}^2 \tag{3.4}$$

A similar approach is used to obtain the total potential energy of the system, which is given by the summation of the gravitational potential energy of the cable and the equipment, and the elastic potential energy of the cable:

$$\mathbb{V} = \frac{(m' - \rho A)gL}{2}(w_0 + w) + \big(M_{eq} - \rho V\big)gw + \frac{1}{2}\frac{EA}{L}(w_0 - w)^2 \tag{3.5}$$

The hydrodynamic force acting on the equipment, modeled by Morison's equation [118], is considered to be an external non-conservative force. Consequently:

$$\mathbb{Q} = -M_{add}\ddot{w} - \frac{1}{2}\rho C_d A_p \dot{w}|\dot{w}| \tag{3.6}$$

Substituting Equations (3.4) to (3.6) into Equation (3.1), and considering that the cable's length is variable within time, it is possible to obtain the following equation of motion for the system[1]:

$$\begin{aligned}\left(M_{eq} + M_{add} + \frac{1}{3}m'L\right)\ddot{w} + \left(\frac{m'\dot{L}}{3} + \frac{1}{2}\rho C_d A_p|\dot{w}|\right)\dot{w} + \frac{EA}{L}w \\ = -\frac{(m' - \rho A)gL}{2} - \big(M_{eq} - \rho V\big)g + \frac{EA}{L}w_0 - \frac{m'\dot{L}}{6}\dot{w}_0 - \frac{m'L}{6}\ddot{w}_0\end{aligned} \tag{3.7}$$

This equation must be solved for the displacement of the equipment (w) as a function of the imposed movement of the top of the cable (w_0, $\dot{w}_0$, and $\ddot{w}_0$), considering that the cable's length is variable with the time: $L = L(t)$. In comparison with the equation presented by [71], some differences arise: the terms $m'L\ddot{w}/3$ and $-m'L\ddot{w}_0/6$ were introduced because of the assumption that the cable's mass is considered in the analysis; while the terms $m'\dot{L}\dot{w}/3$ and $-m'\dot{L}\dot{w}_0/6$ were included due to the fact that the cable's length is variable within time. Further, the influence of the weight of the cable and of the equipment is included as an external force; therefore, the static deformation due to these loads will be part of the solution. Lastly, the hydrodynamic force acting on the equipment sums the added mass on the inertia term, and introduces a quadratic force, making the system nonlinear.

In order to solve Equation (3.7), it is necessary to specify the displacement (w_0), the velocity

[1] The equation of motion presented in this study is similar to the equation obtained by Quan and Chang [86] for a finite element representation of an unidimensional variable-length cable, except for one momentum flux term ($m'V_c^2/2$) due to the variation of mass in the system. This term is negligible for the example presented in this study (i.e. maximum value of 12.3 N, compared to other terms in the order of hundreds of kN). For different applications, this term might be significant and included in the analysis.

($\dot{w}_0$) and the acceleration ($\ddot{w}_0$) on the top of the cable. In this scenario, they may be considered as:

$$w_0 = h(t) + \int V_c(t)dt \tag{3.8}$$

$$\dot{w}_0 = \dot{h}(t) + V_c(t) \tag{3.9}$$

$$\ddot{w}_0 = \ddot{h}(t) + \dot{V}_c(t) \tag{3.10}$$

where $h(t)$ is a function that represents the movement of the lifting point under the influence of the ocean waves, and $V_c(t)$ is a function for the payout speed (being positive when recovering cable and negative when releasing cable). The movement of the lifting point may be given by a specified sinusoidal signal or by the product of the displacement RAO of the vessel and the wave spectrum, as detailed by [156].

It is also required to set the length of the cable and its variation through time to solve Equation (3.7):

$$L = L_0 - \int V_c dt \tag{3.11}$$

$$\dot{L} = -V_c \tag{3.12}$$

Finally, the efforts on the top of the cable and on the equipment[2] are given by:

$$F_{top} = \frac{EA}{L}(w_0 - w) + \frac{(m' - \rho A)gL}{2} \tag{3.13}$$

$$F_{eq} = \frac{EA}{L}(w_0 - w) - \frac{(m' - \rho A)gL}{2} \tag{3.14}$$

3.2.1 Numerical implementation

Equation (3.7) is integrated over the time domain via a predictor-corrector form of the Newmark β-method [157]. This choice is made due to the fact that this algorithm has successfully been

[2] The term named force on the equipment (F_{eq}) actually refers to the force on the bottom part of the cable. This nomenclature might be misleading, as the equipment, in addition to the force due to the cable, is also subjected to hydrodynamic, inertia, gravitational and buoyancy forces. Nonetheless, the force obtained in Eq. (3.14) is the correct term to be compared against design criteria presented in Section 3.3, as this is the force acting on the pad-eyes of the equipment and on the cable.

used on similar applications [71] and is unconditionally stable when using the undamped trapezoidal rule.

Further, in order to avoid high dynamic transients at the beginning of the simulation, two approaches are taken into consideration. The static solution of the system is used as an initial condition for the displacement of the equipment. And a pre-simulation time is included, when the values for $h(t)$ and $V_c(t)$ are ramped from zero to their final values via a sigmoid function.

3.3 Operational weather window

The operations of installing and recovering subsea equipment are usually classified as weather restricted (as defined by DNV-OS-H101 [158]). Therefore, during the planning phase, it is necessary to specify the weather conditions that guarantee the safety of the operation, which is known as the operational weather window. According to DNV-RP-H103 [146], a safe procedure should check if the maximum efforts are not higher than the safe working load (SWL) of any component of the lifting system, and if the minimum efforts are 10% higher than the static load on each point of cable (F_{static}), in order to prevent slack conditions.

Given that, Table 3.1 presents the algorithm considered to define the weather window in an installation-retrieval operation of subsea equipment for the model proposed in this paper.

Table 3.1: Algorithm for the evaluation of the operational weather window for the proposed model.

1. Set the data for a given operation;
2. For each sea state (Significant Height and Peak Period), calculate:
    a. The movement of the equipment over the time according to Equation (3.7);
    b. The efforts on the top of the cable and on the equipment over the time according to equations (3.13) and (3.14);
    c. Check for the acceptance criteria ($F_{cable} \leq SWL$, and $F_{cable} \geq 0.1F_{static}$):
        i. If both criteria are fulfilled, the sea state is acceptable;
        ii. Otherwise, the sea state is unacceptable;
3. Build the operational weather window with the acceptable sea states.

If an irregular wave approach is considered, it is then necessary to perform several runs for each sea state (step 2a-b). The design values to be compared against the acceptance criteria may be obtained via a maximum value statistical analysis. In this work, the design value is taken as the maximum and minimum values obtained on 95% of the sea states considered.

3.4 Numerical results and discussion

The scenario considered in the sequence to evaluate the proposed model is presented in Table 3.2. This scenario represents an operation for a medium size manifold, being lifted by a 3 in diameter steel wire rope.

Table 3.2: Input data for the evaluation of the proposed model[3].

	Parameter	Value
Cable	Linear mass (m')	24.6 kg/m
	Area (A)	4098 mm^2
	Axial stiffness product (EA)	315 MN
	Safe Working Load (SWL)	1100 kN
Equipment	Mass (M_{eq})	60 tonnes
	Volume (V)	7.63 m^3
	Area (A_p)	56.95 m^2
	Added mass (M_{add})	300 tonnes
	Drag coefficient (C_d)	7
Newmark method	Time step	0.1 s

3.4.1 Verification of the proposed model for fixed length cases

The first analysis aims to evaluate the system's response considering no payout speed and a sinusoidal displacement imposed on the top of the cable. In this case, to evaluate the dynamics of the system during all the installation/retrieval process, several independent time domain analyses are run, each one considering a fixed cable's length. The results from the proposed model are then compared with those obtained using the commercial software Orcaflex, which discretizes the cable in several elements (in this example, 30 elements were considered) and also includes the nonlinearities due to the hydrodynamic force.

The sinusoidal imposed displacement is considered to have an amplitude of 0.3 m and the time domain analyses are run for 100 s. Figure 3.2 illustrates the maximum (superior curve) and minimum (inferior curve) forces acting on the top of the cable and on the equipment as a function of the depth of the equipment (unstretched cable's length). Figure 3.2 a-b, c-d and e-f consider an imposed sinus with period of 5 s, 9 s and 13 s, respectively.

[3] The terminal velocity for this manifold (the maximum velocity achieved during free fall inside the fluid) is equal to 1.6 m/s. This value can be considered as an upper boundary for the pay-out speed. In this study the maximum pay-out speed considered is 1 m/s, which is less than the terminal velocity.

It is possible to see that the mean traction on the top of the cable increases linearly with the depth, since the total weight of the suspended cable also increases with the depth. Further, the peak of the system's response occurs at different depths when varying the imposed sinus period.

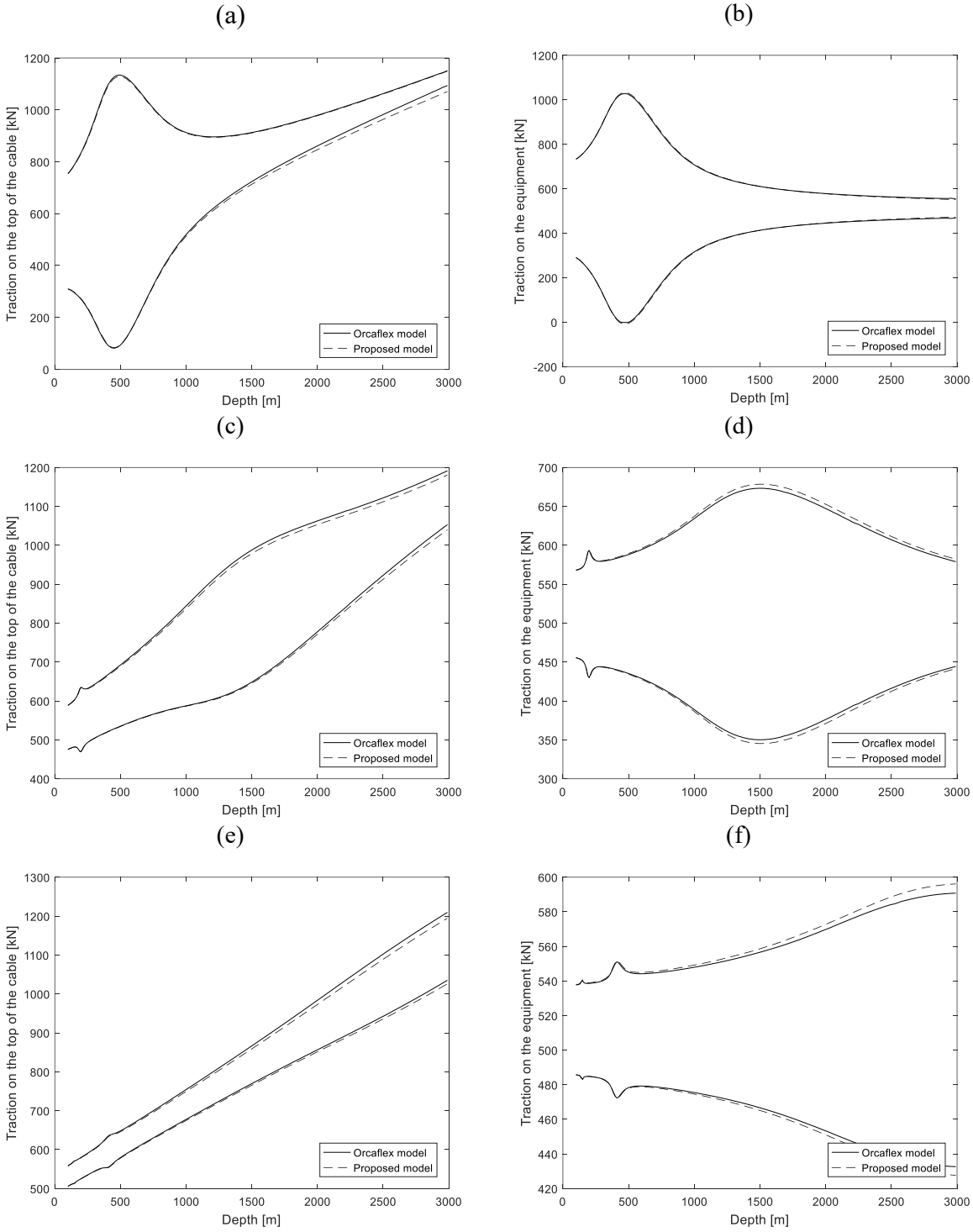

Figure 3.2: Maximum and minimum efforts on the top of the cable and on the equipment as a function of the equipment's depth. The imposed sinus has amplitude 0.3 m and period: (a-b) 5 s, (c-d) 9 s, and (e-f) 13 s.

This is due to the fact that the resonance period of the system varies as a function of the suspended cable's length: for greater depths, the resonance period tends to be higher. Besides, there are other peaks of response at depths where the natural frequency of the system matches an odd harmonic of the exciting frequency. At those depths, there is more than one sinusoidal component on the response of the system, which is known as super-harmonic response [155].

Figure 3.3 represents the traction on the top of the cable considering an exciting sinus of amplitude 0.3 m and period 9 s at the zone where super-harmonic response occurs (200 m depth). Figure 3.3a is the time domain curve and Figure 3.3b is the Fourier transform of that signal. The graphs show the two sinusoidal components on the response of the system. The first one has amplitude equal to 60 kN, and frequency of 0.11 Hz (similar to the forcing frequency);

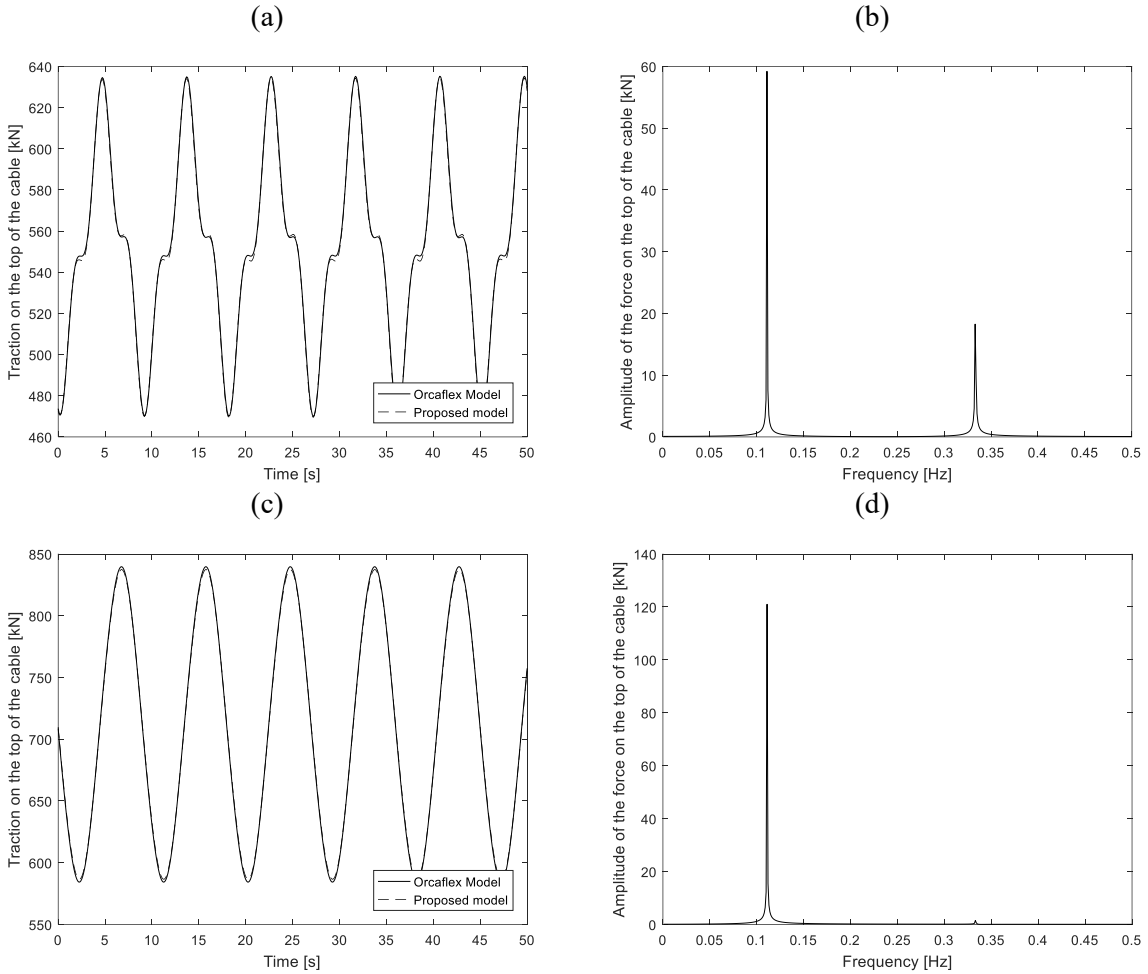

Figure 3.3: Traction on the top of the cable for an exciting sinus of amplitude 0.3 m and period 9 s. (a) Time domain graph for 200 m depth; (b) Fourier transform for 200 m depth; (c) Time domain graph for 1000 m depth; (d) Fourier transform for 1000 m depth.

while the second has amplitude equal to 18 kN, and frequency of 0.33 Hz (three times the forcing frequency and equal to the resonance frequency at this depth). This second component is

the responsible for the increase in the dynamic response of the system at this depth. On the other hand, Figure 3.3c-d show the traction on the top of the cable for the equipment at 1000 m depth. In this case, the natural frequency of the system (0.15 Hz) does not match an odd harmonic of the exciting frequency, and consequently there is only one sinusoidal component on the response.

3.4.2 Verification of the proposed model for variable length cases

Considering a variable length scenario, the results obtained from the proposed model were again compared with the results presented by the commercial software Orcaflex. In this case, an imposed sine wave on the top of the cable was considered of amplitude 0.3 m and period of 9 s, a laying speed of 0.1 m/s, and 30 elements along the full length of the cable for the Orcaflex model. Figure 3.4 presents the maximum and minimum efforts on the top of the cable (Figure 3.4a) and on the equipment (Figure 3.4b) for the two models. These results illustrate the accuracy of the proposed model in comparison with a discretized model in predicting the dynamics of the system when the payout speed is considered in the analysis. Similar results were also obtained for different payout speeds considered. Further, it is possible to see that the zone where the super-harmonic response occurs is extended when the payout speed is considered. At this region, the efforts on the system present a dynamic transient due to the changing in the amplitude of the super-harmonic component from the moment it appears until it vanishes.

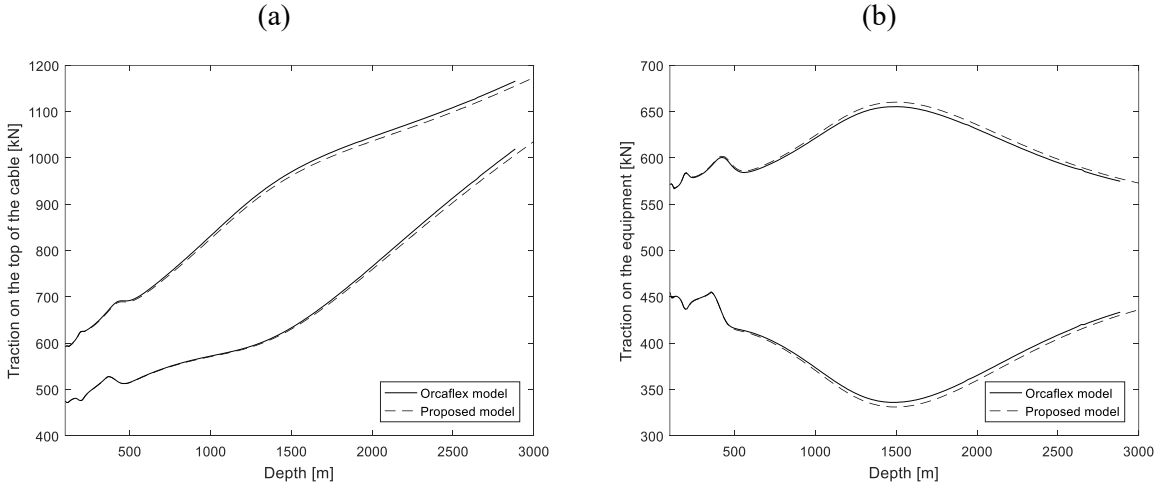

Figure 3.4: Comparison of the system's response for a variable length scenario considering an imposed sinus on the top of the cable of amplitude 0.3 m and period of 9 s, and a laying speed of 0.1 m/s. (a) Force on the top of the cable; (b) Force on the equipment.

The next example of this section considers the response of the system when the payout speed is considerably low. In this case, Figure 3.5 presents the response of the system considering a

laying speed of -0.01 m/s, a retrieving speed of 0.01 m/s, and the response of the system obtained from a fixed length analysis (in a similar way as presented in Figure 3.2c-d). The results obtained from these three analyses are similar, which suggests that the variable length model gives comparable response to fixed length analysis as long as sufficiently low laying or retrieval speeds are considered. This is an expected result since, for low payout speeds, the system has enough time to reach a permanent response at each water depth, mirroring a fixed length analysis.

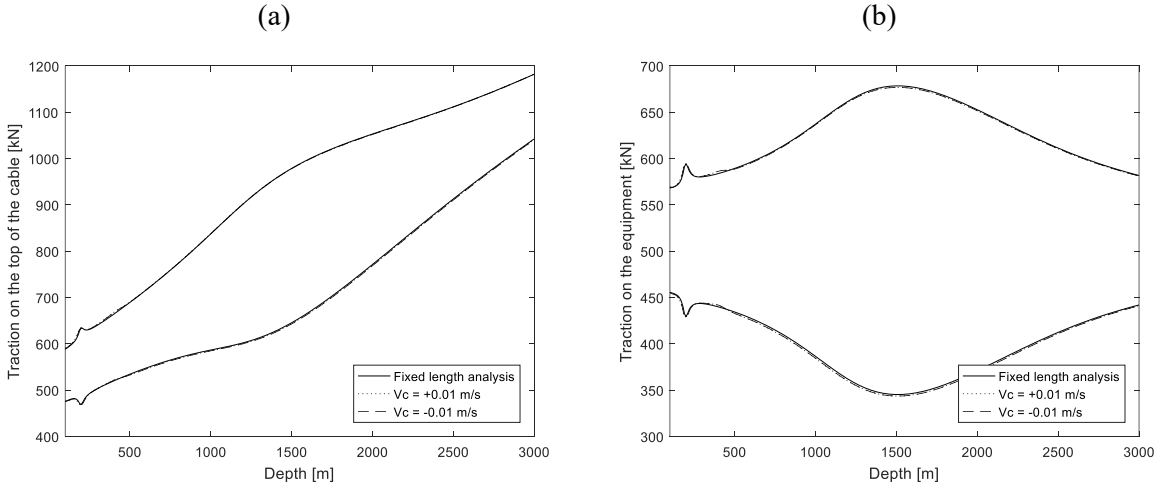

Figure 3.5: Comparison of the system's response for a low payout speed ($0.01\ m/s$) and a fixed length analysis. The imposed displacement at the top has an amplitude of $0.3\ m$ and period of $9\ s$. (a) Force on the top of the cable; (b) Force on the equipment.

The results presented in sections 3.4.1 and 0 showed that the proposed and the Orcaflex models give similar results even at zones where super-harmonic response is present. This adherence of results may be explained by a modal analysis of the cable-equipment system. Table 3.3 presents the 4 first natural vibration periods for the equipment at 3000 m depth (calculated by the Orcaflex model). The first vibration mode refers to the vertical oscillation of the equipment, similar to a one-degree of freedom system. The other modes consider internal axial vibrations along the cable. One may notice that these three higher modes have a natural period in a region that is not excited in installation and retrieval operations, as they are outside of the frequency range of the ocean waves (peak period usually between 5 s and 13 s for the Campos Basin, Brazil). This can be seen as a reason for the similarity of results between a one degree-of-freedom system and a discretized model, since the first vibration mode is the one that is majorly excited in this scenario.

Table 3.3: Natural vibration periods for the system at 3000 m depth.

Vibration mode	Vibration period (s)
1	12.03
2	1.64
3	0.84
4	0.56

Consequently, one-degree of freedom models may be an efficient and accurate way to predict the dynamics of an installation or retrieval operation as long as the modes that result in internal axial vibrations along the cable are not majorly excited.

3.4.3 Influence of the payout speed on the dynamics of the system

The first example of this section illustrates how the payout speed affects the static force acting on the cable during the deployment or recovery of the equipment. For this scenario, it was considered that the vessel remains stationary ($h(t) = 0$), while the cable is laid or recovered with a given speed. Figure 3.6 presents the static force acting on the equipment for several drag coefficients as a function of the laying speed (Figure 3.6a) and hauling speed (Figure 3.6b). For low speeds, the static force on the equipment equals the submerged weigh of the equipment. As the speed is increased, the static force decreases in a quadratic way for the case of laying and increases (also in a quadratic way) for the case of hauling. It is equally noticeable that the drag coefficient has a direct influence on the response. These results suggest that the variation of the static force on the system is due to the action of a constant drag force on the equipment when it is laid or recovered at a given speed.

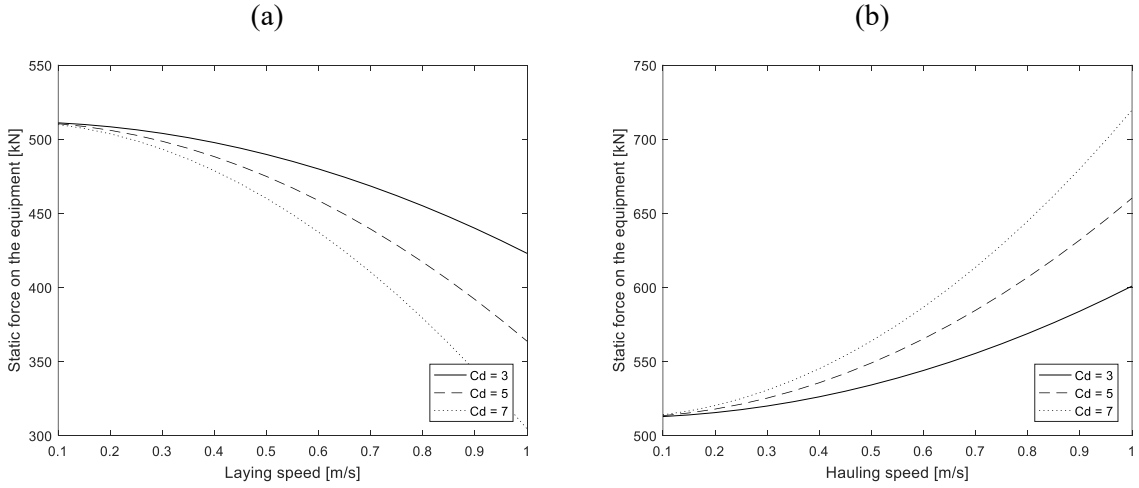

Figure 3.6: Influence of the payout speed on the static force for different drag coefficients. (a) Laying conditions, and (b) recovering conditions.

The second example consists of evaluating the influence of the payout speed on the dynamic efforts on the system. In this scenario, it is considered a sinusoidal imposed displacement of amplitude 0.3 m and period 9 s. Figure 3.7 presents the dynamic effort on the equipment as a function of the water depth for different payout speeds and drag coefficients ($C_d = 3$ in Figure 3.7a and $C_d = 7$ in Figure 3.7b). It is noticeable that there is a transition point when the frequency ratio[4] is about 0.75 (in this case, at 935 m depth). After this point (depths greater than 935 m), as the payout speed is increased, the peak of response tends to reduce and to occur at shallower waters. However, before this point (depths smaller than 935 m), the efforts tend to increase if the speed is also increased. Further, depending on the drag coefficient and payout speed considered, the maximum response may even occur before this transition point (as seen in Figure 3.7b when $V_c \leq -0.8\, m/s$). Additionally, the zone where super-harmonic response occurs is extended and its peak occurs at slightly deeper waters if the speed is considered in the analysis.

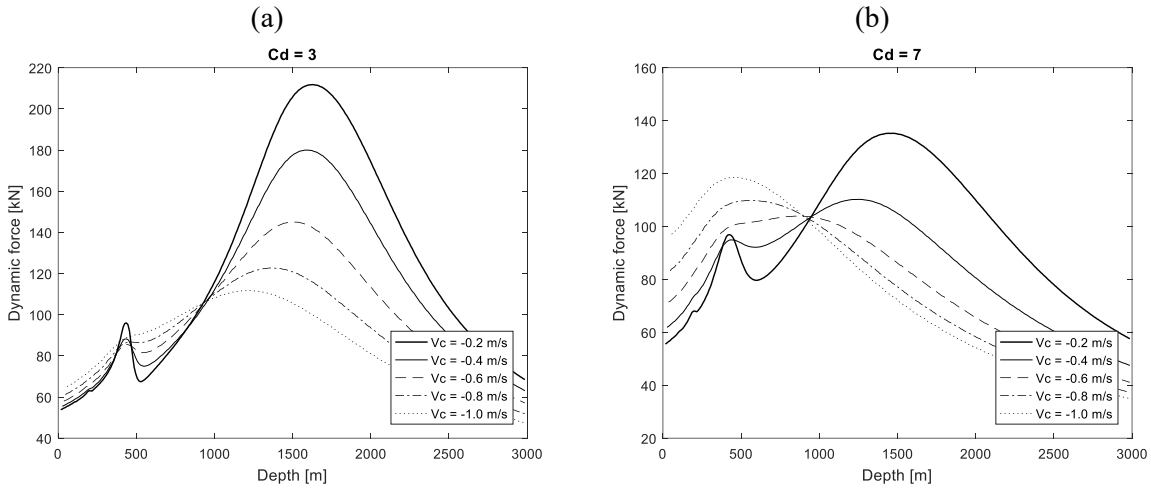

Figure 3.7: Influence of the payout speed on the dynamic force for different laying speeds and considering (a) $C_d = 3$ and (b) $C_d = 7$.

It is also important to mention that the payout speed plays an extra role when the system is exposed to irregular excitations on the top of the cable (representing a real sea state). In this case, the exposure time of the system under the influence of the waves decays in an inversely proportional manner with the payout speed, since the final depth is fixed for a given operation. Therefore, increasing the payout speed reduces the probability of the system to be subjected to high amplitude waves and, consequently, reduces the probability of high efforts on the system.

[4] The frequency ratio in this case is the ratio of the forcing frequency and the fundamental resonance frequency for a given depth.

3.4.4 Influence of the payout speed on the operational weather window

The last example consists in evaluating the operational weather window for several laying and retrieval speeds. This scenario considers an imposed irregular displacement on the top of the cable, given by the product of the displacement RAO of the vessel (Appendix A) and a JONSWAP wave spectrum fitted for the Campos Basin, Brazil. For each sea state, 20 different seeds are considered for the irregular wave train.

The operational weather window obtained from a fixed length analysis is presented in Table 3.4. The cells marked in light gray are considered valid sea states, while blank cells represent unacceptable sea states. This weather window implies an availability of the vessel of 66% and would be used both for installing or retrieving operations if the user decided to plan its operation based on fixed length models.

Table 3.4: Operational weather window for a fixed length analysis

$H_s(m)/T_p(s)$	5	6	7	8	9	10	11	12	13
1.4									
1.6									
1.8									
2.0									
2.2									
2.4									
2.6									
2.8									
3.0									

On the other hand, Figure 3.8 illustrates the difference on the availability of the vessel as a function of the payout speed for installing and retrieving cases. For the installation of the equipment (Figure 3.8a), as the laying speed is increased, the availability of the vessel increases until achieving a maximum when $V_c = -0.4\ \mathrm{m/s}$ and then starts to decrease continually. This is due to the fact that the increase of the speed tends to reduce the maximum efforts at the resonance and reduces the exposure of the system to higher wave amplitudes. However, if the laying speed gets sufficiently high, the steady drag force acting on the equipment makes the cable more prone to slack, restricting the weather window.

For the recovering scenario (Figure 3.8b), the behavior of the system is slightly different. Even though there is a local maximum when $V_c = +0.6\ \mathrm{m/s}$, the availability of the vessel is more likely to decrease as the speed is increased. In this case, the increase on the static force on the system is preponderant over the reduction on the dynamic efforts on the system, and the system tends to violate the criterion of maximum efforts on the cable.

It is important to mention however that the change in the weather window depends on the scenario to be evaluated (combination of equipment, cable, vessel and final installation depth). For example, if the safe working load of the cable is sufficiently high, there might be a scenario where the increase of the retrieval speed will only lead to an increase on the weather window, differently from the example presented before.

As a general outcome, the operational weather window is directly influenced by the payout speed considered for the operation. This influence depends on the combined effect of the variation of the static and dynamic efforts on the system, and the variation of the exposure time of the system under the influence of irregular waves. This might result in an increase or decrease of the availability of the vessel depending on the scenario considered.

This result has a direct impact on the planning of subsea equipment installation and recovery operations since the use of traditional models that consider a fixed cable length may not always lead to a safe or to a cost effective operation. Specifically, for the example presented in this section, if an installation operation was to be executed, the use of variable length analysis would lead to an increase in the availability of the vessel and, thus, in a cheaper operation. On the other hand, if a recovery operation was considered, the use of a fixed length model would indicate as safe some sea states that are not actually acceptable, which could risk the operation.

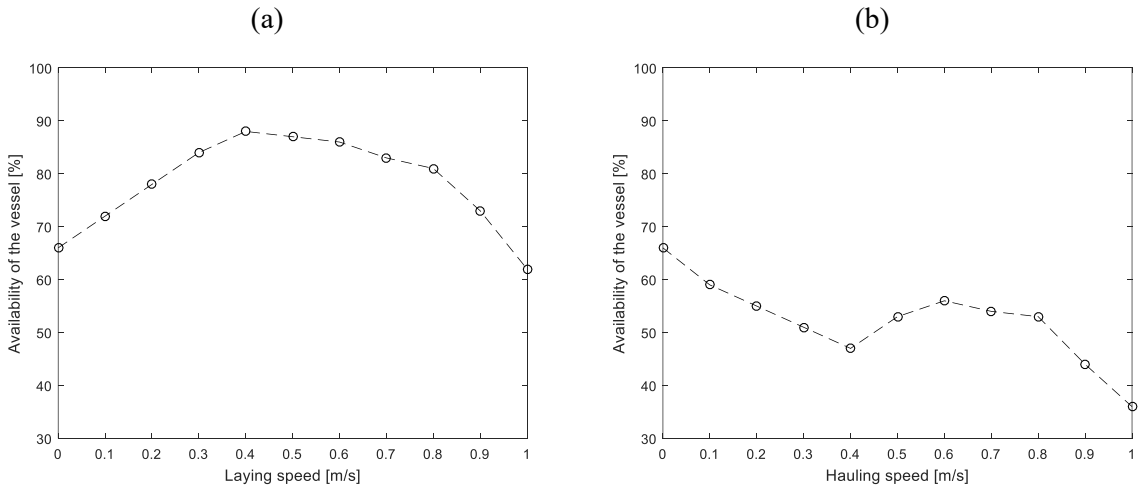

Figure 3.8: Influence of the payout speed on the availability of the vessel for (a) laying conditions and (b) recovering conditions.

Despite the results presented before, some remarks should be made regarding the model proposed. Firstly, the hydrodynamic coefficients considered on Morison's equation are usually given either for an object on a steady flow or for an object on an oscillating flow. The scenario

presented in this work considers the combination of both: the equipment is oscillating and moving at a constant speed. Therefore, it may be necessary to evaluate the hydrodynamic coefficients via an experimental or numerical method as a function of both the payout and oscillating speed. Secondly, the model proposed is only valid for scenarios where internal vibrations modes are not excited by the movements of the vessel. When this assumption is not valid, a discrete model may be the most suitable choice. Finally, a risk analysis may be necessary when deciding to perform an installation or retrieval operation based only on a variable cable's length analysis, since the winch of the vessel may stop working during the operation. In this case, the equipment would be placed at a given depth for an arbitrary period, which could expose the system to unpredicted loads and jeopardize the operation.

3.5 Conclusions

A one-degree of freedom system was developed to evaluate the installation and retrieval of subsea equipment considering the influence of the payout speed. The model considered a variable length cable, included the influence of the cable's mass and used Morison's equation to represent the hydrodynamic forces acting on the equipment. The resulting nonlinear equation of motion was integrated over the time domain via a predictor-corrector form of the Newmark β-method.

The proposed model was evaluated for fixed and variable length scenarios. The results showed that the proposed model gave accurate results in comparison with an Orcaflex model through all the depths evaluated, even at zones where super-harmonic response occurred. Furthermore, the results showed that the increase of the laying speed tended to reduce the static force on the system, while the increase on the retrieval speed led to an increase of the static force. Regarding the dynamic efforts, a transition point was noticed when the frequency ratio was about 0.75. After this point, the maximum dynamic force tended to reduce its value as the payout speed was increased and tented to occur at shallower depths. Before the transition point, the efforts increased if the payout speed increased. Also, the maximum dynamic force could even occur before this point depending on the payout speed and drag coefficient considered.

Finally, the operational weather window and, consequently, the availability of the vessel were directly influenced by the payout speed considered for the operation. Depending on the scenario and payout speed, the availability of the vessel could be increased or decreased due to the combined effect of the variation on the static and dynamic efforts, and the exposure time of the

system under the influence of irregular waves. This is a key point, since the use of traditional models that consider only fixed length scenarios may not always lead to safe or cost effective operations.

3.6 Appendix

Table 3.5 presents the vertical displacement RAO of the lifting point for a typical support vessel used in installation and retrieval operations.

Table 3.5: Displacement RAO for the lifting point.

Angular frequency (rad/s)	Complex value
0.0000	0.9922 - 0.0238i
0.2094	0.9922 - 0.0238i
0.2513	0.9841 - 0.0336i
0.3142	0.9600 - 0.0667i
0.3307	0.9490 - 0.0710i
0.3491	0.9369 - 0.0754i
0.3696	0.9182 - 0.0799i
0.3927	0.8918 - 0.0844i
0.4054	0.8739 - 0.1023i
0.4189	0.8560 - 0.1035i
0.4333	0.8312 - 0.1037i
0.4488	0.8011 - 0.1021i
0.4654	0.7608 - 0.1135i
0.4833	0.7128 - 0.1031i
0.5027	0.6446 - 0.0980i
0.5236	0.5535 - 0.0639i
0.5464	0.4258 + 0.0522i
0.5712	0.4706 + 0.4361i
0.5984	1.0478 + 0.1883i
0.6283	0.8101 - 0.1687i
0.6614	0.5644 - 0.2251i
0.6981	0.3506 - 0.2270i
0.7392	0.1327 - 0.1864i
0.7854	-0.0854 - 0.0903i
0.8378	-0.2526 + 0.0824i
0.8976	-0.2605 + 0.2838i
0.9666	-0.0725 + 0.3160i
1.0472	0.0524 + 0.1229i
1.1424	0.0491 - 0.0246i
1.2566	0.0235 - 0.0319i
1.3963	-0.0092 - 0.0011i
1.5708	-0.0024 - 0.0032i

4. PREDICTION OF DESIGN LOADS FOR DEEP WATER SUBSEA LIFTING OPERATIONS BASED ON NON-STATIONARY TIME RESPONSE

The original version of this paper has been published in Marine Structures (v. 74, n. 102818, 2020) by R. B. Tommasini, R. Pavanello and L. O. Carvalho [159] addressing the objective n. 2 of this thesis (as per Section 1.2.3). This study discusses the determination of the extreme loads in subsea lifting operations modelled by using a variable length cable assumption, such as presented in Chapter 3. In this case, the response of the system under stochastic excitation is non-stationary and specific techniques are required to estimate the design loads. The following study presents two methodologies to deal with this problem.

Abstract

Two methodologies for the prediction of the design loads of deep water subsea lifting operations crossing resonance zones are presented. These methodologies are applicable to models that consider the influence of the payout speed on the dynamics of the operation, leading to a non-stationary time series for the dynamic forces on the system. The first model is based on running several random simulations of the same scenario and using these simulations as a sample in which statistical parameters are inferred. The second model uses a weighted least squares approach to predict a normalizing function that is used to evaluate the statistical parameters of the response. Both models are tested by considering the installation of a typical manifold in the Pre-Salt fields, in Brazil, and are able to predict the general form of the envelope of forces on the cable for various sea states and payout speeds. The models also provided similar results for the availability of the vessel after evaluating the weather window for this operation. Finally, the advantages of using the weighted least squares approach in comparison to the direct method are discussed, since it may considerably reduce the total number of simulations required to perform a real operation assessment, especially during preliminary design phases.

Nomenclature

A_p	Vertical projected area of the equipment
C_a	Added mass coefficient of the equipment
C_d	Drag coefficient of the equipment
EA	Axial rigidity of the cable
D	Axial dynamic force on the cable
F	Axial force on the cable
g	Gravity acceleration
H_s	Significant wave height
h	Vertical displacement of the vessel at the lifting point
k	Number of times steps
L	Suspended length of the cable
L_0	Initial suspended length of the cable
M	Mass of the equipment
m	Linear mass of the cable
m_s	Equivalent submerged linear mass of the cable
N	Normal probability distribution function
n	Number of occurrences of a random process
w	Displacement of the equipment
w_0	Displacement boundary condition on the top of the cable
S	Axial static force on the cable
SWL	Safe Working Load
T_p	Peak period of the wave
T_z	Mean zero up crossing period of the wave
t	Time
V	Volume of the equipment
V_c	Payout speed
α	Ratio for the position of the cable
β	Coefficients of the normalizing function
σ_D	Standard deviation of the dynamic force on the cable
σ_ψ	Standard deviation of the normalized dynamic force on the cable
λ	Weighting function
η	Number of cycles of the dynamic forces
ρ	Density of the sea water

ψ Normalized dynamic force on the cable

Φ Constant value

ϕ Normalizing function

4.1 Introduction

Subsea lifting operations are among the most expensive activities required to develop an offshore oil and gas field. Further, emerging technologies such as the exploration of offshore renewable energy and deep sea mining also require the installation of equipment on the seafloor. Therefore, much effort has been made by the industry and the academy to reduce the global costs of these operations in order to achieve profitable offshore exploration systems.

The beginning of the study of subsea lifting operations trace back to the 1960's, when a report considering the dynamics of underwater ship-suspended loads was published [67]. After this pioneer study and following the increase on the water depth of the offshore oil fields, many studies have been conducted discussing the dynamics of subsea lifts. A highly influential paper was published by Niedzwecki and Thampi [71] which provided means to predict the possibility of slack conditions on the cable based on a simple and effective model. Many other models were also presented by several authors dealing with different features of this problem, such as the presence of snap loads in submerged cables [76,160–162], the dynamics of the system at the wave zone [58,65,144,163,164] and at deep water [93,96,165], the use of passive or active heave compensation systems [78,79,106], and the determination of hydrodynamic coefficients for subsea structures [124,125,132]. Much of this work have been grouped in the recommended practice DNV-RP-H103 [146], which is currently used as the technical basis for the analysis of subsea lifting operations.

In the last years, other different approaches to reduce the cost or even enable otherwise unviable operations has been considered, such as the development of new subsea lift methods. The pendulous installation method provided means to install heavy equipment at ultra-deep water fields without the need of specialized crane vessels [14,166]. Many authors presented technologies based on a wet tow of the equipment by means of a floating structure in order to uncouple the motions of the vessel and the motion of the equipment to be installed [15,18]. Other recurrent approach considered is the use of synthetic cables on the operation [10,81,167], reducing the maximum top tension on the cable and avoiding resonance conditions at specific scenarios.

More recently, the installation of structures for offshore energy production has increased considerably, leading to the publication of various studies [23,28,59].

Among the phases of a typical subsea lifting, the lowering into deep water presents several challenges. Depending on the scenario considered, the motion induced by the ocean waves may lead to a resonance regime, causing high dynamic forces on the system. Another difficulty is the increase in the suspended weight of the cable as the water depth increases, reducing the available load capacity of the crane. In order to perform a safe and cost effective operation, all these features should be previously addressed in a detailed engineering analysis. A common methodology used by the industry to evaluate this phase is to perform several simulations considering the equipment positioned at fixed depths, ranging from sea surface to seafloor in several steps [146]. In this way, it is possible to evaluate the impact of the increase of the suspended weight of the cable and the zones where resonance effects are preponderant. The assumption that the equipment is positioned at a fixed depth, however, restricts the possibility to evaluate the influence of the payout speed on the dynamics of the system.

Recent developments have enabled the analysts to model the operation considering an arbitrary payout speed for the cable. The commercial software Orcaflex, a traditional tool to simulate offshore operations, introduced in its 10.2 version (released in 2017) the line feeding option, which can be used to model a cable being laid or hauled. Other state of art software, such as SIMO by Marintek, aNySIM by Marin, and ANSYS AQWA, are also suitable to analyse transient offshore lifting operations. Further, a study conducted by Tommasini *et al.* [137] presented a one degree of freedom model that was able to deal with a variable length cable. In this study, the authors also showed that the payout speed has several impacts on the dynamics of the systems and its consideration during the planning phase of the operation could lead to safer and cost optimized operations.

A typical feature of variable length models is the generation of non-stationary time series for the forces on the system. Due to the variation of the suspended length of the cable as time progresses, the suspended weight of the cable and the resonance period of the system increases. This phenomena lead to a signal that has a variable mean and standard deviation as a function of time (or the depth of the equipment, since they are related by the payout speed), as presented in Figure 4.1. Due to this behaviour, the determination of the design loads to be compared against the limiting criteria of the system is more challenging.

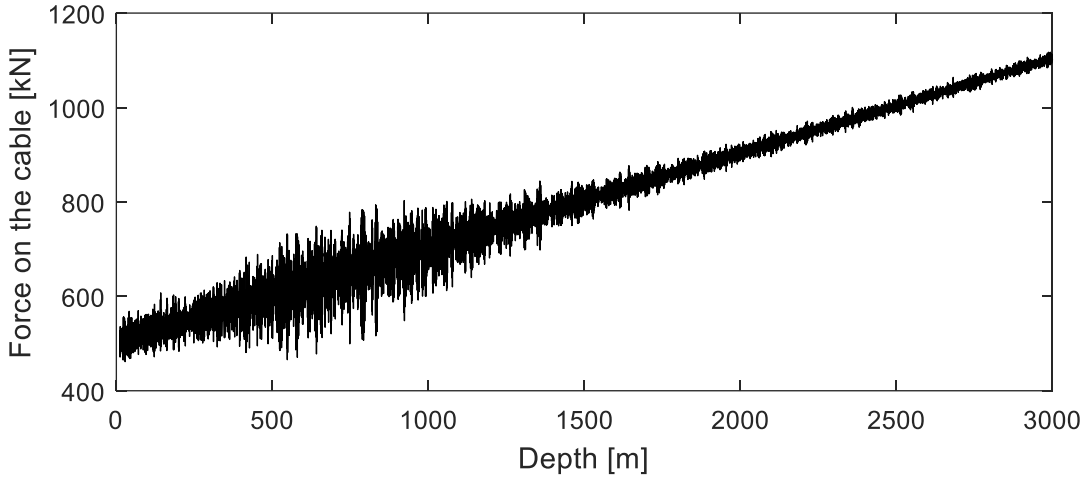

Figure 4.1: Typical signal for the tension on the cable as a function of depth for a variable length model.

In a traditional analysis, where the equipment is considered fixed at constant depths, the design forces on the cable may be estimated considering that the amplitude of the tension follows a Rayleigh distribution. Then, the extreme values for the tension may be obtained considering, for example, the most probable largest value of the series [146]. This procedure is possible because the time signal obtained is stationary, which means that it has a constant mean and variance. For the scenario of a variable length model, this approach is not possible due to the variation of the statistics of the signal with the depth.

The typical methodology considered for the non-stationary case is to run several simulations and obtain the statistical description of the random variable at each time instant; or to find a way to eliminate the trend of the signal by a variable transformation or by fitting a regression model [168]. These procedures are common in statistical modelling, and are typically used to model climate changes for example [169–171]. Regarding marine operations, several studies have been published dealing with the dynamics of system and the prediction of the availability of the vessel under non-stationary conditions [60,61,172–178]. Nevertheless, in most of these studies, the non-stationary response is introduced by impact loads, such as the slamming conditions when the equipment is lifted through the wave zone or due to collisions on other structures during the operation. The study of non-stationary behaviour that is introduced by the passage through a resonance zone in deep water subsea lifting operations has not been entirely addressed so far.

Based on this scenario, this work has two main objectives: (1) to present a methodology capable of defining the design loads of a deep water subsea lifting operation obtained by a variable

length model that generates a non-stationary time signal due to the passage through a resonance zone; and (2) to evaluate the effectiveness and the impacts of this methodology on typical deep water subsea lifting scenarios. Additionally, the focus of the study is on the deep water lifting phase; the lifting through the wave zone and the landing on the seabed phases are not covered in this paper.

To this end, two different techniques are presented here. The first one is based on running several random simulations for the same scenario and to predict the design forces at each time step via a parameter estimation made from the samples produced. The second one focuses on eliminating the trend of the time response by means of a normalizing function. This function is obtained after solving a weighted least squares constrained optimization problem. Both models are then tested for a typical scenario of the Pre-Salt fields in Brazil.

4.2 Variable length cable-equipment model

The model considered to generate the dynamic response of the system may be any one that is capable of treating the length of the cable as variable throughout time. In this work, a one degree of freedom model, as presented by Tommasini *et al* [137] is selected because it proved to be coherent with more complex models, such as those used by Orcaflex, for typical deep water subsea lifting scenarios [179].

The assumptions considered to construct this model are: (1) the system has one degree of freedom, which is the vertical displacement of the equipment (w); (2) the vessel and the cable-equipment system are dynamically uncoupled; (3) the length of the cable is variable; and (4) the hydrodynamic forces act only on the equipment and are modelled by Morison's equation [118]. The representation of this model is presented in Figure 4.2. The equation of motion for this system is given by:

$$\left(M + \rho V C_a + \frac{1}{3}mL\right)\ddot{w} + \left(\frac{m\dot{L}}{3} + \frac{1}{2}\rho C_d A_p |\dot{w}|\right)\dot{w} + \frac{EA}{L}w = -\frac{m_s g L}{2} - (M - \rho V)g + \frac{EA}{L}w_0 - \frac{m\dot{L}}{6}\dot{w}_0 - \frac{mL}{6}\ddot{w}_0 \tag{4.1}$$

where M, V, A_p are respectively the mass, volume and projected area of the payload; C_a and C_d are the added mass and drag coefficients; m, m_s, EA, L are respectively the mass per unit length, the equivalent submerged mass per unit length, the rigidity and the length of the cable; ρ is the density of the water and g is the gravity acceleration.

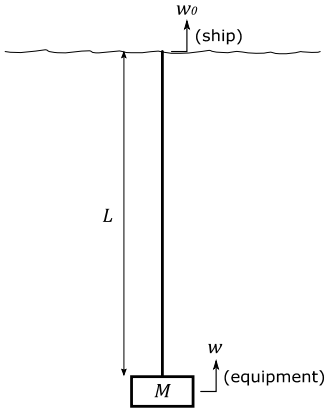

Figure 4.2: Representation of the one degree of freedom model for the evaluation of the deep water subsea lifting operations.

The prescribed motion on the top of the cable is set as the boundary condition for this equation, which, in this case, is given by a function h that specifies the vertical displacement of the lifting point, and by the integral of the payout speed V_c, which is considered positive for hauling and negative for laying conditions, as shown in Eq. (4.2). In this study, the displacement of the lifting point is given by the product of the displacement RAO of the vessel and a JONSWAP spectrum fitted for the Santos Basin, Brazil.

$$w_0 = h + \int V_c dt \tag{4.2}$$

It is also necessary to specify the equation for the variation of the cable length as a function of time:

$$L = L_0 - \int V_c dt \tag{4.3}$$

The suspended length of the cable L is equivalent to the current depth of the equipment, so these variables will be used as synonymous throughout this study. Finally, the force on a specific point of the cable is given by:

$$F(L) = \frac{EA}{L}[w_0 - w] + \frac{m_s g L[2\alpha - 1]}{2} \tag{4.4}$$

In this case, $0 \leq \alpha \leq 1$ is a ratio that defines the position of the cable which is being evaluated ($\alpha = 0$ represents the lower end of the cable, and $\alpha = 1$ represents the upper end of the cable). Eq. (4.1) is solved in the time domain via a Newmark-β algorithm, leading to a time signal for the displacement of the equipment. Eq. (4.4) is then used to obtain the time signal for the forces on the cable, which is going to be the basis for the subsequent analyses.

4.3 Determination of the design loads from non-stationary series

It is historically recognized that the ocean surface elevation constitutes a random process [180]. This characteristic introduces randomness on all structural response of systems that are excited by the ocean waves, including on the dynamics of cable-equipment systems during subsea lifting operations. However, even though the ocean surface elevation may be classified as a stationary random process for some period, the forces on the cable will suffer from other effects that lead to a non-stationary response.

As introduced previously, as time progresses during a subsea lifting operation, the suspended length of the cable varies. Consequently, two main effects are noticeable: (1) the variation of the suspended weight of cable, and (2) the variation of the fundamental resonance period of the cable-equipment system. These two behaviours are responsible to introduce the non-stationarity on the dynamic response of the cable.

In order to separate the influence of each of these behaviours, Equation (4.4) may be split in two separate terms:

$$F(L) = S(L) + D(L) \tag{4.5}$$

The first term is the static force (S) acting on the cable, given by the submerged weight of the system and a drag force generated by the payout speed; the second term is the dynamic force (D), which is generated by the axial vibration of the cable-equipment system. It is also important to mention that, in the sequence of this study, the suspended length of the cable (or the depth of the equipment) will be used as the independent variable, since the suspended length introduces the non-stationarity in the system, not the time.

The static force is known previously, because it depends only on given data, such as the payout speed prescribed for the operation. So, it may be written as:

$$S(L) = [M - \rho V]g + m_s g L\alpha + \frac{1}{2}\rho C_d A_p \left|\dot{V}_c\right| V_c \tag{4.6}$$

This force is responsible only to represent the linear trend on the mean response of the cable, as represented in Figure 4.1. On the other hand, the dynamic force is a random variable with null mean[5] and non-constant variance that is not known a priori. Consequently, its modelling

[5] The mean force on the system might be different from zero in some scenarios due to nonlinear dynamic effects. In this study, this effect is considered negligible in comparison to the variation of the standard deviation throughout the depth when the payload crosses the fundamental resonance zone.

needs a different treatment. In this work, two approaches are considered and presented in the next sections.

4.3.1 Evaluation of the dynamic forces via a direct approach

The direct approach consists in obtaining the statistics of the dynamic force via parameter estimation from a sample of n random occurrences. In this case, each of the j-th occurrence is considered to be independent and represents the same scenario: combination of the type of equipment, cable, vessel, and environmental conditions. The generation of each of the n random occurrences is done by considering random phases for the harmonic components of the ocean waves, as detailed by Chakrabarti [180] in chapter 4.7. More details regarding similar approach to calculate statistics of offshore operations may be found in [181].

Since the mean of the dynamic force is null, only its standard deviation needs to be obtained:

$$\sigma_D(L) = \sqrt{\sum_{j=1}^{n}\left[\frac{D_j^2(L)}{n-1}\right]} \tag{4.7}$$

where $D_j(L)$ represents the dynamic force on the cable for j-th occurrence. Also, because the values of $D_j(L)$ at each depth are considered independent random variables, some random variability will also be present in the standard deviation, resulting in a noisy signal. In order to obtain a smoother representation, a moving mean procedure is applied on $\sigma_D(L)$.

After obtaining the representation of the standard deviation of the dynamic force as a function of the depth, it is necessary to estimate the maximum forces on the cable in order to compare it against the structural limits of the system. According to Chakrabarti [180], the surface elevation and the amplitude of the ocean waves in a narrow-band spectrum is verified to follow, respectively, a Gaussian and a Rayleigh distribution. Considering that the only source of randomness in the system is the ocean waves, it is assumed that the response of the system keeps a similar distribution after eliminating the non-stationarity. Therefore, the amplitude of $D(L)/\sigma_D(L)$ is supposed to follow a Rayleigh distribution. Then, the maximum force on the cable is obtained by the most probable largest value for the dynamic load:

$$D_{max}(L) = \sigma_D(L)\sqrt{2\ln(\eta)} \tag{4.8}$$

where η is the number of cycles of the dynamic force during the operation, which is considered

to be:

$$\eta = \frac{L_{max}}{T_z V_c} \tag{4.9}$$

where L_{max} is the final length of the cable during the operation and T_z is the mean zero up crossing wave period. Consequently, the maximum and minimum forces on the cable as a function of the depth will be given by:

$$F_{max}(L) = S(L) + \sigma_D(L)\sqrt{2\ln(\eta)} \tag{4.10}$$

$$F_{min}(L) = S(L) - \sigma_D(L)\sqrt{2\ln(\eta)} \tag{4.11}$$

The values of $F_{max}(L)$ and $F_{min}(L)$ may be seen as the envelope of the forces on the cable as a function of the depth of the equipment during the operation. These values should be compared against the acceptance criteria prescribed in DNV-RP-H103: the maximum forces should be lower than the safe working load (SWL) of the system, and the minimum forces should be higher than 10% the static force. So, the algorithm to construct the weather window of a given subsea lifting operation using the direct approach is presented in Table 4.1.

Table 4.1: Algorithm to evaluate a deep water subsea lifting operation via the direct approach.

1. Set the data for the operation (type of equipment, cable, and vessel);
2. For each sea state (significant height and peak period):
    a. For each of the n cases, calculate:
        i. The motion of the equipment over the time according to Equation (4.1);
        ii. The forces on the cable over the time according to Equation (4.4);
    b. Calculate the static force according to Equation (4.6);
    c. Calculate the dynamic force according to Equation (4.5);
    d. Calculate the standard deviation of the dynamic force according to Equation (4.7);
    e. Calculate the maximum and minimum forces according to Equations (4.10) and (4.11);
    f. Check the acceptance criteria ($F_{max} \leq SWL$, and $F_{min} \geq 0.1S$):
        i. If both criteria are fulfilled, the sea state is acceptable;
        ii. Otherwise, the sea state is unacceptable;
3. Build the operational weather window with the acceptable sea states.

4.3.2 Evaluation of the dynamic forces via a weighted least squares estimation

A common methodology used to deal with time series of non-constant variance is to use trend decomposition via a regression model [168]. So, it is assumed that the dynamic force on the cable is given by a random variable (ψ) multiplied by a normalizing function (ϕ) that depends on the depth ($\phi = \phi(L)$):

$$D(L) = \phi(L)\psi \tag{4.12}$$

In this case, ψ is assumed to be stationary and normally distributed, such that $\psi \sim N\left(0, \sigma_{\psi}^2\right)$; and $\phi(L)$ is a normalizing function that transforms the non-stationary signal $D(L)$ into a stationary one. The assumption that ψ is normally distributed relies once again on the fact the only source of randomness in the system is the ocean waves, and that the response of the system keeps a similar distribution of the waves after eliminating the non-stationarity.

Since the idea of the normalizing function is only to eliminate the variation with the cable length on the standard deviation of the dynamic force, we may assume that $\phi(L)$ is always greater than one without any loss of generality. In this way, the normalizing function will always increase the random variable ψ. A typical function that follows this requirement, and which is recurrently used in this kind of procedure [168,169,182], is:

$$\phi(L) = 1 + \exp(\beta_0 + \beta_1 L + \beta_2 L^2) \tag{4.13}$$

The selection of this expression also relies on its flexibility to represent different scenarios of amplification of the dynamic force depending on the coefficients selected. Some possible forms of this function are presented in Figure 4.3, which illustrate scenarios of shallow-water, mid-water, and deep-water resonances. Important to remark here that this function is not able to represent multiple peaks of the dynamic force throughout the depth, a limitation of the method presented.

The problem, then, consists in determining the coefficients β_1, β_2, and β_3 that leads to the correct representation of the resonance region. This may be achieved by minimizing the sum of all the time steps of the squared quotient $D(L)/\phi(L)$. In this way, the function ϕ tends to present higher values where the value of the dynamic forces are also higher. This optimization problem may be stated in a weighted least squares form as follow:

$$\text{minimize:} \quad \sum_{i=1}^{k} \left[\lambda(L) \frac{D(L)}{\phi(L)} \right]^2 \tag{4.14}$$

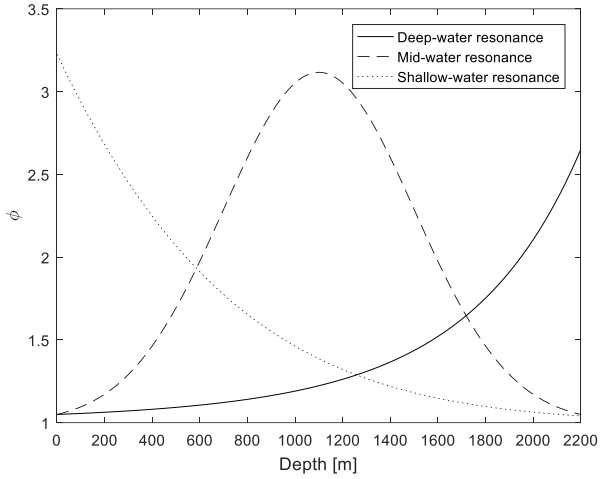

Figure 4.3: Different forms of the normalizing function representing various resonance conditions.

where k is the number of time steps used to obtain the solution of Equation (4.1), and $\lambda(L)$ is a weighting function. As the interest of this methodology is to represent the resonance area, the weighting function is considered to be equal to the dynamic forces: $\lambda = D$; therefore, higher weight is given at the zones of higher forces.

Further, since the normalizing function appears in the denominator of the quotient, this optimization would lead to an arbitrarily high value for the coefficients β, forcing the minimized function to go to zero. This is not the objective of this procedure, since this resulting normalizing function would not be able to eliminate the non-stationarity from the dynamic force.

A possible procedure to overcome this difficulty is to introduce some constrain to this minimization problem. In this case, restricting the area of the normalizing function would lead to a valid solution. So, the optimization problem becomes:

$$\begin{aligned} &\text{minimize:} \quad \sum_{i=1}^{k} \left[\frac{D^2(L)}{\phi(L)} \right]^2 \\ &\text{subject to:} \quad \int \phi(L) dL = \Phi \end{aligned} \tag{4.15}$$

where Φ is a constant value. This problem may be solved by any constrained optimization technique. In this work, it was chosen to use the interior point algorithm [183] due to its reliability. Further, in order to ease the convergence of the algorithm, the variables D and L are

scaled as follows:

$$\bar{L} = \frac{L}{\max(L)} \tag{4.16}$$

$$\bar{D} = \frac{D}{\max(|D|)} \tag{4.17}$$

In this way, $0 \leq \bar{L} \leq 1$ and $-1 \leq \bar{D} \leq 1$. Considering this scaling, an effective value for the area restriction is $\Phi = 2$, which leads to an unitary area for the exponential part of the normalizing function.

After the solution of this minimization problem, it is possible to calculate the standard deviation of the stationary random variable ψ by:

$$\sigma_{\psi} = \max(D) \sqrt{\frac{1}{k-1} \sum_{i=1}^{k} \left[\frac{\bar{D}(\bar{L})}{\phi(\bar{L})}\right]^2} \tag{4.18}$$

Similarly, as presented in the direct approach, the amplitude of the random variable ψ is assumed to follow a Rayleigh distribution, and the design loads are obtained by its most probable largest value. In this particular case, since the dynamic force is given by the product of $\phi(L)$ and ψ, the maximum dynamic forces must be written as:

$$D_{max}(L) = \phi(L)\sigma_{\psi}\sqrt{2\ln(\eta)} \tag{4.19}$$

Consequently, the maximum and minimum forces on the cable may be estimated by:

$$F_{max}(L) = S(L) + \phi(L)\sigma_{\psi}\sqrt{2\ln(\eta)} \tag{4.20}$$

$$F_{min}(L) = S(L) - \phi(L)\sigma_{\psi}\sqrt{2\ln(\eta)} \tag{4.21}$$

Finally, the algorithm considered to calculate the operational weather window using the weighted least square estimation for the design loads is presented in Table 4.2.

Table 4.2: Algorithm to evaluate a deep water subsea lifting operation via the weighted least square estimation.

1. Set the data for the operation (type of equipment, cable, and vessel);
2. For each sea state (significant height and peak period), calculate:
    a. The motion of the equipment over the time according to Equation (4.1);
    b. The forces on the cable over the time according to Equation (4.4);
    c. The static force according to Equation (4.6);
    d. The dynamic force according to Equation (4.5);
    e. Scale the variables according to Equations (4.16) and (4.17);
    f. Solve the optimization problem according to Equation (4.15) and obtain β_1, β_2, and β_3;
    g. Build the normalizing function according to Equation (4.13);
    h. Calculate the standard deviation of the stationary random variable ψ according to Equation (4.18);
    i. Calculate the maximum and minimum forces according to Equations (4.20) and (4.21);
    j. Check the acceptance criteria ($F_{max} \leq SWL$, and $F_{min} \geq 0.1S$):
        i. If both criteria are fulfilled, the sea state is acceptable;
        ii. Otherwise, the sea state is unacceptable;
3. Build the operational weather window with the acceptable sea states.

4.4 Numerical results and discussion

In order to test the methodologies presented in this study, the installation of a typical WAG (Water Alternating Gas) Manifold used in the Pre-Salt fields is selected as the example scenario. The cable considered in the analysis is a multi-strand compact construction rope of six inches of diameter. The vessel responsible for the lifting operation is a PLSV (Pipe Laying and Support Vessel) that has a high capacity crane and A&R (Abandonment and Recover) winch to perform the installation or recovery of the equipment. Most of the Pre-Salt fields in Brazil are located at Santos Basin. At this location, nearly 80% of the sea states are within 5 to 13 s peak period (T_p) and 1.0 to 3.0 m of significant height (H_s); also, the typical water depth is 2200 m. So, the data considered for the vessel, the equipment, the cable, and the environmental conditions for this scenario are presented in Table 4.3. Furthermore, the vertical displacement RAO of the vessel at the lifting point is presented in Annex A.

Table 4.3: Input data for the evaluation of the methodologies presented in this study.

	Parameter	Value
Vessel (PLSV)	Length overall	145.9 m
	Breadth moulded	29.9 m
	Max displacement	27012 ton
Cable (Multi-strand – 6in)	Linear mass (m)	111 kg/m
	Subsea equivalent linear mass (m_s)	98 kg/m
	Axial rigidity (EA)	1220 MN
	Safe Working Load (SWL)	5900 kN
Equipment (WAG manifold)	Mass (M)	190 ton
	Volume (V)	24 m^3
	Area (A_p)	147 m^2
	Added mass coefficient (C_a)	73.1
	Drag coefficient (C_d)	4
Environmental conditions	Peak period (T_p)	5 to 13 s
	Significant wave height (H_s)	1.0 to 3.0 m
	Water depth	2200 m
Newmark-β method	Time step	0.1 s

4.4.1 Verification tests for the direct method

The first analysis aims to verify the adequacy of the direct approach to estimate the design loads on the cable for this specific scenario. To this end, it is necessary, first of all, to evaluate how many simulations are necessary to obtain a converged solution for the statistics of the forces on the cable. The mean value of the force on the top of the cable at the beginning of the simulation is selected as the control parameter. In this case, since the mean value of the dynamic force is null, the mean value of the force on the cable should tend to the value of the static force, which is known a priori. The minimum number of simulations required for the mean force to become bounded by the limiting lines of $S \pm 1\%$ is selected as the convergence criterion. These results are presented in Figure 4.4, which shows that the convergence is achieved after 300 simulations for the scenarios considered. It is also remarkable that the convergence is faster for low excitation periods and do not depend on the payout speed in this case.

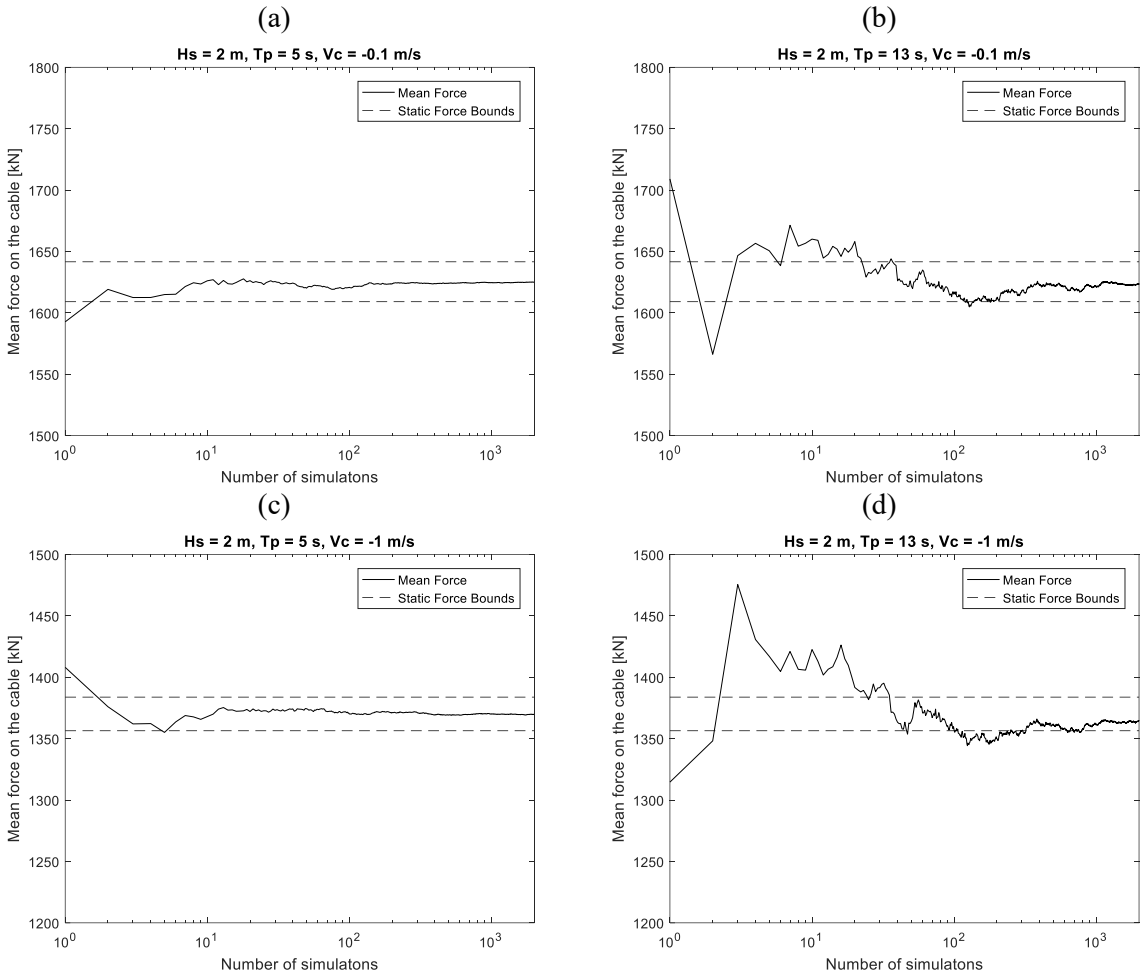

Figure 4.4: Convergence tests of the direct method. The scenario for these tests considered the forces on the top of the cable at the beginning of the simulation for $H_s = 2$ m and (a) $V_c = -0.1$ m/s and $T_p = 5$ s; (b) $V_c = -0.1$ m/s and $T_p = 13$ s; (c) $V_c = -1$ m/s and $T_p = 5$ s; and (d) $V_c = -1$ m/s and $T_p = 13$ s.

Illustratively, the convergence of the envelope of the force on the cable is presented in Figure 4.5 for the scenario of $H_s = 2$ m, $T_p = 13$ s, and $V_c = -1$ m/s, which is the slowest convergence one. This figure shows that the envelope produced by using a reduced value of n is somehow similar to that obtained after convergence is achieved, but presents a noisy behaviour that is reduced as n increases.

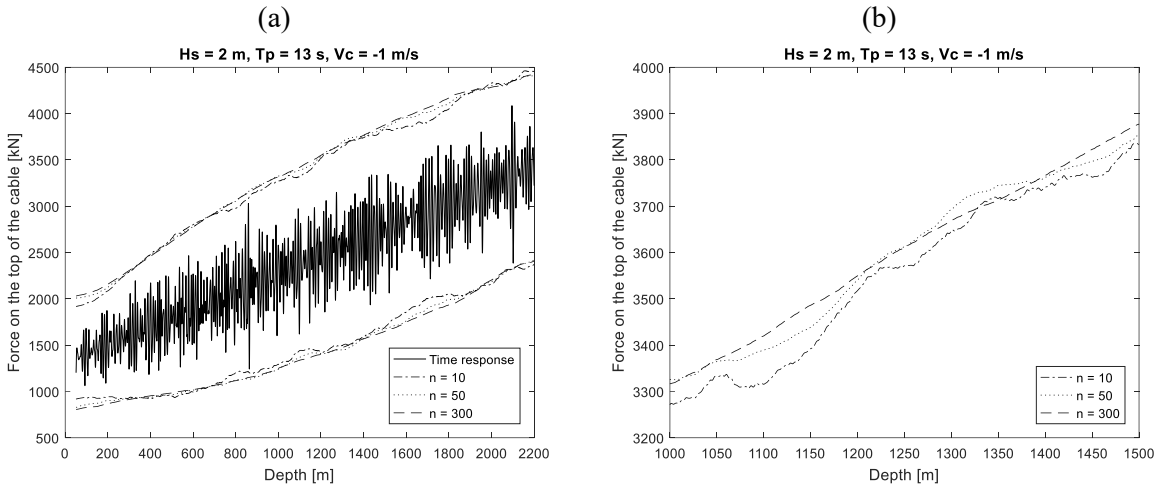

Figure 4.5: Convergence of the envelope of forces on the top of the cable obtained via the direct method for the scenario of $H_s = 2$ m, $T_p = 13$ s, and $V_c = -1$ m/s. (a) Graph of the envelope and a time response for this scenario; (b) zoom of the previous graph.

The next analysis is intended to verify the capacity of the direct method to predict the envelope of forces on the cable using the moving mean procedure. For this case, $V_c = -1$ m/s, $H_s = 2$ m, and $T_p = 5$ s are considered. Figure 4.6a presents the envelope of the forces and one of the time responses for the force on the cable obtained during the analysis. It is possible to see that the maximum and minimum forces encompass the time response and describes the amplification region at the depths of nearly 500 m. Further, Figure 4.6b provides a zoom at this location showing the maximum force on the cable with and without the moving mean procedure. The usage of the moving mean technique avoids the oscillation on the force without compromising the accuracy of the solution. Therefore, next results regarding the direct method will always consider the smoothing via the moving mean.

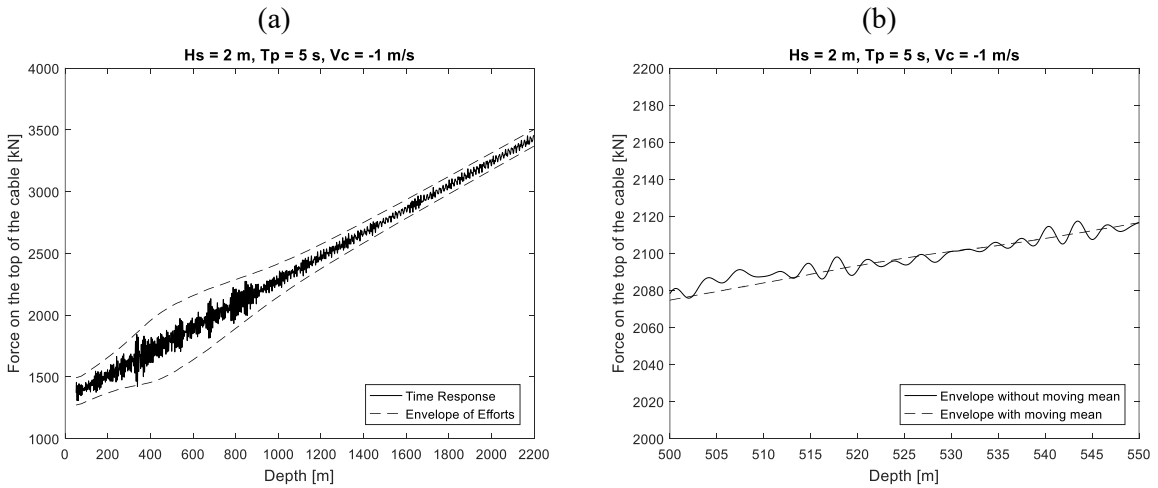

Figure 4.6: Envelope of forces on the top of the cable obtained via the direct method for the scenario of $H_s = 2$ m, $T_p = 5$ s, and $V_c = -1$ m/s. (a) Envelope and a time response for this scenario; (b) zoom of the previous graph showing how the moving mean procedure makes the envelop smoother.

Finally, it is verified the assumption that the amplitude of D/σ_D follows a Rayleigh distribution. Figure 4.7 shows the probability plot for the Rayleigh distribution for scenarios considering $T_p = 5$ and 13 s, and $V_c = -0.1$ and -1 m/s. In this graph, the variable is well represented by the distribution function if the points plotted in the graph form a straight line. Analysing this figure, one may notice some deviation at the tails of the distribution; however, accurate representation is seen in the greatest part of the plot, especially for high payout speeds.

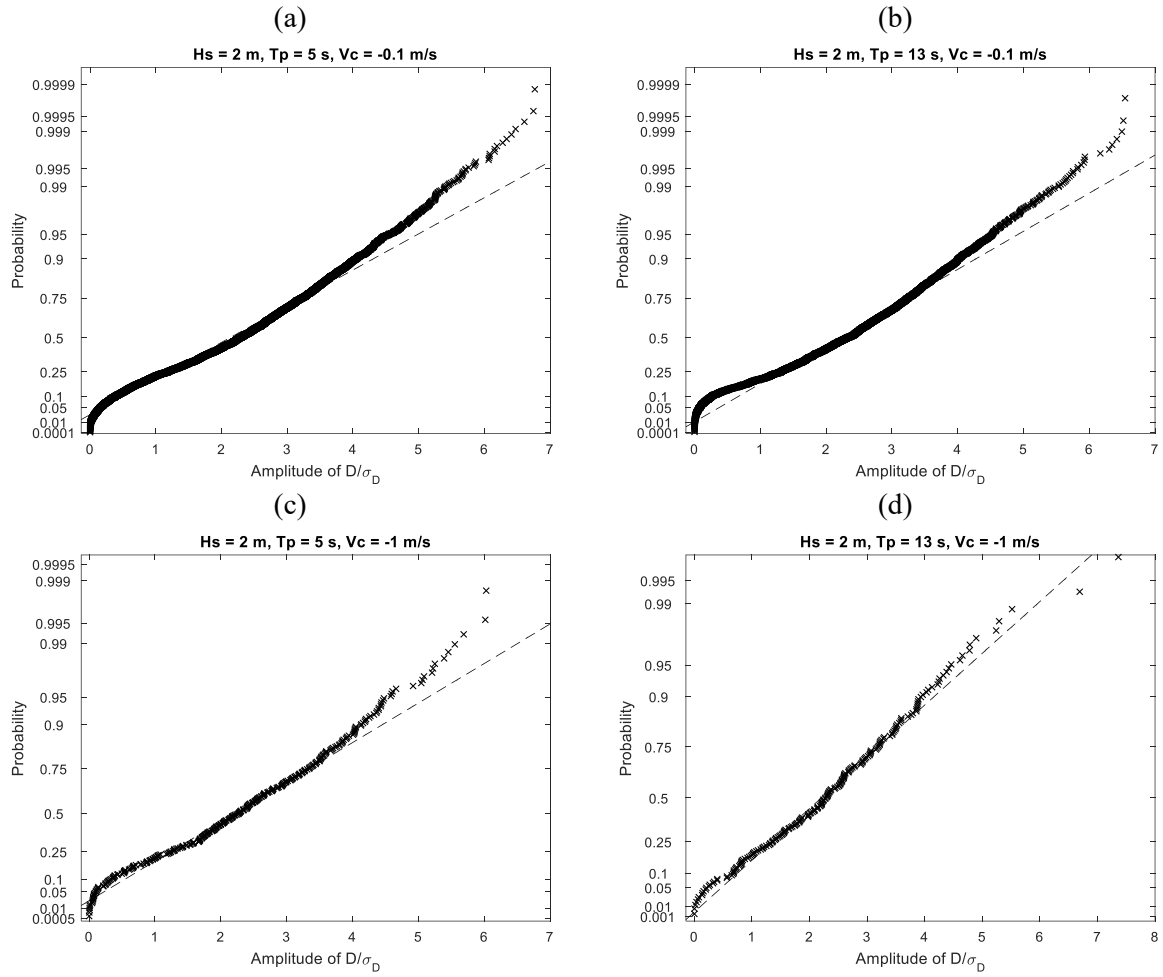

Figure 4.7: Rayleigh probability plot for the amplitude of D/σ_D considering $H_s = 2$ m and (a) $V_c = -0.1$ m/s and $T_p = 5$ s; (b) $V_c = -0.1$ m/s and $T_p = 13$ s; (c) $V_c = -1$ m/s and $T_p = 5$ s; and (d) $V_c = -1$ m/s and $T_p = 13$ s.

Comparatively, the probability plot for other distributions is presented in Figure 4.8 considering the scenario of $T_p = 13$ s and $V_c = -0.1$ m/s. In this case, the Weibull and the Lognormal distributions are used because their data range are only positive values, which is reasonable to model amplitudes. The results obtained show a worse representation in comparison to the Rayleigh distribution. Further, the Weibull and Lognormal probability distributions do not have any

physical justification for their use. Therefore, the assumption that the amplitude of D/σ_D follows a Rayleigh distribution is considered plausible in this study.

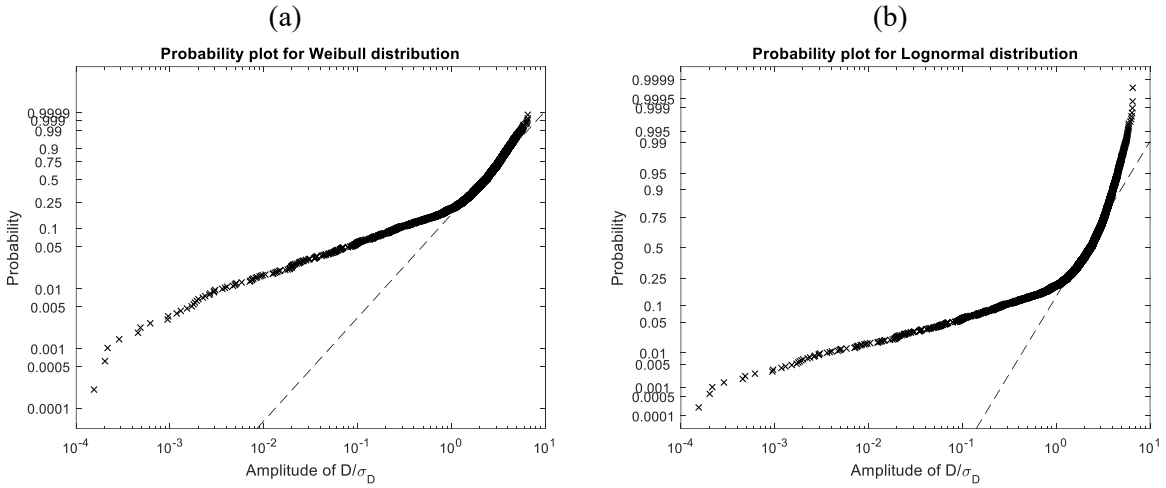

Figure 4.8: Probability plots for the amplitude of D/σ_D considering the scenario of $H_s = 2$ m, $T_p = 5$ s, and $V_c = -1$ m/s. (a) Weibull distribution, and (b) Lognormal distribution.

4.4.2 Verification tests of the least squares method

Following the tests regarding the direct method, it is necessary to verify the adequacy of the weighted least square method to predict the design loads. For this analysis, the method to obtain the envelope of the forces on the cable is presented, and the assumptions considered to construct this method are tested. As a testing scenario, the case of $H_s = 2$ m, $T_p = 8$ s, and $V_c = -0.4$ m/s is selected. The force on the top of the cable as a function of the depth is plotted in Figure 4.9a, and the force on the equipment is plotted in Figure 4.9b. These responses typically represent the non-stationary pattern due to the variation of the cable's length.

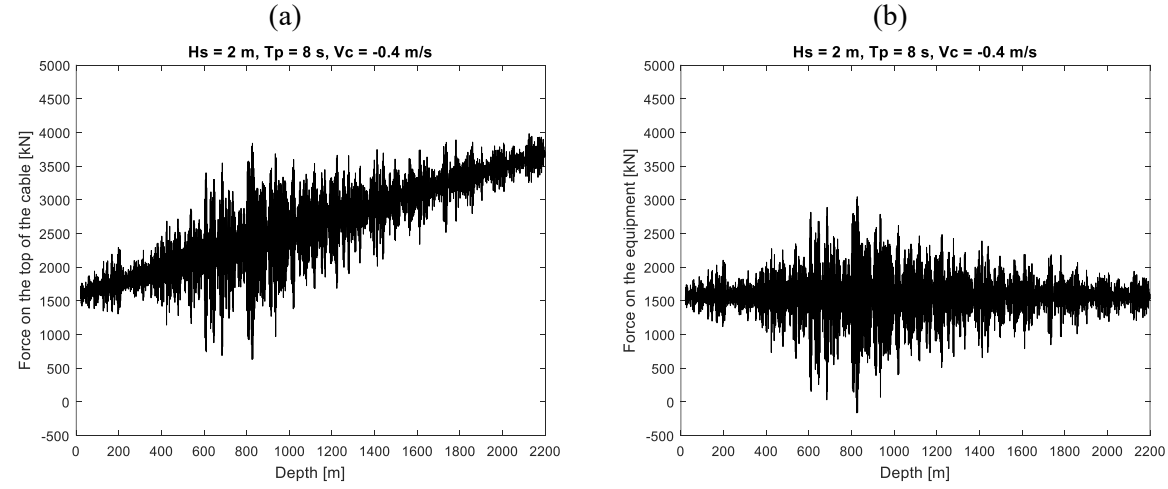

Figure 4.9: Forces on the cable for the scenario of $H_s = 2$ m, $T_p = 8$ s, and $V_c = -0.4$ m/s. (a) Force on the top of the cable, and (b) force on the equipment.

The dynamic force on the cable, obtained via Equation (4.5), is presented in Figure 4.10a. In the sequence, the normalized dynamic force (Figure 4.10b), found after the optimization procedure described in Equation (4.15), is plotted. Visually inspecting these figures, it is possible to see that the normalized dynamic force presents a more stationary behaviour over the depths evaluated in comparison to the untreated dynamic force.

An assumption that was made to build this model was that the normalized dynamic force was normally distributed, so a possible test to verify the adequacy of this procedure is to check if this assumption holds. Figure 4.10c and Figure 4.10d present, respectively, the normal probability plot of the dynamic force and the normalized dynamic force. As expected, a high deviation from normality is presented by the dynamic force (Figure 4.10c), since it is a non-stationary signal. After normalizing this variable, the adequacy to a normal distribution is more plausible (Figure 4.10d), even though some deviation is still observed, especially for

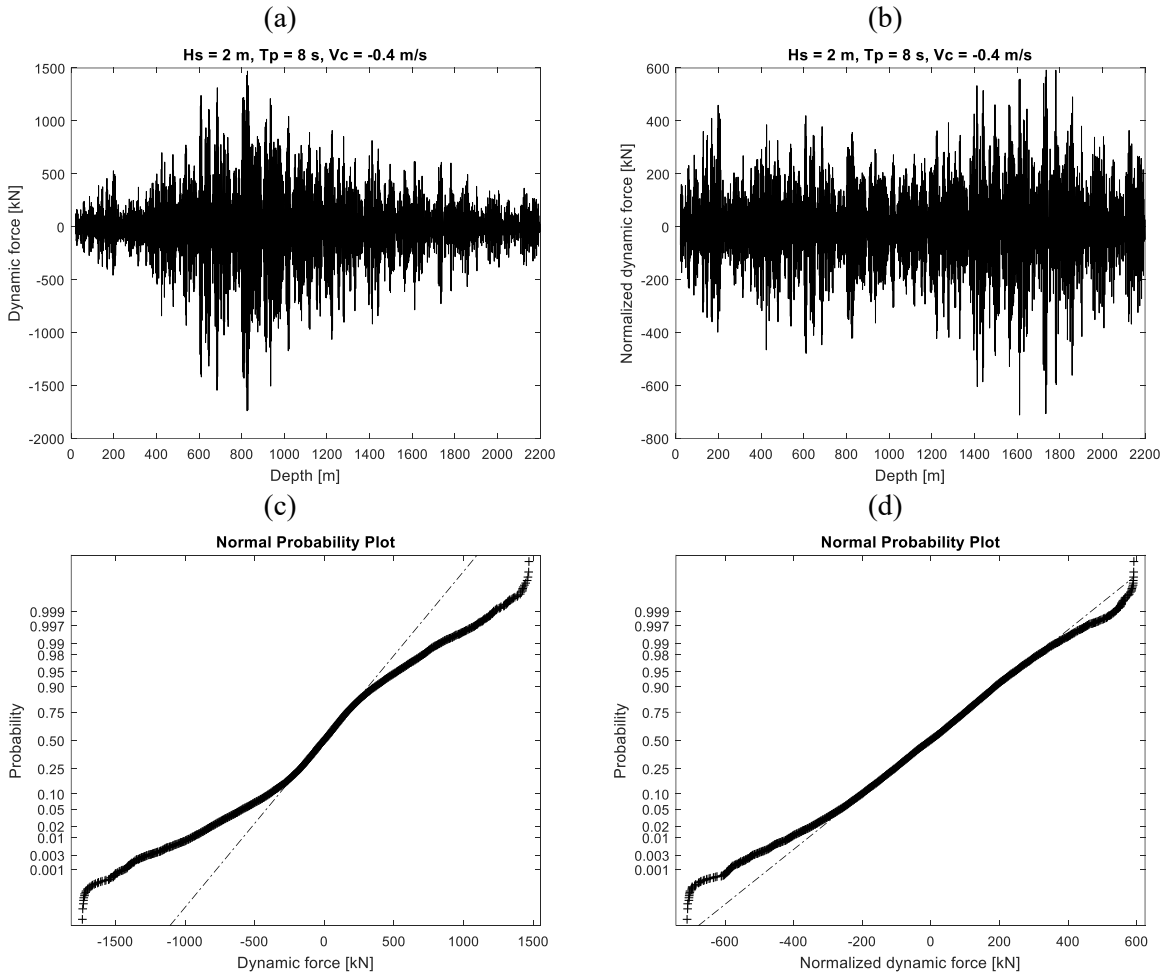

Figure 4.10: Results obtained by the least square method for the scenario of $H_s = 2$ m, $T_p = 8$ s, and $V_c = -0.4$ m/s. (a) Dynamic force; (b) normalized dynamic force; (c) normal probability plot of the dynamic force; and (d) normal probability plot for the normalized dynamic force.

negative values of the variable. Also, this little deviation is expected, since the function selected

to normalize the dynamic force was arbitrary, and does not truly represent the influence of the depth on the dynamic forces for deep water subsea lifting operations.

In the sequence, it is presented in Figure 4.11 the envelope of the forces on the top of the cable (Figure 4.11a) and on the equipment (Figure 4.11b) obtained via the weighted least squares procedure. It is possible to see that the envelope of forces correctly represents the shape of the resonance zone. For this specific scenario, the force on the bottom part of the cable (which is equal to the force on the equipment) is below zero near 900 m depth; so, during the planning phase of a real operation this scenario would not be marked as valid when building the operational weather window.

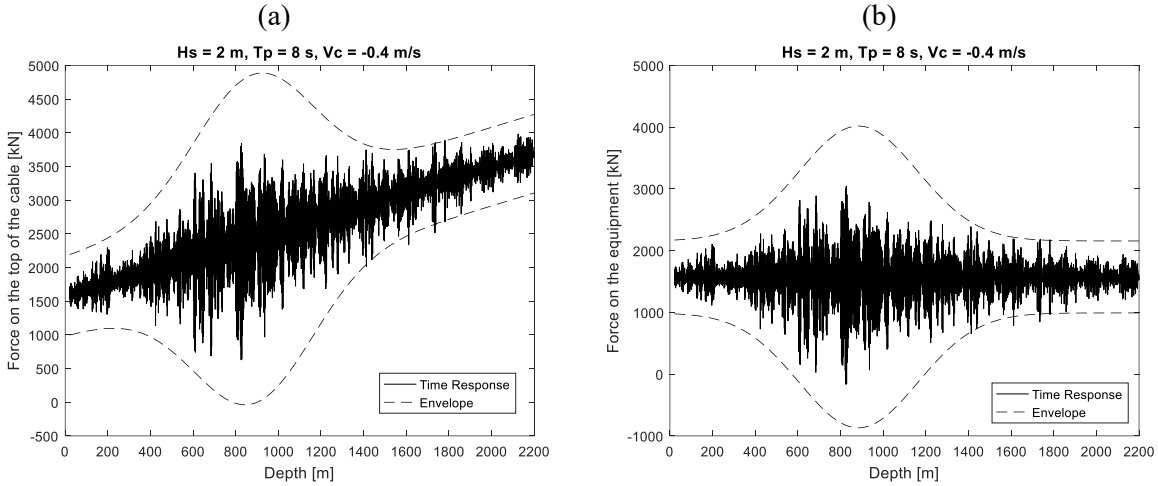

Figure 4.11: Forces on the cable and their envelopes for the scenario of $H_s = 2$ m, $T_p = 8$ s, and $V_c = -0.4$ m/s. (a) Force on the top of the cable, and (b) force on the equipment.

Further, it is necessary to check if the assumptions that the normalized dynamic force follows a Normal distribution and if its amplitude follows a Rayleigh distribution in different scenarios. Figure 4.12 and Figure 4.13 present, respectively, the Normal and the Rayleigh probability plot of ψ and of its amplitude considering the payout speed varying from -0.2 to -1.0 m/s, and the peak period varying from 5 to 13 s. It is again considered the significant wave height of 2.0 m. Analysing these figures, it is possible to assume that the variables are well represented by the distributions considered, confirming the assumptions made in the development of the weighted least squares method.

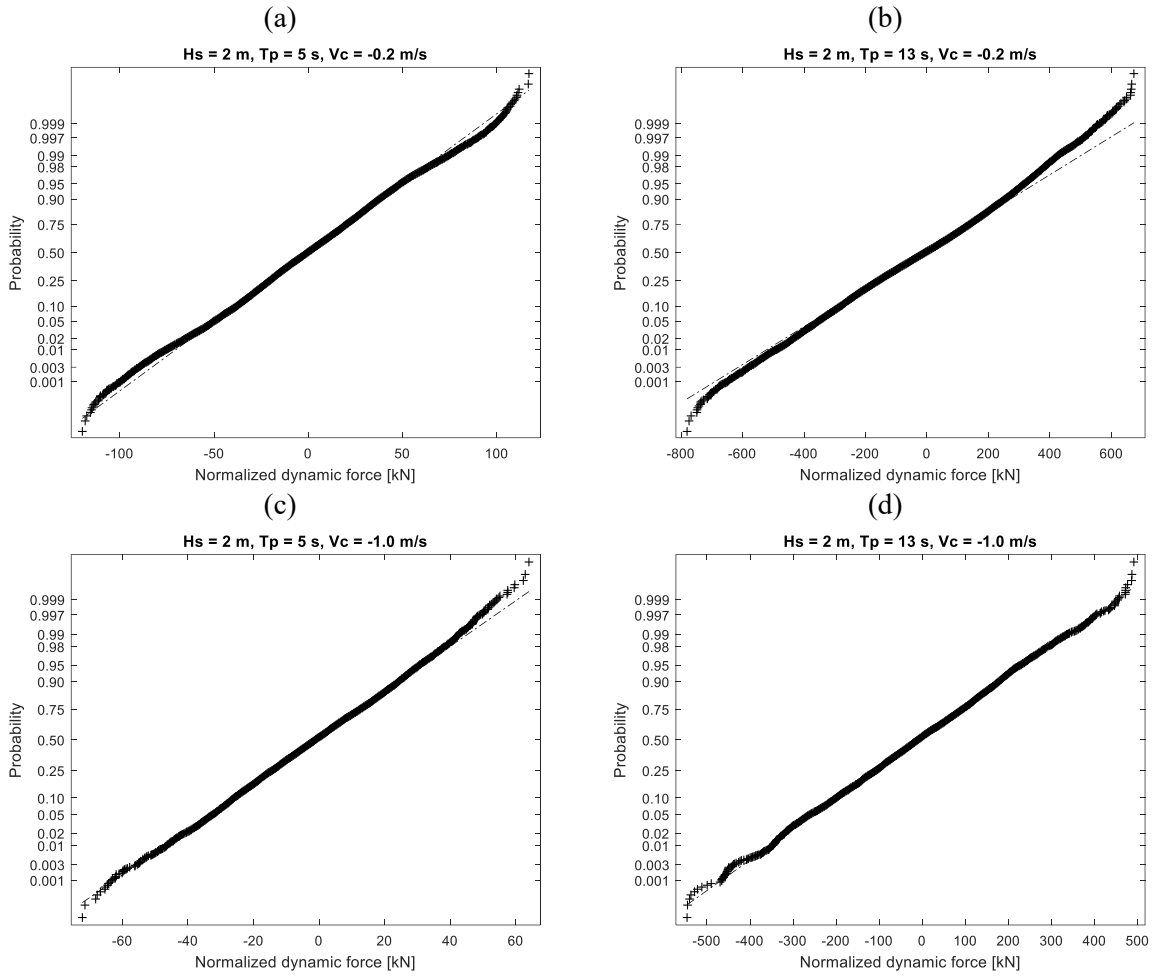

Figure 4.12: Normal probability plot for ψ considering $H_s = 2$ m and (a) $V_c = -0.2$ m/s and $T_p = 5$ s; (b) $V_c = -0.2$ m/s and $T_p = 13$ s; (c) $V_c = -1$ m/s and $T_p = 5$ s; and (d) $V_c = -1$ m/s and $T_p = 13$ s.

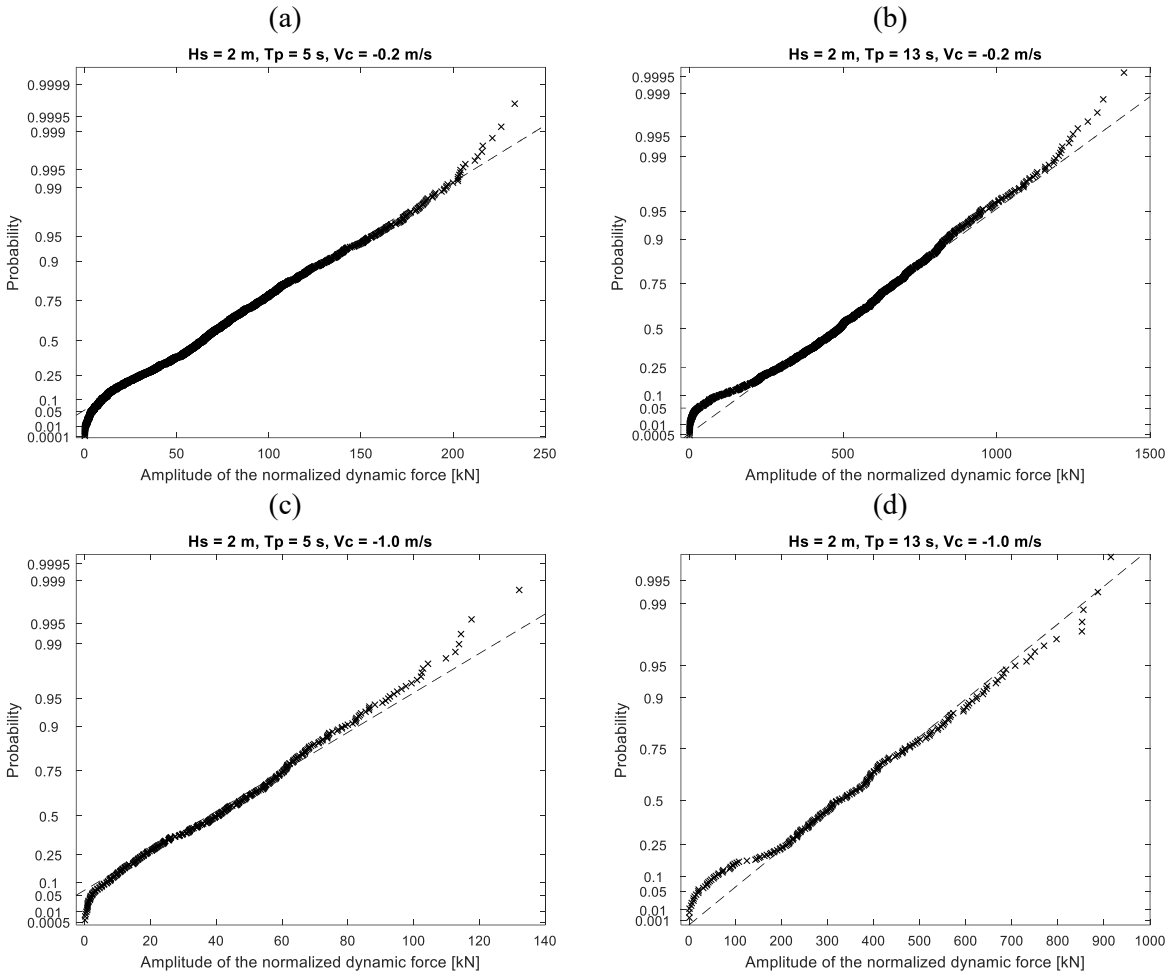

Figure 4.13: Rayleigh probability plot for the amplitude of ψ considering $H_s = 2$ m and (a) $V_c = -0.2$ m/s and $T_p = 5$ s; (b) $V_c = -0.2$ m/s and $T_p = 13\ s$; (c) $V_c = -1$ m/s and $T_p = 5$ s; and (d) $V_c = -1$ m/s and $T_p = 13$ s.

Finally, the influence of a particular wave occurrence in the determination of the envelope of the force by using the weighted least squares method is evaluated. To this end, 20 random seeds for a given sea state are used to obtain the normalizing function ϕ for different scenarios. The mean values obtained for β_1, β_2, and β_3 plus or minus two standard deviations are presented in Table 4.4. In this case, the scenarios of higher payout speeds lead to greater variation on the coefficients, indicating a higher sensitive to the specific wave considered in the simulation. The reason for this behaviour comes from the fact that when the payout speed is high, the number of ocean waves cycles are reduced. Consequently, higher amplitude waves are less prone to occur during the resonance zone of the system. This makes more difficult for the weighted least squares method to identify the resonance zone accurately. This drawback may be circumvented by taking the mean coefficients obtained after running a few simulations, and using them to build the normalizing function.

Table 4.4: Statistical description of the normalizing function for different scenarios.

Scenario		**Normalizing function**		
T_p (s)	V_c (m/s)	β_0	β_1	β_2
5	-0.1	-6.96 ± 0.81	62.23 ± 4.40	-110.75 ± 6.68
9	-0.1	-2.96 ± 0.16	13.98 ± 0.66	-13.23 ± 0.64
13	-0.1	-2.94 ± 0.22	8.72 ± 0.83	-5.39 ± 0.72
5	-0.5	-3.57 ± 1.2	37.60 ± 8.41	-69.13 ± 13.68
9	-0.5	-3.09 ± 0.95	15.64 ± 5.12	-15.73 ± 6.24
13	-0.5	-3.29 ± 1.66	9.65 ± 6.57	-5.98 ± 5.68
5	-1.0	-1.43 ± 1.06	22.02 ± 7.24	-43.96 ± 11.91
9	-1.0	-2.18 ± 2.04	13.21 ± 10.35	-14.89 ± 11.66
13	-1.0	-1.96 ± 0.86	7.46 ± 4.10	-5.83 ± 4.40

Illustratively, Figure 4.14 presents the different envelopes obtained by considering random wave seeds for two specific scenarios. The envelope obtained by taking the mean coefficients of three random simulations are also presented. For the scenario of low payout speed (Figure 4.14a), all the envelopes appear similar and equivalent to the mean envelope. On the other hand, for the scenario of high payout speed (Figure 4.14b), a greater scattering is noticeable. It is important to remark however that high payout speeds such as -1 m/s are extreme conditions, and most of the offshore vessels are not able to achieve this speed when lifting heavy equipment such as manifolds.

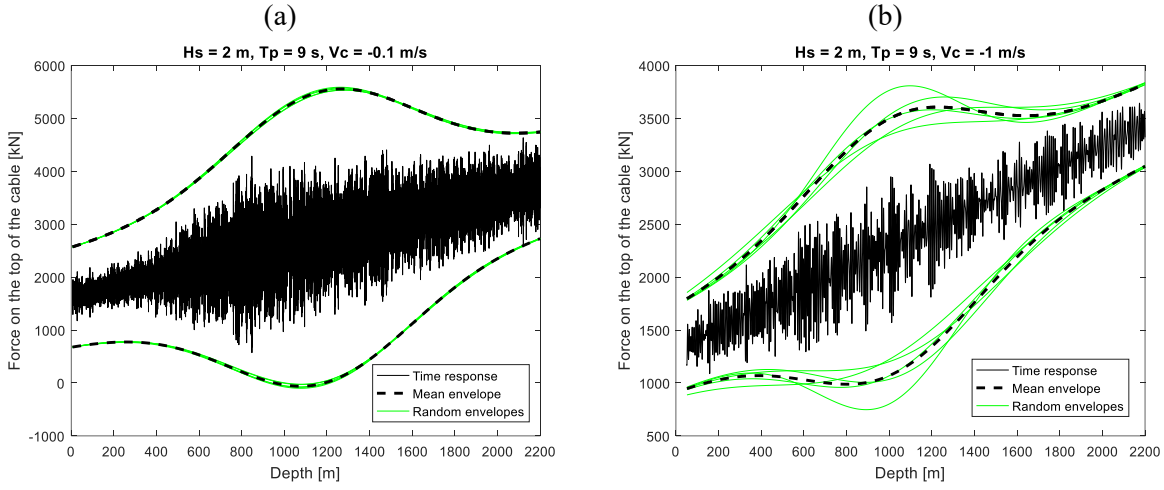

Figure 4.14: Forces on the cable and their envelopes for the scenario of $H_s = 2$ m, $T_p = 9$ s, and (a) $V_c = -0.1$ m/s, and (b) $V_c = -1$ m/s.

4.5 Comparison of the models

Previous sections presented some tests to check the adequacy of the assumptions made to construct the models presented in this study. Now, the adequacy of both models to predict the envelope of the forces on the cable during typical subsea lifting operations is checked. To this end, several cases considering the following scenarios are simulated: $H_s = 2.0$ m, T_p varying from 5 to 13 s, and V_c varying from -0.1 to -1.0 m/s. The results considering the force on the top of the cable are presented in Figure 4.15. The envelope of the weighted least squares method is obtained by using the mean coefficients of 3 random time series, and all the 300 time series obtained when running the direct method are presented in order to verify the accuracy of the envelopes obtained. Firstly, the general forms of the envelope obtained by both models present similar behaviours, amplifying the envelope at the resonance zone. However, since the least squares approach uses a normalizing function that was arbitrarily selected, this method does not truly represent the shape of the envelope. Especially, the scenarios of low payout speed generate multiple peaks due to transient behaviours near the resonance zone; this behaviour is not fully represented by the weighted least squares method. This is expected since the normalizing function selected for this method is only able to represent one peak. In these scenarios, some load cycles trespass the envelope obtained by the least squares method, but not the one obtained by the direct method. Important to remark that, although the envelope of the direct method is violated in some points, the extreme loads predicted at the resonance by this method are still higher than the maximum loads obtained in the 300 simulations, which provides conservative results.

For the scenarios of high payout speed, the envelopes obtained by both methods are eventually trespassed, especially for the scenario considering $T_p = 13$ s. In this specific case, the total number of loading cycles used to build the envelope is equal to 231, the smallest value considered in this study. A minimum number of cycles may be considered by the analyst to increase the envelopes obtained and avoid these cycles to trespass the envelope. Also, instead of using the most probable largest value in the determination of design loads in Equations (4.8) and (4.19), percentile of extreme value distribution, based on the peak over threshold method, could be used to obtain larger safety margin. Further, the recommended practice DNV-RP-H103 states that it is necessary to consider also the largest and smallest loads on the system obtained during the time domain simulations as a design parameter. So, both the envelope and the extreme loads on the time series should be compared against the limiting criteria to build the operational weather window. Notice again that $V_c = -1$ m/s is an extreme speed at which most

of vessels are not able to perform heavy lifting operations.

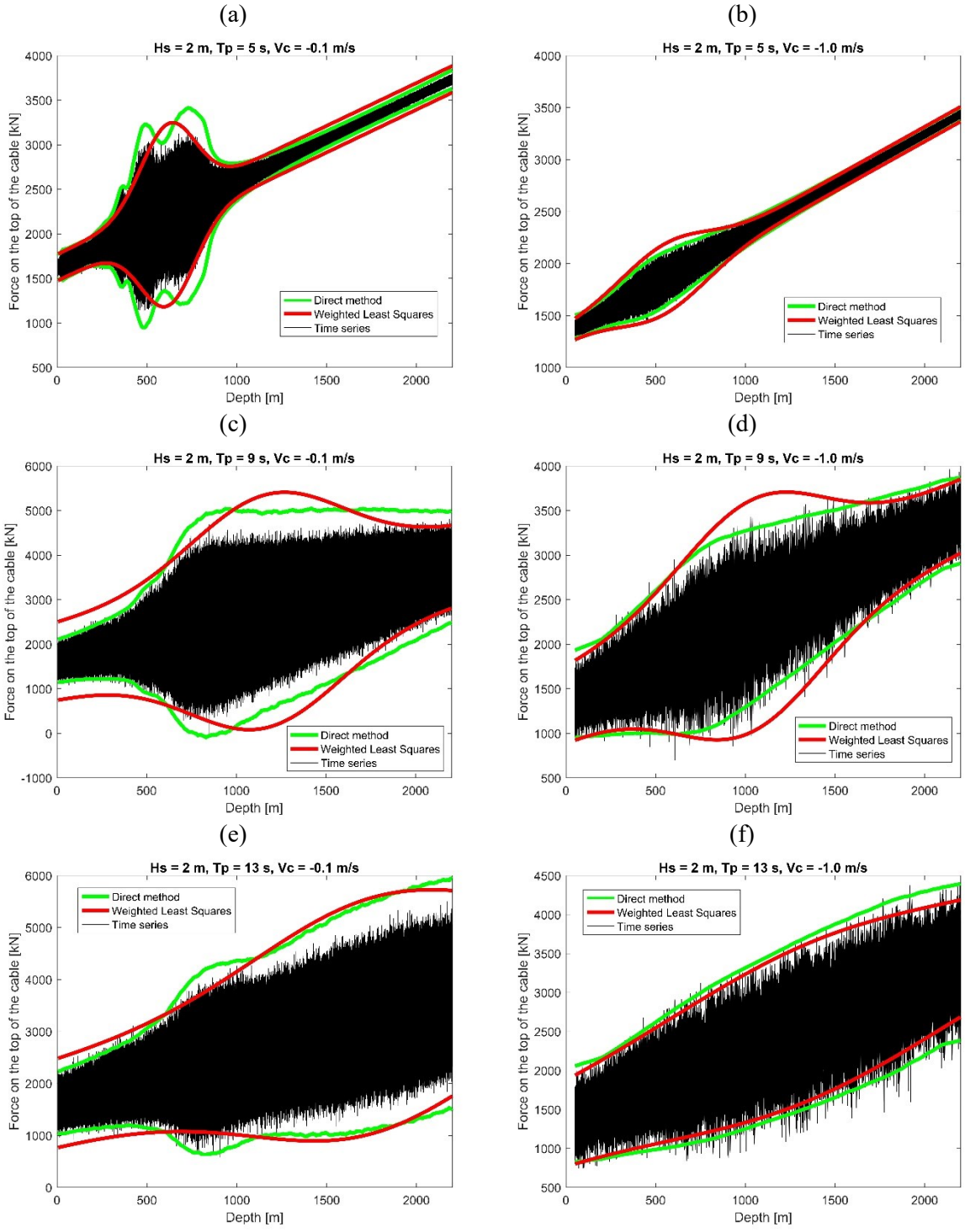

Figure 4.15: Envelope of forces for the direct and the weighted least squares methods, considering $H_s = 2$ m and (a) $V_c = -0.1$ m/s and $T_p = 5$ s; (b) $V_c = -1.0$ m/s and $T_p = 5$ s; (c) $V_c = -0.1$ m/s and $T_p = 9$ s; (d) $V_c = -1$ m/s and $T_p = 9$ s, (e) $V_c = -0.1$ m/s and $T_p = 13$ s; and (f) $V_c = -1$ m/s and $T_p = 13$ s.

4.6 Operational weather window assessment

The final evaluation of the models presented in this study aims to compare the weather window obtained by both models for the operation of installing this manifold. The sea states considered for this analysis are $1.0 \leq H_s \leq 3.0$ m and $5 \leq T_p \leq 13$ s, and the payout speed considered ranges from 0.2 to 1.0 m/s. After running the analysis for each sea state, the availability of the vessel is calculated by summing the relative occurrence of each sea state that is considered valid according to the simulations. The results obtained are presented in Figure 4.16. It is possible to notice an agreement between the models both in the general shape of the curve and in the values found. In this case, a total of 495 scenarios have been analysed (11 significant wave heights, 9 peak periods, and 5 payout speeds), and in only 25 of them (5% of the cases), the two methods presented different results regarding the approval of the operation. Moreover, the limiting criterion of the operation is mainly the possibility of the occurrence of snap loads on the bottom part of the cable; and the increase in the payout speed leads to wider operational weather windows and, consequently, higher availability for the vessel.

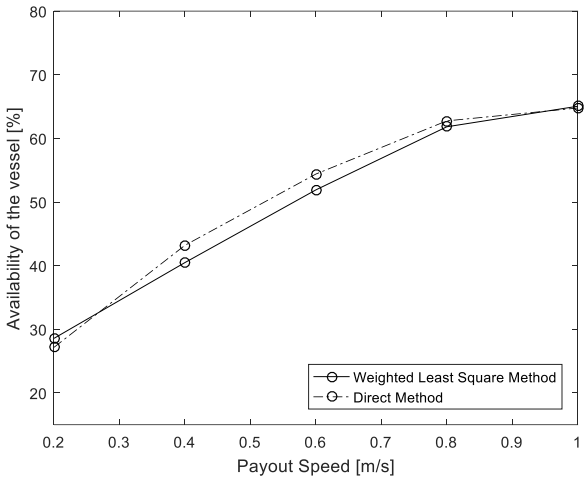

Figure 4.16: Availability of the vessel for the installation of the Pre-Salt manifold obtained using the two methodologies presented in this study.

Based on these results, it is possible to conclude that the models presented in this study to predict the design loads of deep water subsea lifting operations are coherent and present similar results for the scenario considered: the deep water phase of the installation of a manifold in the Pre-Salt fields, in Brazil. Further, it is important to point out that the weighted least squares method needs few time-domain simulations to predict the envelope of forces on the system. This is a significant feature of the method, since it may noticeably reduce the computational

effort needed to plan a real operation. A limitation of this method is the incapacity of representing multiple peaks of response throughout the depth, which can occur due to multimodal wave spectra or multi resonance frequencies of the vessel. On the other hand, the direct method provides better estimation of the form of the envelope of forces on the cable. Further, due to the great amount of time-domain simulations needed for each sea state, the extreme values obtained during all the time series generated can also be used as a design parameter in the direct method, leading to more reliable results.

Finally, as a design guidance, the weighted least squares method may be used in the planning phase of the operation to perform an assessment of different methods to install a given equipment, comparing the results obtained among different vessels and payout speeds. Once one operational procedure is selected, the direct method may be applied to evaluate the weather window to be considered during the real operation. In this way, the analyst can benefit from the speed of the weighted least squares method and from the reliability of the direct method to plan an optimized and safe operation.

4.7 Conclusions

Two methodologies were presented to predict the design loads of deep water subsea lifting operations. These methods are suitable to evaluate non-stationary time series that result from the increase of the suspended weight of the lifting cable and from the passage through a resonance zone during the lifting procedure. In this case, the forces on the cable were split into a static and a dynamic part. The static force could be calculated a priori and was responsible for the variation on the mean force on the cable. The two methods were then used to predict the statistics of the dynamic force, which presented a non-constant standard deviation as a function of the suspended length of the cable.

The first method presented, called the direct method, obtained the standard deviation of the dynamic force after running several simulations for the same scenario and calculating the statistics of the variable at each time step. The second method was based on a weighted least squares procedure that predicted a normalizing function which was used to calculate statistics of the dynamic force. The envelope of the forces, which is used as the design parameter, was constructed for both models assuming the largest most probable value for a Rayleigh distribution of the amplitude of the dynamic force.

The direct method was evaluated and 300 simulations were considered necessary to obtain

convergence on the solution. Further, a moving mean procedure was used to smooth the envelope of the forces obtained. The weighted least squares method was evaluated for different sea states and operational conditions indicating that the assumption that the normalizing function would lead to a stationary normal variable was valid. The comparison of the models, simulating a typical lifting operation on the Brazilian Pre-Salt fields, showed an agreement among the models in most of the scenarios when using three simulations to build the normalizing function of the weighted least squares method. The main limitation of the weighted least squares method was the incapacity of representing envelopes with multiple peaks due to the normalizing function selected.

Finally, the availability of the vessel was assessed using both models. The results obtained were similar in 95% of the scenarios considered, which indicated that both models could be used in the planning of a real operation. Further, it was argued that the computational cost of the weighted least square method was considerable smaller than the direct method. It was then suggested that the least squares method could be used at early phases of the planning, in order to select the most suitable procedure for an operation. After selecting one procedure, the direct method could be used to provide more reliable results for the weather window to be considered in the real operation.

4.8 Appendix

Table 4.5 presents the vertical displacement RAO of the lifting point for a typical PLSV used in installation and retrieval operations.

Table 4.5: Vertical displacement RAO for the lifting point.

$\omega\ (rad/s)$	RAO
0.10	0.9996 + 0.0090i
0.15	0.9983 + 0.0202i
0.20	0.9948 + 0.0359i
0.25	0.9859 + 0.0386i
0.30	0.9681 + 0.0627i
0.35	0.9351 + 0.0577i
0.40	0.8851 + 0.0734i
0.42	0.8586 + 0.0717i
0.43	0.8457 + 0.0783i
0.44	0.8276 + 0.0712i
0.45	0.8124 + 0.0780i
0.46	0.7936 + 0.0852i
0.47	0.7750 + 0.0788i
0.50	0.7118 + 0.0877i
0.55	0.5833 + 0.0917i
0.60	0.4343 + 0.1011i
0.70	0.1082 + 0.1587i
0.80	-0.0794 + 0.2533i
0.90	-0.0417 + 0.1761i
1.00	-0.0393 + 0.0063i
1.10	-0.0261 - 0.0332i
1.20	0.0010 - 0.0092i
1.30	0.0032 + 0.0067i
1.40	-0.0029 + 0.0010i
1.50	0.0009 - 0.0024i
1.60	0.0017 + 0.0005i
1.70	-0.0018 + 0.0002i
1.80	0.0006 + 0.0001i
1.90	0.0004 - 0.0001i
2.00	-0.0008 - 0.0000i

5. THE DYNAMICS OF DEEP WATER SUBSEA LIFTING OPERATIONS IN SUPER-HARMONIC RESONANCE VIA THE HARMONIC BALANCE METHOD

This Chapter is a pre-print of the study by R. B. Tommasini, T. L. Hill, J. H. G. Macdonald, R. Pavanello and L. O. Carvalho, accepted for publication in Marine Structures [184], addressing the objective n. 3 of this thesis (as per Section 1.2.3). This study analyses the dynamics of deep water subsea lifting operations experiencing super-harmonic resonances. Building on the model developed in Chapter 3, a nonlinear non-dimensional equation of motion is presented and solved via the harmonic balance method. The aim is to address the impacts that super-harmonic resonances can have on the dynamics and planning of the operation.

Abstract

The dynamics of deep water subsea lifting operations experiencing super-harmonic resonance is analysed in this study. The harmonic balance method is used to solve the non-dimensional equation of motion of the system and the results are compared with time domain integration and with an equivalent energy dissipation model for typical subsea lifting scenarios. It is demonstrated that 1:3 and 1:5 super-harmonic resonances represent significant features of the response of the system and can lead to large dynamic forces in the cable, which may violate the structural limits of the system in real operations. The harmonic balance method presents results almost as accurate as the time domain integration but up to 25 to 35 times faster, while the equivalent energy dissipation model is not able to represent the super-harmonic resonances. Consequently, taking into account the dynamics introduced by super-harmonic resonances is necessary in the analysis of subsea lifting operations, as it can be the limiting design criterion in certain scenarios, and the harmonic balance method can be used as a fast and accurate method to solve this problem.

Nomenclature

A_i	Coefficients of the polynomial fit
A_p	Vertical projected area of the equipment
C_a	Added mass coefficient
C_d	Drag coefficient
EA	Axial rigidity of the cable
F_{dyn}	Dynamic force on the cable
f	Dimensionless force on the cable
g	Gravity acceleration
H_s	Significant height of the ocean wave
L	Suspended length of the cable
M	Mass of the equipment
m	Mass per unit length of the cable
m_s	Equivalent submerged mass per unit length of the cable
N	Number of harmonic terms
n	Number of input cycles
RAO	Response Amplitude Operator of the vertical displacement at the lifting point
S	Energy density spectrum of the vertical displacement at the lifting point
S_{wave}	Energy density spectrum of the ocean waves
T_p	Peak period of the ocean waves
t	Time
V	Volume of the equipment
W_0	Amplitude of the vertical displacement of the lifting point
w	Vertical displacement of the equipment
w_0	Vertical displacement of the lifting point
w_{st}	Static vertical displacement of the equipment
w_{dyn}	Dynamic vertical displacement of the equipment
y	Dimensionless dynamic displacement
Y_k	Amplitude of the k^{th} dimensionless harmonic component
α	Dimensionless mass ratio
γ	Dimensionless damping
ϕ_k	Phase of the k^{th} harmonic component
Λ	Dimensionless excitation frequency
ρ	Density of the sea water

Ω	Excitation frequency
τ	Dimensionless time
ω_n	Natural frequency of the system
ω_z	Mean zero up-crossing frequency of the vertical displacement of the lifting point
σ	Standard deviation of the vertical displacement of the lifting point
$\mathbb{Q}$	Non-conservative generalized force
$\mathbb{T}$	Kinetic energy of the system
$\mathbb{V}$	Potential energy of the system

5.1 Introduction

Many offshore activities require the installation and recovery of equipment from the seabed. Such equipment is used, for example, for the production of oil and gas, the exploration of wind and tidal energy, and for deep sea mining. An important consideration for such operations is the high cost related to it, especially due to the need for specialist vessels and the possibility of environmental restrictions for the operation. Because of this, precise assessment of the dynamic loads in the system is necessary to ensure minimum costs and to comply with safety requirements.

Throughout previous decades, several works have been published focusing on different aspects of subsea lifting operations. Classical formulations for the problem can be encountered in the work of Niedzwecki and Thampi [71], Huang [72], and Driscoll *et al.* [74], where analytical models were proposed; and in the study by Driscoll *et al.* [76], where a finite element approach was used to calculate the dynamics of the system. More recently, the use of synthetic materials for the cable was covered by de Araújo Neto *et al.* [81], who presented a design methodology to avoid resonances via the use of a combined steel wire and polyester rope for the lifting line. Further, some authors [83,84,86,137,159] have focused their attention on the scenario where the length of the cable may vary, which has provided means to understand how the payout speed could influence the dynamics of the operation. The dynamics of the system in the wave zone has also been covered by some authors: Jeong *et al.* [65] developed a model to account for the possibility of collisions of the equipment with the vessel during this phase, while the influence of vessel shielding effects on the response of the system have been presented in other studies [59,61]. Additionally, a methodology for the assessment of the operational limits of marine operations was presented by Acero *et al.* [178].

An important aspect of the dynamics of subsea lifting operations is the hydrodynamic forces

that act on the payload [124,125,129–132,135]. These forces are typically modelled via Morison's equation [118], which is a semi-empirical equation that considers the hydrodynamic force as the combination of an inertial term, proportional to the acceleration; and a drag term, proportional to the squared velocity. Particularly, the drag term in this formulation is an odd nonlinear function and, consequently, generates odd harmonics when the body is oscillating in sinusoidal motion. This behaviour was observed by Tommasini *et al.* [137] through a theoretical model that predicted increased forces on the cable due to the third harmonic component when the input frequency was $1/3$ of the natural frequency of the system, as illustrated in Figure 5.1. Also, the presence of these harmonics in the response of the system was observed in a real operation, as presented by Driscoll *et al.* [73] in their study about the motion of deep sea remotely operated vehicles. Although Tommasini *et al.* [137] and Driscol *et al.* [73] made some remarks regarding this phenomenon, a greater focus on this type of behaviour and its consequences on real subsea lifting operations was absent in their studies.

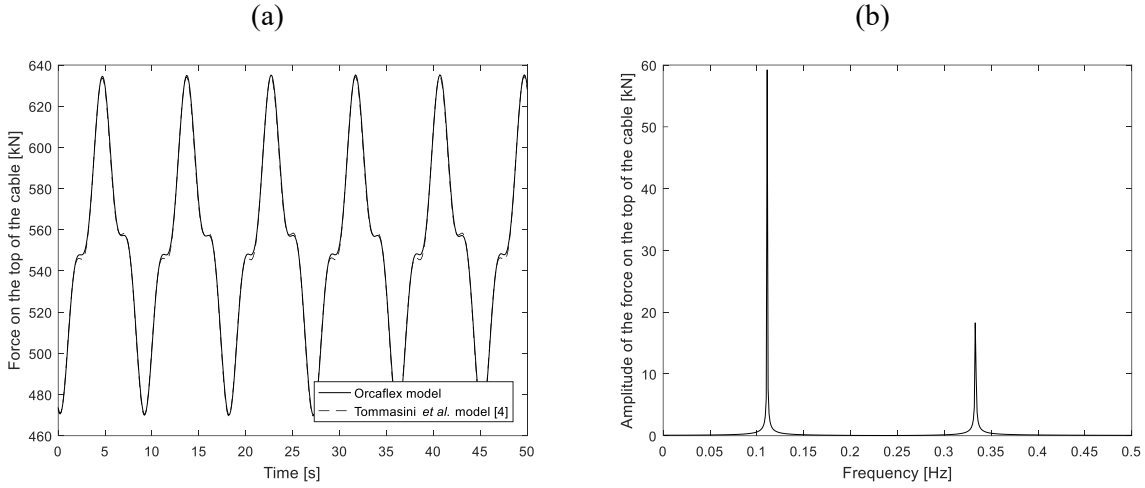

Figure 5.1: Illustration of the super-harmonic resonance on subsea lifting operations for sinusoidal excitation at 0.11 Hz; (a) time domain response, and (b) frequency domain response. Figure extracted from Tommasini *et al.* [137].

The phenomenon observed in [137] is known as super-harmonic resonance and it has been widely studied in other fields. Much of the classical literature on nonlinear dynamics presents ways of dealing with this kind of phenomenon, such as in the book of Nayfeh and Mook [185]. More specific examples can be encountered in numerous works on different applications. For example, Hou *et al.* [186] detailed the local bifurcation characteristics of an aircraft cracked rotor for 2:1 and 3:1 super-harmonic resonances induced by manoeuvre loads. Masana and Daqaq [187] illustrated the use of a nonlinear twin-well oscillator in the super-harmonic frequency band for energy harvesting, showing that it was possible to produce power levels similar to those near the fundamental resonance even from low frequency excitations. In the offshore

engineering area, Liaw *et al.* [188] and Liu *et al.* [189] respectively described the dynamics of an articulated tower and of a deep sea Spar platform hull, both numerically and experimentally, illustrating the possibility of super- and sub-harmonic resonance depending on the wave frequency. Also, Hannan and Bai [64] investigated the dynamical response of a fully submerged payload hanging from a fixed crane vessel, showing that the motion of the payload exhibited various nonlinear phenomena, such as sub-harmonic responses. In this case, the focus was on the dynamics of the system in the wave zone, which resulted in constrained pendulum motions for the payload; this is in contrast to the scenario observed by Tommasini *et al.* [137], where the super-harmonic resonance was due to the axial vibration of the cable-equipment system in deep water. It is important to note that the nonlinearity in most offshore systems is due to a factor of velocity squared in the damping term. Other examples of studies dealing with this type of damping term can also be found in the literature [190,191]. These studies addressed the nonlinear response of moored structures, highlighting the possibility of occurrence of chaos and instabilities. In this case, the quadratic damping term controls the thresholds and limits of the stability domains.

Whilst many works have been conducted regarding super-harmonic resonances, it seems there is a lack of any study dealing specifically with this phenomenon in the scenario of deep water subsea lifting operations. Furthermore, no specific mention is given on the possibility of super-harmonic resonances in subsea lifting operations in the recommended practice DNVGL-RP-N103 [192], which is the standard reference used by the industry for the modelling and analysis of marine operations. Therefore, the main objective of this paper is to conduct such a study, focusing on (1) the solution of the non-dimensional nonlinear equation of motion via the harmonic balance method; (2) illustration of the features and implications of the super-harmonic resonance on the subsea lifting scenario; and (3) extending the solution procedure presented to be used as a design methodology to assess the operational weather window. This study considers conventional nonlinear dynamics methods to study an applied offshore dynamics problem not yet fully addressed in the literature. The originality of this study relies not only on the comprehension of the dynamics of the system in super-harmonic resonance, but also in the use of a non-dimensional formulation for the equation of motion, reducing the number of independent variables of the system; and in the use of an analytical approach to solve the nonlinear dynamical problem, which decreases the computational effort required to solve the problem. These aspects are particularly important during the planning of subsea lifting operations, where numerous combinations of environmental and operational conditions are necessary to be studied.

The sequence of this paper is as follows: an overview of the dynamics of subsea lifting operations, highlighting the presence of super-harmonic resonance in Section 5.2; the non-dimensional equation of motion for the system in Section 5.3; the dynamics of the system using the harmonic balance method in Section 5.4; the numerical results obtained by the proposed method in Sections 5.5 and 5.6, and the assessment of the operational weather window for an example scenario in Section 5.7. The conclusions of this work are finally presented in Section 5.8.

5.2 Overview of the dynamics of subsea lifting operations

The first step to analyse the dynamics of subsea lifting operations is to construct a representative dynamical model for the system. Analysing measurements of the average coherence of the six degree-of-freedom of both the vessel and the payload in a real operation, Driscoll *et al.* [73] showed that the only significant relationship between the lifting vessel and the payload was the vertical motion variables; therefore a one-dimensional model was considered sufficient to predict the payload motion due to vessel forcing. This assumption was considered in several studies dealing with the dynamics of subsea lifting operations [71,72,74,76,85,86,137,193] and is also considered herein.

Further, Tommasini *et al.* [137] showed that when the frequency of internal vibration modes of the cable are not within the waveband and are far from the fundamental axial vibration frequency of the system, the results obtained by using single degree-of-freedom models were similar to those obtained by discretized models (such as by using the commercial software Orcaflex). This is the case in the example considered in this work, hence higher vibration modes are not represented. The use of single degree-of-freedom models is also recurrent in the literature [71,72,91,92,159,193] and is particularly useful to understand dynamical features of the system, which is the main objective of this study.

Subsea lifting operations are typically classified as weather restricted and need to comply with the requirements of DNVGL-RP-N103 [192]. One criterion that should be fulfilled is that the cable does not go slack during the operation to avoid large snap loads in the system. Therefore, the scenarios analysed in this study do not result in compressive loads in the lifting line, and the cable is considered to be always taut, as in [74,86,137]. In applications where slack conditions are not possible to be avoided, the model presented herein is not applicable and low tension dynamic models [141,142] should be used instead.

The effects of subsea currents are also not considered in this study relying on reference [67]

that states that the tension in the cable and the offset of the payload are minor when the vertical force due to the submerged weight of the system is larger than the forces due to theses currents, which is the case in most of the typical applications and in the particular scenario analysed in this study.

It is also assumed that the cable-payload system does not affect the dynamics of the vessel, such as done in [71,76,86,137]. Therefore, the vertical displacement of the lifting point is prescribed as an imposed displacement in the top of the cable. This assumption is in agreement with DNVGL-RP-N103 and it is applicable when the inertia of the vessel is much larger than the inertia of the payload.

The hydrodynamic forces are considered to be present only on the payload and they follow Morison's equation using constant hydrodynamic coefficients, as in [72,74,137,193]. Some remarks on the use of constant hydrodynamic coefficients to analyse super-harmonic resonances are given in Section 5.5.

Finally, a constant length model is considered to allow transient effects of the cable payout to be neglected, as in [71,72,76]. This scenario is particularly important in procedures which require the equipment to be kept at certain depths for relatively long periods, such as in subsea load transfers [194] or when successive introduction of slings in the lifting system is considered [2].

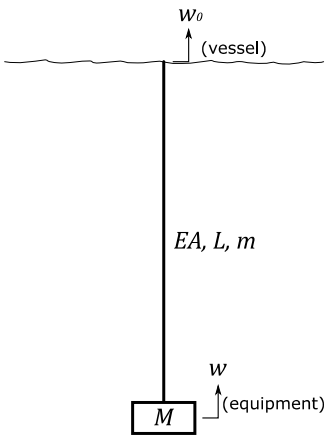

Figure 5.2: Representation of the single degree-of-freedom model for the evaluation of subsea lifting operations.

The equation of motion for the subsea lifting system (Figure 5.2) considering the assumptions presented above was derived in [137], so only the main details are presented here for clarity. The derivation was based on the application of Lagrange's equation and it was assumed that the displacement of the payload was the only degree-of-freedom of the system. Assuming a

linear interpolation for the velocity field within the cable, the kinetic energy of the system ($\mathbb{T}$) was considered to be the sum of the kinetic energy of the cable (obtained by integrating throughout its length) and the payload:

$$\mathbb{T} = \frac{mL}{6}(\dot{w}_0^2 + \dot{w}_0\dot{w} + \dot{w}^2) + \frac{1}{2}M\dot{w}^2 \tag{5.1}$$

where m is mass per unit length of the cable, L is the suspended length of cable, M is the mass of the payload, $\dot{w}_0$ is the velocity of the lifting point, and $\dot{w}$ is the velocity of the payload.

The potential energy of the system ($\mathbb{V}$) was considered to be sum of the potential energy of the cable and payload due to the gravity and the strain energy of the cable:

$$\mathbb{V} = \frac{m_s gL}{2}(w_0 + w) + (M - \rho V)gw + \frac{1}{2}\frac{EA}{L}(w_0 - w)^2 \tag{5.2}$$

where m_s is the equivalent submerged mass per unit length of the cable, g is the gravity acceleration, ρ is the density of the sea water, V is the volume of the payload, EA is the rigidity of the cable, w_0 is the displacement of the lifting point, w is the displacement of the payload.

The hydrodynamic force on the payload was considered to be the only non-conservative generalized force ($\mathbb{Q}$) acting on the system:

$$\mathbb{Q} = -\rho V C_a \ddot{w} - \frac{1}{2}\rho A_p C_d |\dot{w}|\dot{w} \tag{5.3}$$

where C_a and C_d are, respectively, the added mass and drag coefficients, A_p is the vertical projected area of the payload, and $\ddot{w}$ is the acceleration of the payload.

Therefore, the resulting equation of motion for the single degree-of-freedom system was found to be:

$$\begin{aligned}\left(M + \rho V C_a + \frac{1}{3}mL\right)\ddot{w} + \frac{1}{2}\rho A_p C_d |\dot{w}|\dot{w} + \frac{EA}{L}w \\ = \frac{EA}{L}w_0 - \frac{mL}{6}\ddot{w}_0 - \left(M - \rho V + \frac{m_s L}{2}\right)g\end{aligned} \tag{5.4}$$

The nonlinearity of this equation comes only from the quadratic drag term, which is a function of the equipment velocity. Due to this fact, the static displacement due to the weight of the cable and equipment does not influence the nonlinear behaviour of the system and, in this respect, the superposition principle may be applied to split the response of the system into a static and a dynamic term: $w = w_{\mathrm{st}} + w_{\mathrm{dyn}}$. The static displacement is directly obtained by the equilibrium

condition:

$$\frac{EA}{L} w_{\mathrm{st}} = -(M - \rho V + \frac{m_s L}{2}) g \tag{5.5}$$

While the dynamic term comes from the solution of the equation of motion:

$$\left(M + \rho V C_a + \frac{1}{3} mL\right) \ddot{w}_{\mathrm{dyn}} + \frac{1}{2} \rho A_p C_d \left|\dot{w}_{\mathrm{dyn}}\right| \dot{w}_{\mathrm{dyn}} + \frac{EA}{L} w_{\mathrm{dyn}} = \frac{EA}{L} w_0 - \frac{mL}{6} \ddot{w}_0 \tag{5.6}$$

Further, the dynamic force acting on the cable can be computed as:

$$F_{\mathrm{dyn}} = \frac{EA}{L} \left(w_0 - w_{\mathrm{dyn}}\right) \tag{5.7}$$

In order to present an introduction to the dynamical behaviour of this system, the installation of a small size manifold in the Campos Basin (Brazil) is considered as an example. The data used for the operation are presented in Table 5.1. Constant hydrodynamic coefficients are considered in this study, as in [72,74,137,193], and some remarks on this topic are given in Section 5.5.

Table 5.1: Data considered for the example scenario.

	Parameter	**Value**
Cable (3 in six-stranded)	Mass per unit length (m)	24.6 kg/m
	Equivalent submerged mass per unit length (m_s)	20.4 kg/m
	Axial rigidity (EA)	315 MN
	Safe Working Load	1300 kN
Equipment (Small size manifold)	Mass (M)	15 tonnes
	Volume (V)	1.92 m^3
	Vertical projected area (A_p)	15 m^2
	Added mass coefficient (C_a)	30
	Drag coefficient (C_d)	4
	Safe Working Load	200 kN
Environmental conditions	Wave peak period (T_p)	5 to 13 s
	Wave significant height (H_s)	1.0 to 3.0 m
	Water depth	700 m

A typical engineering analysis would start by checking the natural frequency of this system as a function of the water depth, aiming to identify the risk of resonance:

$$\omega_n = \sqrt{\frac{EA}{L\left(M + \rho V C_a + \frac{1}{3}mL\right)}} \tag{5.8}$$

This result is presented in Figure 5.3 and reveals that the natural period ($T_n = 2\pi/\omega_n$) of the system is always below the wave peak periods found near the Brazilian shore (typically between 5 and 13 s). Consequently, one could conclude that amplifications in the cable force due to resonance would not be a risk in this scenario, and that the maximum dynamic loads would occur at 700 m depth, since at this depth the natural period is closest to the excitation periods. However, this conclusion is not correct as it ignores the effects introduced by the nonlinear drag term in the dynamics of the system.

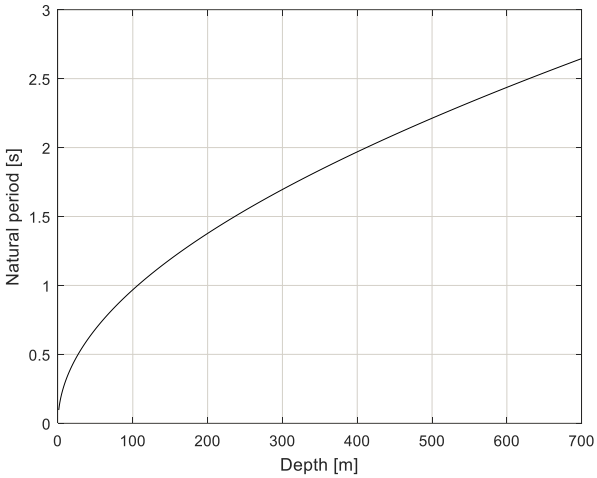

Figure 5.3: Natural period of the system as a function of depth.

A more accurate and useful representation of the dynamics of the system can be obtained by plotting the maximum value of the dynamic force on the cable as a function of depth. This way, it is possible to identify the zones where structural limits of the system may be violated during the operation. As an example, a sinusoidal input displacement (w_0) of amplitude 0.5 m and frequency (Ω) 1 rad/s is considered.

The results, obtained using a fourth order Runge-Kutta algorithm to integrate Eq. (5.6) in the time domain, implemented via Matlab function 'ode45', are presented in Figure 5.4. The solution of an equivalent equation, substituting the quadratic drag term with a linear one that dissipates the same amount of energy per cycle [71], is also presented. This last model is usually considered as a first guide to analyse subsea lifting operations [192] and is used as a comparative model in this study.

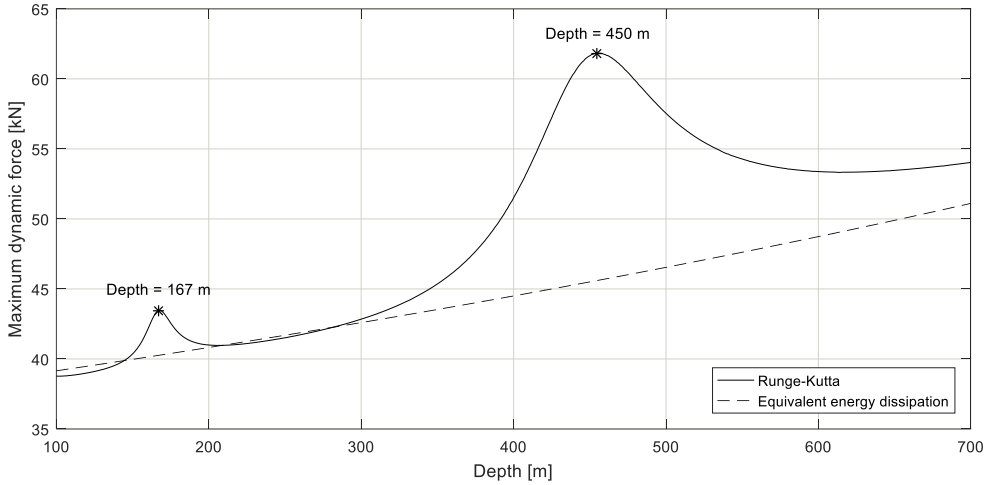

Figure 5.4: Maximum dynamic force on the cable as a function of depth for the nonlinear equation of motion (Eq. (5.6)) and for an equivalent linear equation considering equivalent energy dissipation per cycle. Input frequency $1\ \mathrm{rad/s}$ and input amplitude 0.5 m.

In this figure, the Runge-Kutta results exhibit two peaks in the dynamical response of the system that do not occur for the equivalent energy dissipation model. The higher peak occurs at a depth of 450 m, where the natural frequency of the system is $3\ \mathrm{rad/s}$ ($\Omega = \omega_n/3$), while the smaller peak occurs at 167 m, where the natural frequency is $5\ \mathrm{rad/s}$ ($\Omega = \omega_n/5$). This increase in the dynamical response of a system in zones where the input frequency is an integer fraction of the natural frequency is known as super-harmonic resonance [185], which is characterized by the presence of higher harmonic components in the response of the system (as indicated in Figure 5.1).

Considering that unexpected higher loads may violate the structural limits of the system, comprehension of the features of the super-harmonic resonance is necessary. The rest of this paper presents this study.

5.3 Non-dimensional equation of motion

Although Eq. (5.6) can be directly used to calculate the dynamics of the system, using an equivalent non-dimensional equation permits the simplification of the problem by reducing the number of parameters necessary to evaluate it. So, assuming a harmonic input for the displacement on the top of the cable:

$$w_0 = W_0 \cos(\Omega t) \tag{5.9}$$

and introducing the following dimensionless variables:

$$\tau = \omega_n t \tag{5.10}$$

$$\Lambda = \frac{\Omega}{\omega_n} \tag{5.11}$$

$$y = \frac{w_{\mathrm{dyn}}}{W_0} \tag{5.12}$$

it is possible to re-write Eq. (5.6) in non-dimensional form:

$$y'' + \gamma |y'| y' + y = (1 + \alpha \Lambda^2) \cos(\Lambda \tau) \tag{5.13}$$

In this case, y' and y'' mean differentiation of y with respect to τ, and the new parameters of the system are defined as:

$$\alpha = \frac{mL}{6\left(M + \rho V C_a + \frac{1}{3} mL\right)} \tag{5.14}$$

$$\gamma = \frac{\rho A_p C_d}{2\left(M + \rho V C_a + \frac{1}{3} mL\right)} W_0 \tag{5.15}$$

The dimensionless mass ratio (α) represents $1/6$ of the ratio of the mass of the cable to the effective mass of the system and the dimensionless damping (γ) relates the drag force to the effective mass of the system. It is interesting to note that it has been possible to incorporate the amplitude of the input in this last parameter, rather than needing a separate input parameter, as is usual. This representation of the equation of motion enables the analysis of the dynamics of this system as a function of only three parameters: α, γ, and Λ, simplifying the understanding of the general behaviour of the system in different scenarios.

Finally, as the interest in this type of analysis is to calculate the force on the cable, a non-dimensional form of the dynamic force on the cable can be obtained by taking:

$$f = \frac{F_{\mathrm{dyn}}}{W_o \left(M + \rho V C_a + \frac{1}{3} mL\right) \Omega^2} \tag{5.16}$$

Applying this relation into Eq. (5.7), it is possible to obtain the dimensionless force as:

$$f = \frac{1}{\Lambda^2} (y_0 - y) \tag{5.17}$$

where $y_0 = \cos(\Lambda \tau)$.

5.4 Analysing the dynamics of the system via the harmonic balance method

Despite the fact that Eq. (5.13) may be solved numerically in the time domain, analytical or semi-analytical approaches may be used to provide more rapid solutions and also insight into the mechanisms that underpin the nonlinear dynamical behaviour. Therefore, the focus of this section is to present the solution of the equation of motion in the super-harmonic zone analytically.

Approximate solutions of nonlinear equations, such as Eq. (5.13), may be obtained using techniques such as the method of multiple scales, the method of averaging or the harmonic balance method (HBM). These techniques represent the solution of the full problem by the first few terms of a perturbation or series expansion [195]. The procedure selected for this study is the harmonic balance method [196–199]. This choice is made due to its intuitive approach and also the fact that numerical simulations can be easily used to check the harmonic components that are present in the dynamic response of the system.

The harmonic balance method employs the fact that the steady state response of the of system to sinusoidal excitation is periodic in the vicinity of a centre (the static equilibrium position, in this case) and, hence, it can be represented by a Fourier series. Therefore, the non-dimensional dynamic displacement is assumed to be equal to [185]:

$$y = \sum_{k=1}^{N} Y_k \cos(k\Lambda\tau + \phi_k) \tag{5.18}$$

This approximation is substituted into the equation of motion, and the amplitudes and phases are determined by balancing the harmonic terms with the same frequencies.

5.4.1 Harmonic balance method considering 1 harmonic component

A first approximation to solve the problem may be obtained by considering just one harmonic component for the response of the system. So, the non-dimensional displacement has the form:

$$y = Y_1 \cos(\Lambda\tau + \phi_1) \tag{5.19}$$

In this case, the system responds at the same frequency as the excitation, but it has a different amplitude and phase. Substituting Eq. (5.19) into Eq. (5.13) leads to the following equation:

$$-Y_1\Lambda^2\cos(\Lambda\tau+\phi_1)-Y_1^2\Lambda^2\gamma|\sin(\Lambda\tau+\phi_1)|\sin(\Lambda\tau+\phi_1)+Y_1\cos(\Lambda\tau+\phi_1)=(1+\alpha\Lambda^2)\cos(\Lambda\tau) \tag{5.20}$$

The quadratic term is a periodic function, and thus can be represented via a Fourier series:

$$|\sin(\Lambda\tau+\phi_1)|\sin(\Lambda\tau+\phi_1)=\frac{8}{3\pi}\sin(\Lambda\tau+\phi_1)-\frac{8}{15\pi}\sin(3\Lambda\tau+\phi_1)-\frac{8}{105\pi}\sin(5\Lambda\tau+\phi_1)+\cdots \tag{5.21}$$

Substituting Eq. (5.21) into Eq. (5.20), expressing the sines and cosines in imaginary exponential form and balancing the coefficients of the terms with frequency Λ, after some algebraic manipulation, the following equation is obtained:

$$-Y_1\Lambda^2+\frac{8Y_1^2\Lambda^2\gamma}{3\pi}\mathrm{j}+Y_1-(1+\alpha\Lambda^2)\mathrm{e}^{-\mathrm{j}\phi_1}=0 \tag{5.22}$$

Separating the real and imaginary parts of this equation results in:

$$(1-\Lambda^2)Y_1=(1+\alpha\Lambda^2)\cos\phi_1 \tag{5.23a}$$

$$-\frac{8\Lambda^2\gamma}{3\pi}Y_1^2=(1+\alpha\Lambda^2)\sin\phi_1 \tag{5.23b}$$

The amplitude of the displacement can be obtained taking the square of both sides and adding the equations, which leads to:

$$\left(\frac{8\Lambda^2\gamma}{3\pi}\right)^2Y_1^4+(1-\Lambda^2)^2Y_1^2-(1+\alpha\Lambda^2)^2=0 \tag{5.24}$$

This is a quadratic equation in Y_1^2, so it can be easily solved for Y_1. Then, the phase of the non-dimensional displacement can be obtained from:

$$\phi_1=\arctan\left[\frac{-8\Lambda^2\gamma Y_1}{3\pi(1-\Lambda^2)}\right] \tag{5.25}$$

Eqs. (5.24) and (5.25), obtained to calculate Y_1 and ϕ_1, are the same as those found when the assumption of equivalent energy dissipation is made. Therefore, the results obtained using only one harmonic component to represent the dynamics of the system are equal to those obtained from the equivalent energy dissipation model, as presented in Figure 5.4, which is not able to represent the super-harmonic resonance that the system experiences.

5.4.2 Harmonic balance method considering 2 or 3 harmonic components

The above analysis shows that selecting only one harmonic component is not sufficient to represent the super-harmonic resonance, so more harmonics are required in the assumed solution. Only odd harmonics need be included, since the only nonlinear term in the equation of motion, $\gamma|y'|y'$, is an odd function. Considering the results presented in Figure 5.1, a rational choice is the selection of two harmonic components for the response of the system. The first harmonic is assumed to have the same frequency as the excitation and the second one to have three times the excitation frequency. Therefore, the non-dimensional displacement has the form:

$$y = Y_1 \cos(\Lambda\tau + \phi_1) + Y_3 \cos(3\Lambda\tau + \phi_3) \tag{5.26}$$

The direct substitution of Eq. (5.26) into Eq. (5.13) leads to algebraic difficulties in obtaining a Fourier series representation for the quadratic drag term, as obtained in Eq. (5.21) for one harmonic. This is because there is no simple equation for the time at which y', based on Eq. (5.26), changes sign, as the phase of each harmonic term is not known *a priori*. In order to retain the analytical treatment of the problem, the product $y'|y'|$ is approximated by an odd polynomial, due to the anti-symmetry of the function:

$$y'|y'| = A_1 y' + A_3 {y'}^3 + A_5 {y'}^5 + \cdots \tag{5.27}$$

Since the function $y'|y'|$ does not have smooth derivatives, the coefficients A_i cannot be calculated directly via a Taylor series. So, the coefficients may be found by fitting a regression model of the function $y'|y'|$ via a least squares technique [200]. In this case, the values of the coefficients are dependent on the range of values considered for the non-dimensional velocity when fitting the curve.

Taking the maximum value of the non-dimensional velocity to perform this fit as the amplitude of the velocity of the first harmonic, the coefficients A_i are obtained by solving the following minimization problem:

$$\text{min:} \quad \int_0^{\Lambda Y_1} \left({y'}^2 - A_1 y' - A_3 {y'}^3 - A_5 {y'}^5 - \cdots\right)^2 \mathrm{d}y' \tag{5.28}$$

Due to the anti-symmetry of $y'|y'|$, only positive values of y' need be included in the integral. The validity of the approach for dealing with the $y'|y'|$ term is addressed in Section 5.5.

Taking only the two first terms of the polynomial approximation for the nonlinear function, and solving the least squares problem, leads to the following equation of motion:

$$y'' + \gamma\left(\frac{5}{16}\Lambda Y_1 y' + \frac{35}{48\Lambda Y_1}y'^3\right) + y = (1 + \alpha\Lambda^2)\cos(\Lambda\tau) \tag{5.29}$$

Substituting Eq. (5.26) into Eq. (5.29), balancing the coefficients of the first and the third harmonic components, and after some algebraic manipulation, the following system of nonlinear algebraic equation is obtained:

$$64(1-\Lambda^2)Y_1 - 105\gamma\Lambda^2 Y_1 Y_3 \sin(3\phi_1 - \phi_3) - 64(1+\alpha\Lambda^2)\cos(\phi_1) = 0 \tag{5.30a}$$

$$55\gamma\Lambda^2 Y_1^2 + 630\gamma\Lambda^2 Y_3^2 - 105\gamma\Lambda^2 Y_1 Y_3 \cos(3\phi_1 - \phi_3) + 64(1+\alpha\Lambda^2)\sin(\phi_1) = 0 \tag{5.30b}$$

$$192(1-9\Lambda^2)Y_3 + 35\gamma\Lambda^2 Y_1^2 \sin(3\phi_1 - \phi_3) = 0 \tag{5.30c}$$

$$162 Y_1^2 Y_3 + 567 Y_3^3 - 7 Y_1^3 \cos(3\phi_1 - \phi_3) = 0 \tag{5.30d}$$

This is a nonlinear system of equations for Y_1, ϕ_1, Y_3 and ϕ_3 which can be solved numerically. The results for this study, shown in Section 5.5, uses the interior trust region method [201], implemented via the Matlab function 'fsolve', to compute the solutions of this system of equations assuming zero as initial estimates.

Given the existence of another super-harmonic resonance when $\Omega = \omega_n/5$ (Figure 5.4), it is also worth considering the solution of the system adding another harmonic term. In this case, the assumed solution for the dynamic displacement of the equipment is:

$$y = Y_1\cos(\Lambda\tau + \phi_1) + Y_3\cos(3\Lambda\tau + \phi_3) + Y_5\cos(5\Lambda\tau + \phi_5) \tag{5.31}$$

However, the expansion in Eq. (5.27) then needs to include the $A_5 y'^5$ term, in order to generate the harmonic at five times the input frequency. So, solving the least squares minimization problem and substituting the polynomial approximation into the equation of motion leads to:

$$y'' + \gamma\left(\frac{105}{512}\Lambda Y_1 y' + \frac{315}{256\Lambda Y_1}y'^3 - \frac{231}{512\Lambda^3 Y_1^3}y'^5\right) + y = (1+\alpha\Lambda^2)\cos(\Lambda\tau) \tag{5.32}$$

Applying a similar procedure as presented in the case for two harmonics, it is possible to obtain a system of nonlinear algebraic equations for the variables Y_1, ϕ_1, Y_3, ϕ_3, Y_5 and ϕ_5. These expressions are presented in Appendix A.

5.5 Numerical results for the dynamics of the example system in super-harmonic resonance

Having presented the solution of the equation of motion via the harmonic balance method using different combinations of harmonic components, a deeper analysis of the dynamics of the system in super-harmonic resonance can be conducted. To this end, the steady state maximum value of the dynamic force on the example cable is presented in Figure 5.5, using direct integration of Eq. (5.13) by a Runge-Kutta solver and using the HBM with different combinations of harmonic components. The dimensional form of the variables is obtained using Eqs. (5.10) to (5.12) and (5.16), following the solution of the non-dimensional equation of motion. The HBM using only the first harmonic (HBM 1) is unable to represent any of super-harmonic peaks (as addressed in Section 5.4.1), the HBM using the first and the third harmonics (HBM 1,3) reproduces the higher peak, and both peaks are reproduced using the HBM with the first, third, and fifth harmonics (HBM 1,3,5). Comparing the results obtained via the harmonic balance method to the Runge-Kutta solution, the values obtained are considered accurate: the error of the maximum value of the dynamic force, at 450 m depth, is 0.21 % for HBM 1,3 and 0.42 % for HBM 1,3,5, while the error at the other maximum, at 167 m, is 2.01 % for HBM 1,3,5. Furthermore, HBM 1,3 is around 35 times faster than the Runge-Kutta method when considering a total integration time of 50 dimensionless periods and a relative tolerance of 10^{-5} for the non-dimensional displacement and velocity; while HBM 1,3,5 is up to 25 times faster than the Runge-Kutta method in similar conditions. The increased speed with which the equation of motion is solved via the harmonic balance method is particularly important during the planning of subsea lifting operations, when several combinations of environmental and operational conditions must be evaluated. For example, the construction of a typical operational weather window requires the evaluation of 3 vessel headings, 13 wave peak periods, 16 wave heights, and 70 depths (considering the maximum water depth equal 700 m). This would lead to a total of 43680 independent simulations. The total simulation time, considering a 1.7 GHz Core i7 processor, would thus be around 8 hours for the time domain integration in comparison to few minutes for the harmonic balance method (12 min for the HBM 1,3 and 17 min for the HBM 1,3,5). This is crucial if some analysis must be conducted whilst the operation is underway, where high daily rates are common for the vessels.

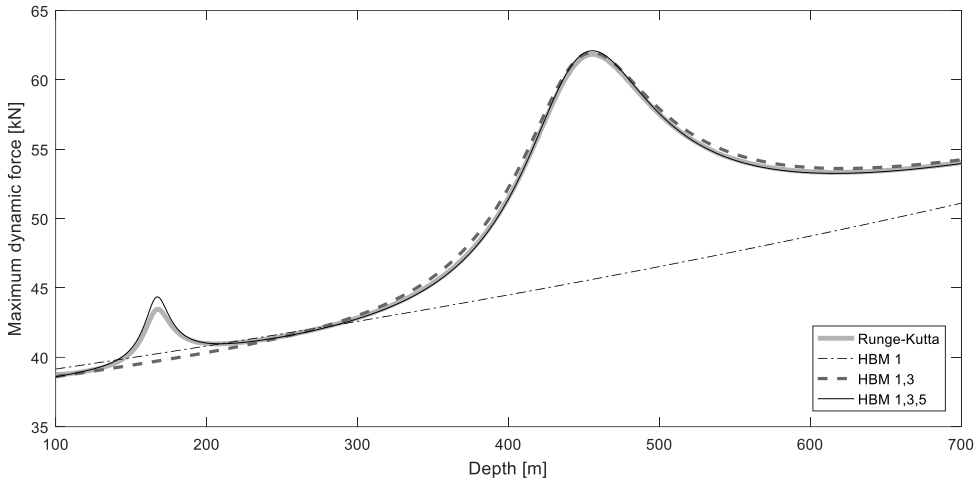

Figure 5.5: Maximum steady state dynamic force on the cable as a function of depth using different solutions. Input frequency $1\ \mathrm{rad/s}$ and input amplitude 0.5 m.

The behaviour of the harmonic components near the super-harmonic resonances are presented in Figure 5.6 (in this case, the amplitude of each harmonic is scaled to its dimensional form: $W_1 = Y_1 W_0$, $W_3 = Y_3 W_0$, and $W_5 = Y_5 W_0$). The amplitude of the first harmonic (W_1) is similar regardless of the number of harmonic components considered in the HBM, and it replicates the results obtained from the equivalent energy dissipation model. Further, when the equipment is at around 450 m depth, the value of W_3 is a maximum, indicating a resonance condition (since the frequency of W_3 matches the natural frequency of the system at this depth). Also, in this case, the phases ϕ_1 and ϕ_3 are both close to zero so the first and third harmonics reach their maxima simultaneously, which increases the total magnitude of the non-dimensional displacement, and consequently increases the force on the system relative to the solution with only one harmonic (i.e. the equivalent energy dissipation model). Similar behaviour occurs at a depth of 167 m, but in this case, the harmonic component that experiences a resonance condition is W_5, which also has a phase close to zero at this depth, so adds to the maximum displacement and force. These conclusions explain the features of the super-harmonic resonance that the system experiences and also explains why the smaller peak is only reproduced using the harmonic balance method considering the first, third, and fifth harmonic components.

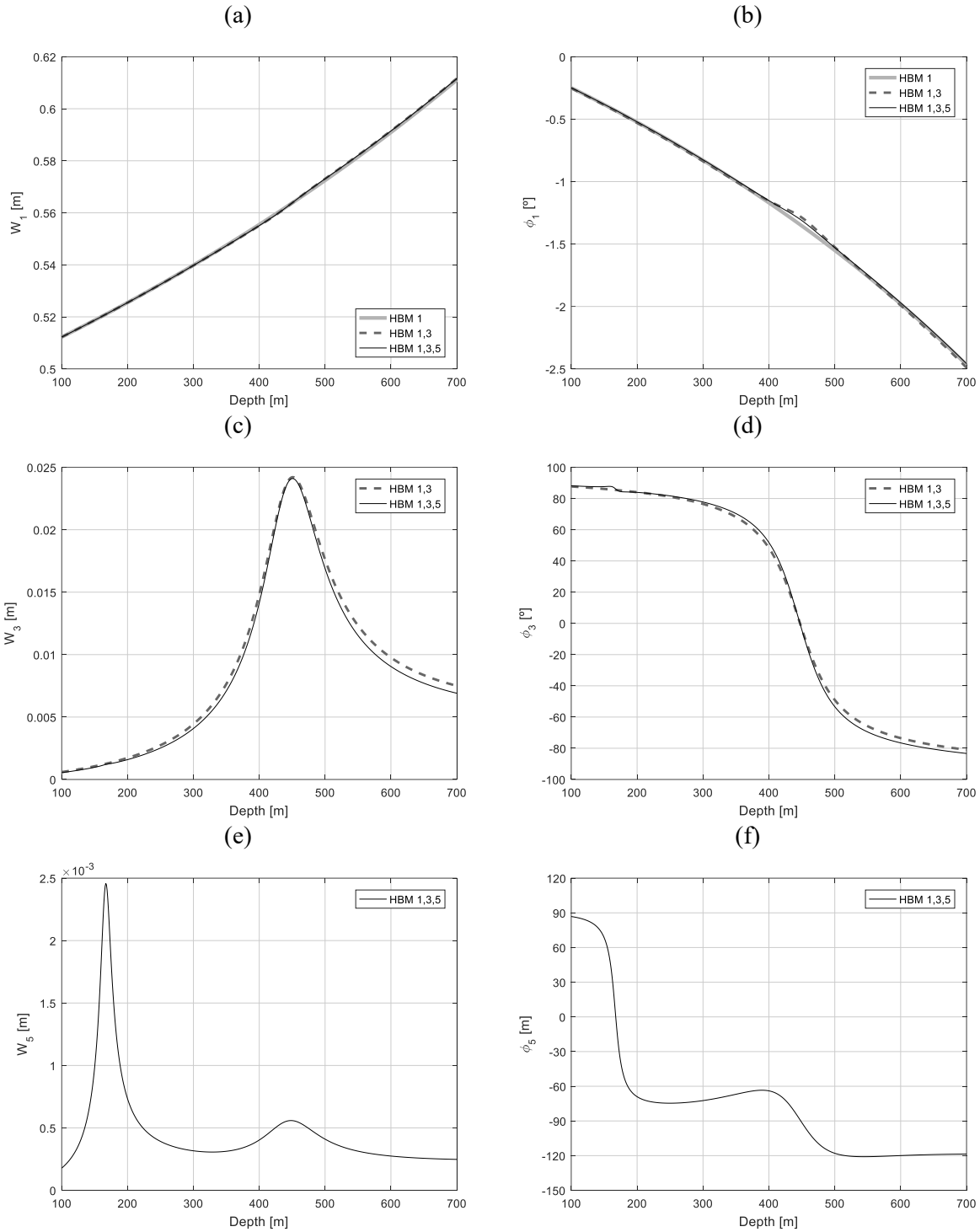

Figure 5.6: Amplitude and phase of each harmonic component as a function of depth. Input frequency 1 rad/s and input amplitude 0.5 m; (a) amplitude of the first harmonic, (b) phase of the first harmonic; (c) amplitude of the third harmonic, (d) phase of the third harmonic, (e) amplitude of the fifth harmonic, and (f) phase of the fifth harmonic.

More details of the dynamics of the system can be understood by observing the total magnitude of the dynamic displacement and of the velocity of the system as a function of depth for the different solutions, as presented in Figure 5.7. The maximum value of the dynamic displace-

ment increases due to the third and the fifth harmonics in the zones where super-harmonic resonance occurs, but the maximum velocity actually decreases for the second peak. This can be explained by the combination of the first and third harmonic components both with phases close to zero. The maximum velocity of the first harmonic then coincides with the minimum velocity of the third harmonic and vice versa. It is also notable that, comparing with the equivalent energy dissipation model (equivalent to HBM 1), at 450 m depth, an increase of only 4% in the maximum dynamic displacement leads to an increase of 35% in the maximum dynamic force. This is because the majority of the displacement of the equivalent energy dissipation model is quasi-static, directly from the motion of the vessel, whereas all of the additional displacement in the nonlinear case is dynamic. Hence, although there is only a small increase in the absolute displacement of the equipment, there is a large increase in its displacement relative to the vessel, which is what governs the dynamic force. This effect is important since, in some scenarios, as a result, dynamic amplification due to super-harmonic resonance may actually be the limiting design criterion. This reinforces the importance of understanding this type of behaviour and to take it into consideration when planning real operations. This conclusion also supports the use of constant hydrodynamic coefficients (i.e. neglecting the influence of the amplitude of oscillation via the Keulegan-Carpenter number) in this study since, in the super-harmonic resonances zones, the amplitude of the response is only slightly changed (4% in this example), which translates to minor variations of the hydrodynamic coefficients due to the variation of the Keulegan-Carpenter number.

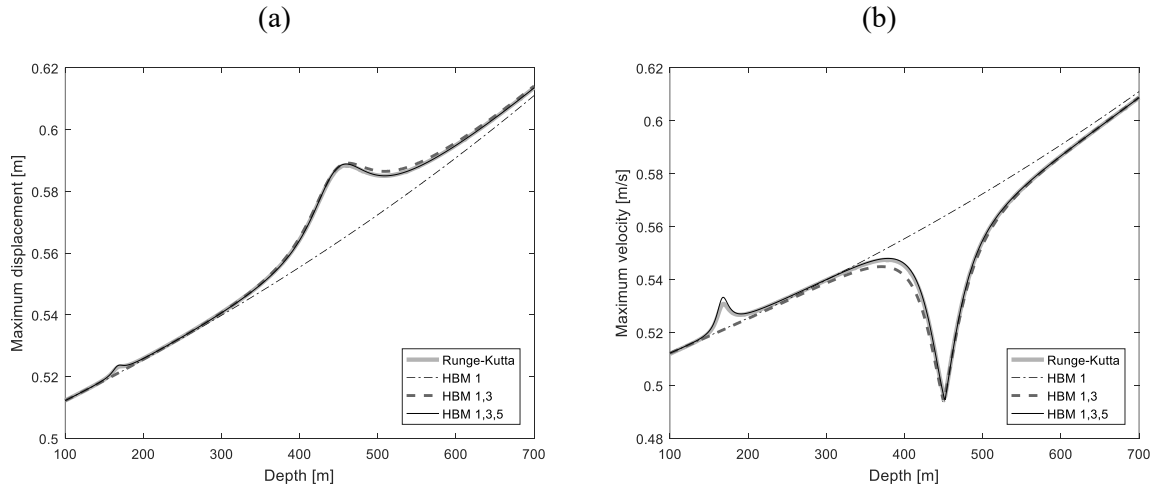

Figure 5.7: Maximum value of (a) the displacement and (b) the velocity of the equipment as a function of depth for the different solutions. Input frequency 1 rad/s and input amplitude 0.5 m.

The application of the harmonic balance method considering two or three harmonic components, as presented in Section 5.4.2, relies on the approximation of the quadratic drag term by an odd polynomial. This approximation depends on the maximum value considered for the velocity when applying the least squares procedure in Eq. (5.28). Observing Figure 5.7(b), the maximum deviation between the velocity amplitude of the first harmonic (almost the same as the maximum velocity obtained by HBM 1) and the velocity found by the Runge-Kutta solver is around 12%, at a depth of 450 m. In this case, the error introduced by the least squares fit (discounting the error introduced by considering a finite number of terms in the harmonic balance method) is lower than 1% in the dynamic force. This is mirrored in the low errors observed in Figure 5.5 and validates the approximation of using the velocity amplitude of the first harmonic as the range for the least squares fit in Eq. (5.28).

For illustration, the time domain solutions, at a depth of 450 m, are presented in Figure 5.8. As shown above, the deviations in the displacement for the different solutions are quite minor. The velocity plot shows a decrease in the peak values due to the combination of the odd harmonics; and the force plot exhibits a significant increase in its maximum values. Regarding the phase plane, the results obtained from the HBM 1,3, HBM 1,3,5, and Runge-Kutta solver deviate from the typical elliptical solution exhibited by the HBM using only the first harmonic, showing a flatter geometric form, indicating the presence of harmonics which are generated by nonlinearity.

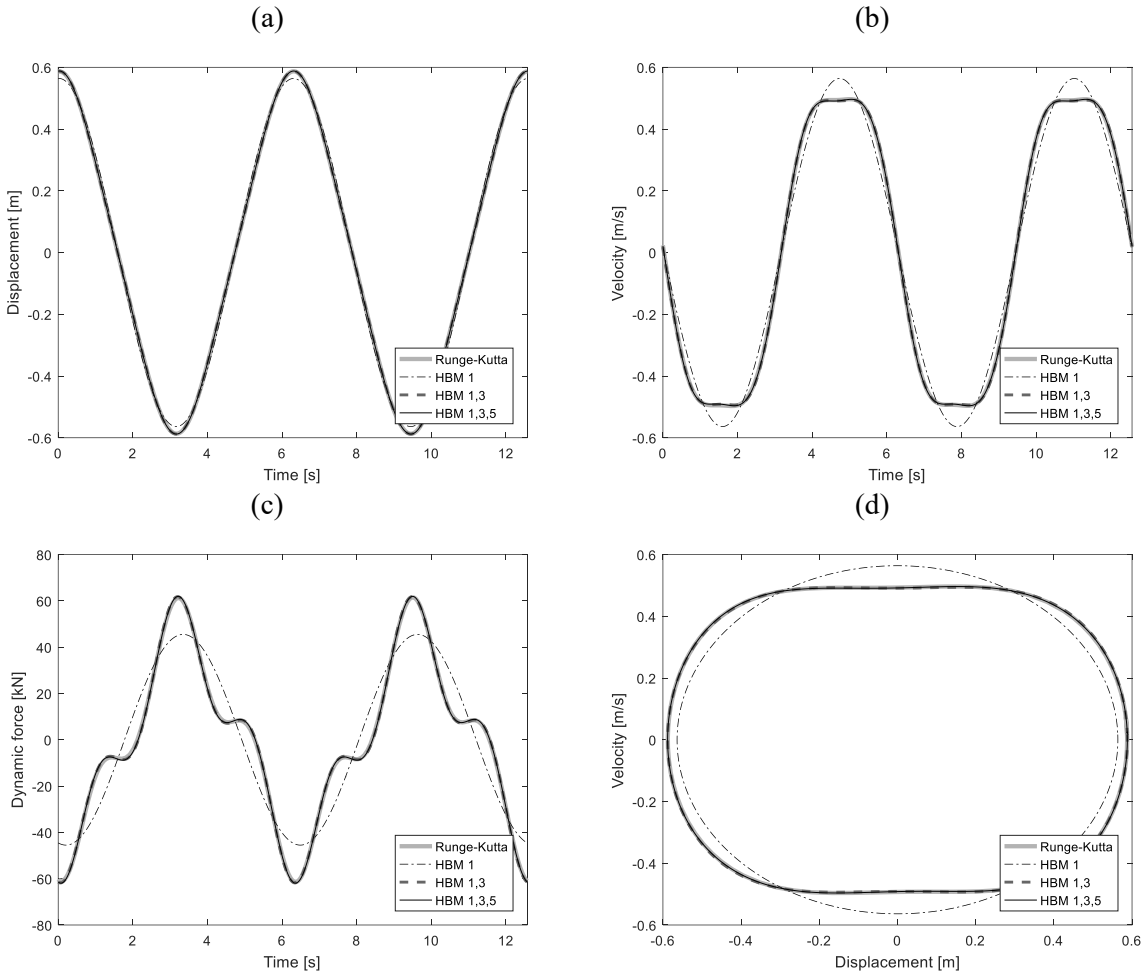

Figure 5.8: Time history responses and phase plane of the response of the system at a depth of 450 m for the different solutions. Input frequency 1 rad/s and input amplitude 0.5 m, (a) time response of the displacement, (b) time response of the velocity, (c) time response of the dynamic force, and (d) phase plane.

5.6 Dynamics of general subsea lifting systems under general conditions

The results presented in Section 5.5 illustrate the details of the super-harmonic resonance experienced by the example system in one specific condition: input frequency equal to 1 rad/s and input amplitude equal to 0.5 m, which corresponds to $0.192 \leq \gamma \leq 0.205$, $0.154 \leq \Lambda \leq 0.421$ and $0.006 \leq \alpha \leq 0.036$. More general conclusions about the dynamics of general subsea lifting systems and the accuracy of the harmonic balance method in different conditions can be obtained by plotting the maximum non-dimensional force as a function of the non-dimensional parameters of the system. In this case, the analysis can be simplified by noting that the term $\alpha\Lambda^2$ (which is equal to $mL^2\Omega^2/6EA$) in Eq. (5.13) can often be neglected. The ratio m/EA is a constant value, being equal to $8 \cdot 10^{-8}$ s^2/m^2 for a typical six-stranded steel wire cable, and the maximum value of the input frequency is around 1.5 rad/s in the Campos Basin, Brazil,

for example. Based on these conditions, the term $\alpha\Lambda^2$ is less than 0.1 when the length of the cable is less than 1800 m, which is applicable to many locations, including the Campos Basin. Consequently, the term $(1+\alpha\Lambda^2)$ can be approximated to unity (i.e. $\alpha\Lambda^2$ can be neglected) in Eq. (5.13) and hence only the parameters Λ and γ are needed to construct contour plots of the maximum dimensionless force.

The maximum dimensionless force and its percentage error when compared to the Runge-Kutta solution are presented in Figure 5.9 as a function of Λ and γ. Observing Figure 5.9(a), which accounts for the solution using HBM 1, the dimensionless force monotonically increases as a function of both Λ and γ. This is the expected behaviour of the equivalent energy dissipation model, which predicts higher forces when Λ approaches unity, but ignores the effects of the super-harmonic resonances. This lack of accuracy is highlighted in Figure 5.9(b), where the errors of HBM 1 compared to the Runge-Kutta solver are presented. In this case, the errors reach values up to -27 % when γ is lower than 0.4 and Λ is near $1/3$. The results obtained using HBM 1,3 are presented in Figure 5.9(c), which represents the 1:3 super-harmonic resonance by downward curves of the contour lines around $\Lambda = 1/3$. The other super-harmonic resonances are not represented, and the errors of HBM 1,3 (Figure 5.9(d)) are mainly observed around $\Lambda = 1/5$, reaching values up to 10 % when γ is close to 0.75. Finally, HBM 1,3,5 (Figure 5.9(e)) captures the 1:3 and 1:5 super-harmonic resonances, and the errors for this method (Figure 5.9(f)) are near zero for the majority of the range analysed, the maximum value obtained being 4 %, when $\Lambda = 1/7$.

The influence of the parameter γ on the dynamics of the system can be assessed by observing the results obtained using HBM 1,3,5 (Figure 5.9(e)). The impact of the super-harmonic resonances on the amplification of the dimensionless force is relatively higher when γ is smaller. When γ tends to zero and $\Lambda = 1/3$, the dimensionless force increases from 1.2 to 1.5, an increase of 25 % in a narrow range of Λ.

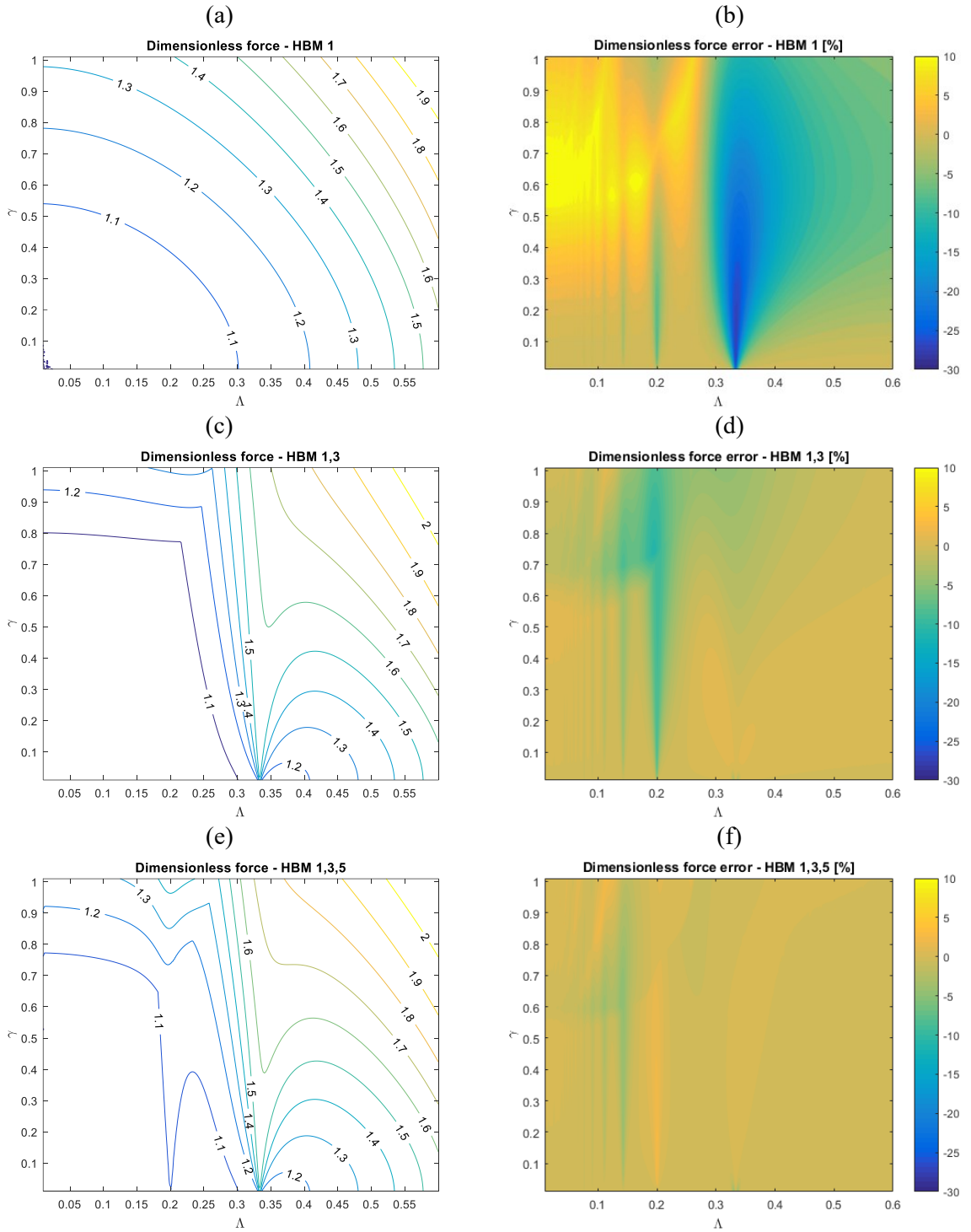

Figure 5.9: Dimensionless force and its percentage error in comparison to the Runge-Kutta solution as a function of the parameters Λ and γ, and assuming $\alpha = 0$. (a) Dimensionless force obtained by HBM 1, (b) dimensionless force error obtained by HBM 1, (c) Dimensionless force obtained by HBM 1,3, (d) dimensionless force error obtained by HBM 1,3, (e) Dimensionless force obtained by HBM 1,3,5, (f) dimensionless force error obtained by HBM 1,3,5.

Based on these results, it is possible to conclude that the introduction of more harmonic components reduces the errors of the harmonic balance method compared to the Runge-Kutta solution. Further, the introduction of higher harmonics in the HBM enables the representation of the super-harmonic resonance corresponding to the frequency of the harmonic components added. The 1:7 super-harmonic resonance and the subsequent ones could thus be represented by adding the harmonic term at seven times the input frequency and so on in the HBM. However, this would not lead to significant improvements in the results, as the HBM 1,3,5 has already presented errors close to zero in almost all the ranges of Λ and γ studied. Also, these higher super-harmonic resonances tend to occur in shallow waters (less than 100 m), where the influence of the ocean waves are important for the dynamical response of the system and, consequently, the model presented in Eq. (5.4) is not applicable anymore. The dimensionless force obtained by HBM 1,3,5 (Figure 5.9(e)) can thus be used as a simple and effective representation of the dynamics of general subsea lifting operations.

5.7 Operational weather window assessment

The main objective of a subsea lifting engineering analysis is to calculate the weather window for the operation, that is: the maximum significant wave height (H_s) where the operation can be performed safely as a function of the wave peak period (T_p). The goal of this section is therefore to conduct this analysis for the scenario presented in Table 5.1, comparing the results obtained by direct time domain integration using the Runge-Kutta solver, by the harmonic balance method considering the first, third, and fifth harmonics, and by the equivalent energy dissipation model (which is equivalent to HBM 1).

The lifting operation is considered to be performed by a typical subsea construction vessel, modelled by its vertical displacement Response Amplitude Operator (RAO) at the lifting point (i.e. the vessel frequency response function). The analysis is conducted assuming an equivalent regular excitation, according to the recommendations of DNVGL-RP-N103 [192]. In this case, the spectral response of the lifting point is given by:

$$S = |\mathrm{RAO}|^2 S_{\mathrm{wave}} \tag{5.33}$$

where S_{wave} is modelled, in this example, by a JONSWAP spectrum fitted for the Campos Basin, Brazil. Next, the standard deviation and the mean zero-up crossing angular frequency of the vertical displacement of the lifting point can be obtained via the moments of the spectrum

of the response:

$$\sigma = \sqrt{\int S \mathrm{d}\omega} \tag{5.34}$$

$$\omega_z = \sqrt{\frac{\int \omega^2 S \mathrm{d}\omega}{\int S \mathrm{d}\omega}} \tag{5.35}$$

The equivalent regular excitation amplitude can be found by considering the most probable largest value of a Rayleigh distribution:

$$W_0 = \sigma\sqrt{2\ln(n)} \tag{5.36}$$

where n is the number of input cycles expected during the operation, and considered equal to 1000, a common value used in real operations [180]. Further, the input frequency is considered equal to the mean angular frequency $\Omega = \omega_z$. Finally, the weather window is obtained by calculating the maximum significant wave height, as a function of the wave peak period, that does not violate the acceptance criteria: the maximum forces on the cable must be below the safe working loads of the system and the cable must always be taut. In this case, the equipment is considered to be initially positioned at 100 m depth since in shallower waters the effects of the ocean waves are relevant in the calculation of the hydrodynamic loads and, thus, the models presented in Sections 5.2 to 5.4 are not applicable.

The results are presented in Figure 5.10. The operational weather window obtained by the Runge-Kutta solver and by the HBM 1,3,5 are equal, supporting the outcomes of Sections 5.5 and 5.6, where low deviations between these models have been presented. On the other hand, the results obtained by the equivalent energy dissipation model predict higher values for the allowed significant wave height, especially in the range of wave peak periods varying from 6 to 9 seconds. The reasons for this behaviour can be addressed by analysing the path followed by the system on the $\gamma - \Lambda$ plot (Figure 5.11) as the equipment is lowered from 100 m to 700 m (Λ increasing). When $H_s = 2$ m and $T_p = 6$ s, the equipment crosses the 1:5 and 1:3 super-harmonic resonance zones, leading to a maximum non-dimensional force of 1.57 (Figure 5.11(b)). Since the equivalent energy dissipation model is not able to predict the super-harmonic resonance, the maximum non-dimensional force obtained is 1.30 (Figure 5.11(a)), corresponding to the maximum depth of 700 m. This explains the higher wave height limit found in the

weather window for this wave peak period using the equivalent energy dissipation model (Figure 5.10). When $H_s = 2.9$ m and $T_p = 8$ s, HBM 1,3,5 predicts a maximum non-dimensional force of 1.60, in contrast to the maximum of 1.22 obtained by the equivalent energy dissipation model, i.e. 23.8 % lower. This higher deviation of the dimensionless force between the models at this wave peak period ($T_p = 8$ s) is directly reflected in the operational weather window, where the equivalent energy dissipation model considers H_s up to 2.9 m acceptable, while HBM 1,3,5 and the Runge-Kutta method only allow H_s up to 2.2 m. For the scenario when $H_s = 2$ m and $T_p = 12$ s, only the 1:5 super-harmonic resonance zone is crossed and the non-dimensional force obtained by all the models is 1.34. Consequently, at this peak period, the limiting H_s is the same for all the models.

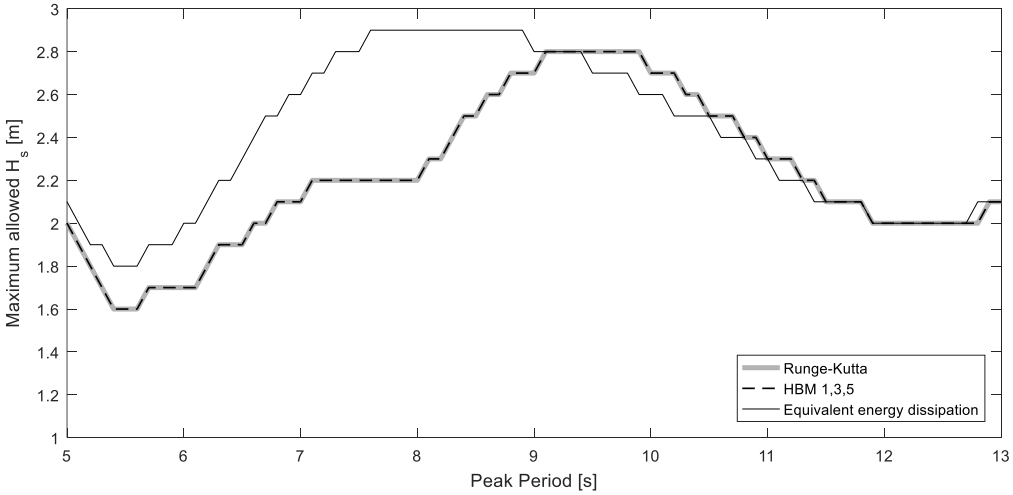

Figure 5.10: Maximum allowed significant wave height for the subsea lifting operation as a function of wave peak period for different solutions.

Based on these results, it is clear the importance of analysing the dynamics of the system by nonlinear models that are able to predict the amplification of forces due to the super-harmonic resonance. As presented in Figure 5.10, the use of equivalent energy dissipation models, typically used as a first guide to analyse subsea lifting operations [192], can lead to over-estimation of the safe operational wave height and thus could jeopardize the operation. Also, the assumption that the maximum loads on the system occur at the deepest condition when the system does not cross the fundamental resonance zone is equally not correct, and again can lead to risks for the operation. In this context, the harmonic balance method considering the first, third and fifth harmonic components can be used as an accurate and effective method to assess the dynamics of the system, as it presents results similar to those obtained via time domain integration, but up to 25 times faster (as per Section 5.5). Further, the graph of the dimensionless force in the

$\Lambda - \gamma$ space, such as presented in Figure 5.11(b), is an important tool for the analysis of subsea lifting operations, since the dynamic forces on the cable during a given operation can be directly obtained using this graph by just tracing the $\Lambda - \gamma$ path that the system follows as the payload is transported. In this case, direct interpretation of the dynamics of the system and the critical scenarios are obtained in a clear and concise way.

(a)

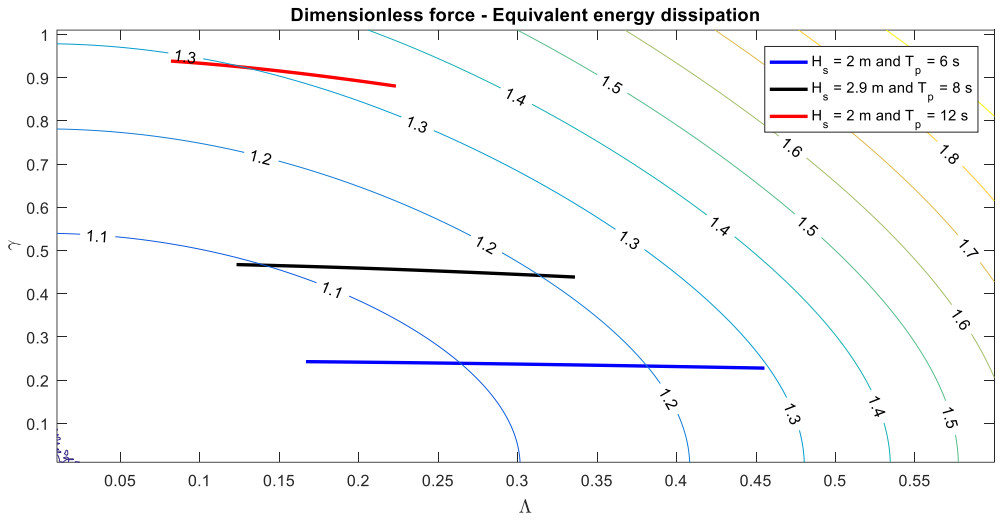

(b)

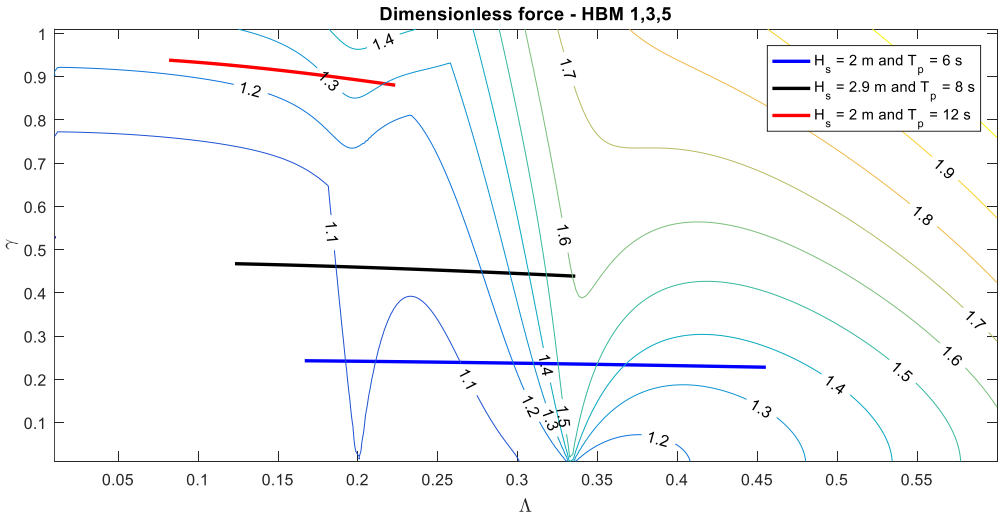

Figure 5.11: Path followed by the system, during a lowering operation, in $\gamma - \Lambda$ space in different representative sea states, with respect to contours of the dimensionless force, considering (a) the equivalent energy dissipation model and (b) the harmonic balance method using the first, third, and fifth harmonics.

5.8 Conclusions

The dynamics of deep water subsea lifting operations in super-harmonic resonance has been analysed in this study. Initially, a Runge-Kutta algorithm was used to integrate the nonlinear equation of motion of the system in the time domain. The results showed that the maximum

force on the lifting cable presented amplifications at depths where the input frequency was equal to an integer fraction of the natural frequency of the system, in contrast to the predictions obtained by the traditional equivalent energy dissipation model.

Then, a non-dimensional form of the equation of motion was presented, and the harmonic balance method was used to solve it and to identify the features of the super-harmonic resonance. The use of only one harmonic component for the response of the system yielded equal results to those obtained via the equivalent energy dissipation model, which motivated the inclusion of more harmonic components in the response of the system. In order to ease the algebraic calculations to apply the harmonic balance method using more than one component, the nonlinear quadratic drag term was expanded as an odd polynomial, whose coefficients were obtained by the least squares method.

For the scenario considered, the harmonic balance method using the first and third harmonic components was able to represent the 1:3 super-harmonic resonance, while the harmonic balance method considering the first, third, and fifth harmonic components could represent both the 1:3 and the 1:5 super-harmonic resonances. Further, in the super-harmonic resonance zones, the higher frequency harmonic terms showed an increase of their amplitudes, and their phases became equal to the phase of the first harmonic term, increasing the dynamic loads on the cable. In the example case, an increase of only 4 % in the maximum displacement of the equipment led to an increase of 35 % in the maximum force on the cable.

Next, the general dynamical behaviour of a generic subsea lifting system was presented by plotting the dimensionless maximum dynamic force and its error relative to the Runge-Kutta solution as a function of the dimensionless excitation frequency and the dimensionless damping using the different solutions. The results showed that the errors of the harmonic balance method using the first, third, and fifth harmonics were close to zero, except in the zone of the 1:7 super-harmonic resonance, where it could reach 4 %. This zone, however, is unlikely to be important, as it occurs in shallow waters where the influence of the ocean waves is important so different models are necessary. The use of the harmonic balance method considering the first and the third harmonics led to errors of up to 10 % in the zone of the 1:5 super-harmonic resonance, and less than 4 % otherwise.

Finally, the operational weather window was presented for the example scenario, comparing the different solutions and assuming regular equivalent excitation. The Runge-Kutta results were equal to those presented by the harmonic balance method using the first, third, and fifth

harmonics. In contrast, the equivalent energy dissipation model presented higher operational limits. This deviation was due to the dynamic amplifications when the system crossed the super-harmonic resonance zones, that were not represented by the equivalent energy dissipation model. This final result reinforced the importance of taking into account the super-harmonic resonances when analysing subsea lifting operations, as they can be the limiting design criterion in certain scenarios. In this context, the harmonic balance method considering the first, third and fifth harmonic components can be used as an accurate and effective method to assess the dynamics of the system, as it presented results similar to those obtained via time domain integration, but up to 25 times faster.

5.9 Appendix

This appendix presents the system of nonlinear algebraic equations for the harmonic balance method considering the first, third, and fifth harmonics as per Section 5.4.2.

$$\begin{aligned}
&8192Y_1^4\frac{(1-\Lambda^2)}{\Lambda^2\gamma}-8192Y_1^3\frac{(1+\alpha\Lambda^2)}{\Lambda^2\gamma}\cos(\phi_1)-12285Y_1^4Y_3\sin(3\phi_1-\phi_3)\\
&\quad-5775Y_1^4Y_5\sin(5\phi_1-\phi_5)-88200Y_1^3Y_3Y_5\sin(2\phi_1+\phi_3-\phi_5)\\
&\quad+187110Y_1^2Y_3^3\sin(3\phi_1-\phi_3)\\
&\quad+28350Y_1^2Y_3^2Y_5\sin(\phi_1-2\phi_3+\phi_5)\\
&\quad+1039500Y_1^2Y_3Y_5^2\sin(3\phi_1-\phi_3)\\
&\quad+1871100Y_1Y_3^3Y_5\sin(2\phi_1+\phi_3-\phi_5)\\
&\quad+5197500Y_1Y_3Y_5^3\sin(2\phi_1+\phi_3-\phi_5)\\
&\quad-1871100Y_3^4Y_5\sin(\phi_1-2\phi_3+\phi_5)\\
&\quad+1559250Y_3^3Y_5^2\sin(\phi_1+3\phi_3-2\phi_5)\\
&\quad-7796250Y_3^2Y_5^3\sin(\phi_1-2\phi_3+\phi_5)=0
\end{aligned}\tag{5.37a}$$

$$\begin{aligned}
&8192Y_1^3\frac{(1+\alpha\Lambda^2)}{\Lambda^2\gamma}\sin(\phi_1)+6930Y_1^5-5355Y_1^4Y_3\cos(3\phi_1-\phi_3)\\
&\quad-5775Y_1^4Y_5\cos(5\phi_1-\phi_5)+11340Y_1^3Y_3^2\\
&\quad+50400Y_1^3Y_3Y_5\cos(2\phi_1+\phi_3-\phi_5)+31500Y_1^3Y_5^2\\
&\quad+187110Y_1^2Y_3^3\cos(3\phi_1-\phi_3)\\
&\quad-595350Y_1^2Y_3^2Y_5\cos(\phi_1-2\phi_3+\phi_5)\\
&\quad+1039500Y_1^2Y_3Y_5^2\cos(3\phi_1-\phi_3)-561330Y_1Y_3^4\\
&\quad+1871100Y_1Y_3^3Y_5\cos(2\phi_1+\phi_3-\phi_5)-6237000Y_1Y_3^2Y_5^2\\
&\quad+5197500Y_1Y_3Y_5^3\cos(2\phi_1+\phi_3-\phi_5)-4331250Y_1Y_5^4\\
&\quad-1871100Y_3^4Y_5\cos(\phi_1-2\phi_3+\phi_5)\\
&\quad+1559250Y_3^3Y_5^2\cos(\phi_1+3\phi_3-2\phi_5)\\
&\quad-7796250Y_3^2Y_5^3\cos(\phi_1-2\phi_3+\phi_5)=0
\end{aligned}\tag{5.37b}$$

$$8192Y_1^2Y_3\frac{(1-9\Lambda^2)}{\Lambda^2\gamma}+1365Y_1^4\sin(3\phi_1-\phi_3)$$
$$-14700Y_1^3Y_5\sin(2\phi_1+\phi_3-\phi_5)-20790Y_1^2Y_3^2\sin(3\phi_1-\phi_3)$$
$$-18900Y_1^2Y_3Y_5\sin(\phi_1-2\phi_3+\phi_5)$$
$$-115500Y_1^2Y_5^2\sin(3\phi_1-\phi_3)$$
$$+311850Y_1Y_3^2Y_5\sin(2\phi_1+\phi_3-\phi_5)$$
$$+866250Y_1Y_5^3\sin(2\phi_1+\phi_3-\phi_5)$$
$$+1247400Y_3^3Y_5\sin(\phi_1-2\phi_3+\phi_5)$$
$$+1559250Y_3^2Y_5^2\sin(\phi_1+3\phi_3-2\phi_5)$$
$$+5197500Y_3Y_5^3\sin(\phi_1-2\phi_3+\phi_5)=0 \quad (5.37c)$$

$$13Y_1^5\cos(3\phi_1-\phi_3)-282Y_1^4Y_3+140Y_1^4Y_5\cos(2\phi_1+\phi_3-\phi_5)$$
$$-594Y_1^3Y_3^2\cos(3\phi_1-\phi_3)-180Y_1^3Y_3Y_5\cos(\phi_1-2\phi_3+\phi_5)$$
$$-1100Y_1^3Y_5^2\cos(3\phi_1-\phi_3)+1620Y_1^2Y_3^3$$
$$-8910Y_1^2Y_3^2Y_5\cos(2\phi_1+\phi_3-\phi_5)+9000Y_1^2Y_3Y_5^2$$
$$-8250Y_1^2Y_5^3\cos(2\phi_1+\phi_3-\phi_5)$$
$$+23760Y_1Y_3^3Y_5\cos(\phi_1-2\phi_3+\phi_5)$$
$$-14850Y_1Y_3^2Y_5^2\cos(\phi_1+3\phi_3-2\phi_5)$$
$$+49500Y_1Y_3Y_5^3\cos(\phi_1-2\phi_3+\phi_5)+5346Y_3^5+89100Y_3^3Y_5^2$$
$$+123750Y_3Y_5^4=0 \quad (5.37d)$$

$$8192Y_1^2Y_5\frac{(1-25\Lambda^2)}{\Lambda^2\gamma}+231Y_1^4\sin(5\phi_1-\phi_5)+8820Y_1^3Y_3\sin(2\phi_1+\phi_3-\phi_5)$$
$$+5670Y_1^2Y_3^2\sin(\phi_1-2\phi_3+\phi_5)$$
$$-187110Y_1Y_3^3\sin(2\phi_1+\phi_3-\phi_5)$$
$$-519750Y_1Y_3Y_5^2\sin(2\phi_1+\phi_3-\phi_5)$$
$$-374220Y_3^4\sin(\phi_1-2\phi_3+\phi_5)$$
$$-623700Y_3^3Y_5\sin(\phi_1+3\phi_3-2\phi_5)$$
$$-1559250Y_3^2Y_5^2\sin(\phi_1-2\phi_3+\phi_5)=0 \quad (5.37e)$$

$$11Y_1^5\cos(5\phi_1-\phi_5)+420Y_1^4Y_3\cos(2\phi_1+\phi_3-\phi_5)-2350Y_1^4Y_5$$
$$-270Y_1^3Y_3^2\cos(\phi_1-2\phi_3+\phi_5)-6600Y_1^3Y_3Y_5\cos(3\phi_1-\phi_3)$$
$$-8910Y_1^2Y_3^3\cos(2\phi_1+\phi_3-\phi_5)+27000Y_1^2Y_3^2Y_5$$
$$-74250Y_1^2Y_3Y_5^2\cos(2\phi_1+\phi_3-\phi_5)+37500Y_1^2Y_5^3$$
$$+17820Y_1Y_3^4\cos(\phi_1-2\phi_3+\phi_5)$$
$$-29700Y_1Y_3^3Y_5\cos(\phi_1+3\phi_3-2\phi_5)$$
$$+222750Y_1Y_3^2Y_5^2\cos(\phi_1-2\phi_3+\phi_5)+133650Y_3^4Y_5$$
$$+742500Y_3^2Y_5^3+343750Y_5^5=0 \quad (5.37f)$$

6. NONLINEAR DYNAMICS OF DEEP WATER SUBSEA LIFTING OPERATIONS CONSIDERING KC-DEPENDENT HYDRODYNAMIC COEFFICIENTS

The original version of this paper has been published in Ocean Engineering (v. 233, n. 109172, 2021) by R. B. Tommasini, T. L. Hill, J. H. G. Macdonald, R. Pavanello and L. O. Carvalho [202] addressing the objective n. 4 of this thesis (as per Section 1.2.3). This study analyses the dynamics of deep water subsea lifting operations considering KC-dependent hydrodynamic coefficients, building on the model proposed in Chapter 3 and on the analytical solution procedure described in Chapter 5. The aim is to address the impacts that variable hydrodynamic coefficients can have on the dynamics and planning of the operation.

Abstract

The dynamics of deep water subsea lifting operations considering hydrodynamic coefficients that depend on the Keulegan-Carpenter (KC) number are analysed in this study. Firstly, experimental data from the literature is presented for a typical subsea manifold, relating the added mass and drag coefficients to the amplitude of oscillation, represented by the KC number. Then, the nonlinear non-dimensional equation of motion, that considers the variable hydrodynamic coefficients, is presented. The solution of this equation is obtained via the harmonic balance method and by iterative time domain integration, and the results are compared to those of a conventional model with constant hydrodynamic coefficients. The results obtained via the harmonic balance method are considered almost as accurate as from the time domain integration, but require significantly less computational effort. Also, it is shown that the amplitude-dependent model predicts variations in the natural frequency and damping of the system as a function of the amplitude of the response of the payload. This results in significant differences in the maximum cable tension and the payload depth at which it occurs, compared with the constant hydrodynamic coefficient model. Hence this shows the importance of considering variable hydrodynamic coefficients when analysing subsea lifting systems.

Nomenclature

A_p	Vertical projected area of the payload
C_a	Added mass coefficient
C_d	Drag coefficient
D	Characteristic dimension of the payload
EA	Axial rigidity of the cable
F_{hyd}	Hydrodynamic force
F_{dyn}	Dynamic force on the cable
f	Dimensionless force on the cable
g	Gravity acceleration
KC	Keulegan-Carpenter number
L	Length of the cable
m	Mass per unit length of the cable
m_s	Equivalent submerged mass per unit length of the cable
M	Mass of the payload
N	Number of harmonic components in the Harmonic Balance Method
Re	Reynolds number
V	Volume of the payload
t	Time
w	Displacement of the payload
w_{st}	Static displacement of the payload
w_{dyn}	Dynamic displacement of the payload
w_0	Displacement of the input on the top of the cable
W	Amplitude of the displacement of the payload
W_0	Amplitude of the input displacement on the top of the cable
y	Dimensionless displacement of the payload
Y	Amplitude of the non-dimensional displacement of the payload
α	Dimensionless mass ratio
β	Dimensionless amplitude-dependent drag coefficient
γ	Dimensionless damping
μ	Dimensionless amplitude-dependent added mass coefficient
ϕ	Phase of the displacement of the payload
Λ	Frequency ratio

ρ	Density of sea water
Ω	Input frequency
ω_{n0}	Natural frequency of the system when KC $\rightarrow 0$
τ	Dimensionless time

6.1 Introduction

The exploration of offshore resources has progressively increased throughout past decades, led by the pioneering efforts of the oil and gas industry, and followed by the renewable energy and deep sea mining sectors. The construction of the subsea infrastructure required to enable these activities is usually done by subsea lifting operations via specialist barges or vessels, and correspond to a major part of the capital expenditure necessary to start the production of the field. Therefore, there is a pursuit in the industry to continuously improve these operations and reduce their costs. According to Job *et al.* [11], the costs of subsea manifold installations in the Brazilian shore has dropped by 86% since 2010 due to the improvements on the operational procedures and to the use of new technologies such as passive heave compensation and synthetic ropes. Further, Lacal-Arantégui *et al.* [28] reported the reduction of up to 70% on the installation time of offshore wind turbines and their foundations, which is one of the reasons for the overall cost reduction of offshore wind electricity last years. These studies strengthen the importance of new improvements to reduce the costs of subsea lifting operations and the positive impacts these enhancements can have on the viability of offshore exploration.

A common approach to improve these operations is to conceive more accurate models to predict the dynamics of subsea lifting systems. This gives more confidence in predictions of maximum cable tensions to ensure safety of the operation and more accurately define the operational weather window, hence saving costs, which can be extremely high for specialist vessels. In this direction, several works have been published dealing with the dynamics of the system when the payload crosses the wave zone. Li *et al.* [61] considered the installation of a spool piece by taking into account the influence of vessel shielding and transient load effects; Jeong *et al.* [65] presented a model that accounts for the possibility of collisions between the payload and the vessel during the operation; and Hannan and Bai [64] studied the nonlinear dynamics of a barge and a submerged payload subjected to constrained pendulum motions. Further, crane flexibility effects during the lift off phase of operations was covered by Park *et al.* [43] and Hong *et al.* [44]. The dynamics of the system when the equipment is lowered into deep waters is also an important phase to be analysed due to the possibility of resonance of the cable-payload system

at certain water depths. Classical approaches for this problem can be found in the works by Niedzwicki and Thampi [71], Huang [72], Driscoll *et al.* [73,74,76] where the dynamics of the system were modelled considering constant length cables. More recently, variable length models have been presented by Tommasini *et al.* [137,159], Gao *et al.* [85], Quan *et al.* [203] and Quan and Chang [86] highlighting the influence of the winch speed in the response of the system. Other examples of recent studies in this field cover the use of synthetic ropes to avoid resonance amplifications by de Araujo Neto *et al.* [81]; the development of a virtual reality simulation system to analyse the installation of subsea equipment by Zhang *et al.* [98]; and the analysis of the coupled dynamics of the vessel and the cable-equipment system, both numerically and experimentally, by Nam *et al.* [78]. Finally, a methodology for the assessment of the operational limits of marine operations was presented by Acero *et al.* [178].

A crucial aspect of the subsea lifting modelling is the hydrodynamic forces that are applied to the system due to the relative motion of the payload and the water. The traditional approach to model these forces is to use Morison's equation [118], which is a semi-empirical equation that considers the hydrodynamic force as the combination of an inertial term, proportional to the acceleration; and a drag term, proportional to the squared velocity. The use of this equation requires the knowledge of two coefficients: the added mass and the drag coefficient, which are usually a function of the geometry of the equipment and of dimensionless quantities, such as the Reynolds (Re) or Keulegan-Carpenter (KC) numbers.

Extensive research has been done describing these coefficients for simple geometries, especially for cylinders due to their recurrent use as a structural member in offshore structures. A classical reference on this subject is the book by Sarpkaya [120], which presented a review of the state-of-the-art on this topic and stressed the dependence of these coefficients on KC and Re in time-dependent flows. The hydrodynamics of flat plates have also been considered in several studies. Molin [124] presented a summary of his studies on the calculation of added mass and damping coefficients for perforated structures in oscillatory flows by using a theoretical model. His results indicated the dependence of the coefficients on the amplitude of oscillation and on the perforation of the plate, which was represented by a porous Keulegan-Carpenter number ($\widetilde{KC}$). Further, An and Faltinsen [125] showed a numerical and experimental study to evaluate the added mass and damping coefficients of perforated rectangular plates, taking into account the effects of perforation ratio, plate submergence, forcing period, and KC. Especially, dependence of the coefficients on KC was found to be higher than on the frequency when the plate was

deeply submerged. More recently, Mentzoni and Kristiansen [129–131] presented a series of numerical and experimental studies to evaluate the hydrodynamic coefficients of perforated plates. The results obtained were in agreement with previous references, reinforcing the dependence on the amplitude of oscillation. Other examples of studies addressing the determination of the hydrodynamics of simple shapes that highlight the influence of KC can be found in [126–128,204].

Subsea structures are usually more complex, and correlation to simple geometries are not always possible when evaluating their hydrodynamic coefficients. Although more scarce, direct evaluation of the coefficients for specific cases can also be found in the literature, for example Fernandes and Mineiro [132] calculated the translational and rotational hydrodynamic coefficients of subsea manifolds. The hydrodynamic coefficients of an ROV (Remotely Operated Vehicle) were presented by Avila and Adamowski [205], who showed that the influence of the amplitude of oscillation was higher than that of the period on the coefficients. A similar conclusion was obtained in the study by Mentzoni *et al.* [206], where simplified subsea structures were experimentally tested, and by Du *et al.* [135], analysing the hydrodynamic coefficients of a subsea manifold. Further, Solaas and Sandvik [134] presented a series of results for the hydrodynamic coefficients of suction anchors; and Computational Fluid Dynamics (CFD) was used by Holmes *et al.* [207] to evaluate the hydrodynamics of Blow-Out Preventers (BOP) as a function of KC. Finally, a summary of hydrodynamic coefficients for subsea structures was presented by Oritsland [208].

According to these references, there is strong dependence of the hydrodynamic coefficients on the amplitude of the oscillation, which is commonly represented by the KC number. Despite this conclusion, the majority of studies dealing with the dynamics of deep water subsea lifting operations considers constant added mass and drag coefficients in their models [71–74,76,85,86,137,159]. To the best knowledge of the authors, the only studies considering the influence of the amplitude of oscillation on the dynamics of the system are due to Ireland *et al.* [91] and Pestana *et al.* [136]. In the study by Ireland *et al.* [91], only the hydrodynamic damping was considered variable and the solution of the equation of motion was obtained iteratively. While in Pestana *et al.* [136], the dynamics of an example operation were assessed by running independent simulations considering all the pairs of added mass and drag coefficients obtained experimentally for different KC numbers. Therefore, the objective of this work is to extend the study about the dynamics of subsea lifting operations in deep waters considering the effects of KC-dependent hydrodynamic coefficients, focusing on (1) the deduction of a non-dimensional

nonlinear equation of motion for the system; (2) solution of the equation of motion by the harmonic balance method and by an iterative time domain integration algorithm; and (3) illustration of the dynamical features of the system when the hydrodynamic coefficients are KC-dependent.

The sequence of this paper is as follows: an overview of the hydrodynamics of oscillating bodies including the experimental results from the literature of the KC-dependent hydrodynamic coefficients of a typical subsea manifold in Section 6.2, the deduction of the non-dimensional nonlinear equation of motion in Section 6.3, the solution of the equation of motion via the harmonic balance method and via the iterative time domain integration in Section 6.4, the results obtained in Section 6.5, and the conclusions in Section 6.6.

6.2 KC-dependent hydrodynamics of a subsea manifold

An object lifted in deep waters by typical crane vessels experiences an oscillatory motion as a result of the movement of the vessel being excited by the ocean waves. This oscillatory flow introduces hydrodynamic forces on the payload that must be assessed in order to predict the dynamics of the system during the operation. According to Sarpkaya [120], in time-dependent flows such as this, the direction of the wake changes from upstream to downstream as the velocity of the payload changes sign, the flow may alter from laminar to turbulent regimes, and the equipment may oscillate inside its own wake. Due to the complexity of this flow and to the non-trivial geometry of real equipment, no closed solution is available to represent the hydrodynamic forces that are generated. The representation of these forces must rely on empirical or semi-empirical relations calibrated via experiments or Computational Fluid Dynamics (CFD).

Historically, Morison's equation [118] has been used to approximate these forces. In this formulation, the hydrodynamic load is split into a term proportional to the acceleration and a term proportional to the squared velocity. Therefore, for a body oscillating in a stationary fluid, the hydrodynamic force is given by:

$$F_{\mathrm{hyd}} = -\rho V C_a \ddot{w} - \frac{1}{2}\rho C_d A_p \dot{w}|\dot{w}| \tag{6.1}$$

where ρ is the density of the sea water, V is the volume of the structure, A_p is the vertical projected area, $\dot{w}$ is the velocity, $\ddot{w}$ is the acceleration, C_a is the added mass coefficient, and C_d is the drag coefficient. These two coefficients must be determined to represent the forces on the system.

Experimental data for KC-dependent added mass and drag coefficients of typical subsea manifolds were presented by Pestana *et al.* [136]. In their study, 1:35 scale models were used to perform oscillatory tests in a calm fluid for various $\mathrm{KC} = 2\pi W/D$, where W is the amplitude of the oscillation and D is the characteristic length of the body (i.e. its width). The influence of the frequency was not considered, relying on several references [205,206,209] that indicate the preponderance of the amplitude of oscillation in comparison to the frequency. The frequency of the tests was equal to 0.59 Hz, which corresponds to a period of 10 s in the true scale. The test water depth was 2.5 m and oscillations were performed horizontally. Each test consisted of twenty cycles that were repeated three times for each amplitude and the coefficients were obtained via a least squares algorithm. The base plate of the manifold presents some small perforations, but they are less than 5% of the total vertical projected area. Further details of the experimental set-up and methodology can be found in Pestana *et al.* [136].

One piece of equipment analysed in [136] is considered as an example payload to evaluate the dynamics of the deep water subsea lifting operation. The geometric data for this subsea manifold is presented in Table 6.1 and a photograph of the scale model is presented in Figure 6.1.

Table 6.1: Geometric data for the manifold used as the example in this study (extracted from Pestana *et al.* [136]).

Variable		Value
Subsea manifold	Mass (M)	170 tonnes
	Volume (V)	21.8 m^3
	Projected area (A_p)	144.5 m^2
	Length	14.9 m
	Width	9.7 m
	Height	3.8 m

The experimental results obtained in Pestana *et al.* [136] for the added mass and drag coefficients as a function of KC are presented in Figure 6.2, together with the fitted curves obtained by using the least squares method. Note that, for consistency with the dynamic models used in this study, the inertia coefficient based on the envelope of the manifold (as in Pestana *et al.* [136]) is replaced by the added mass coefficient based on the actual volume of the manifold[6]. For the range of KC considered, a linear trend in the added mass coefficient and a shifted reciprocal behaviour for the drag coefficient as KC increases are observed. This general behaviour is

[6] In this study, the added mass coefficients are larger than those presented by Pestana *et al.* [136] since the actual volume of the manifold is less than the envelope volume. Nonetheless, the added mass is still equal in both studies.

in agreement with the data for other pieces of equipment tested by Pestana *et al.* [136] and other results in the literature [126,128,129].

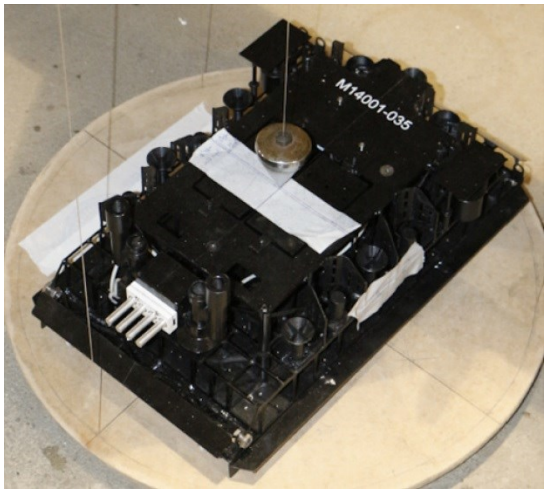

Figure 6.1: 1:35 scale model manifold considered in this study and analysed by Pestana *et al.* [136] (picture courtesy of Petrobras).

(a) (b)

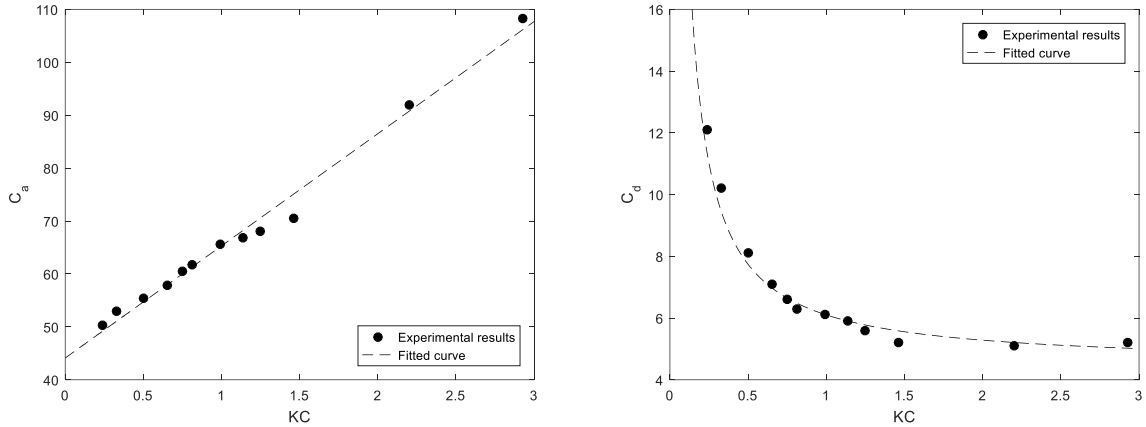

Figure 6.2: Hydrodynamic coefficients for the subsea manifold as a function of KC: (a) added mass coefficient, and (b) drag coefficient (data extracted from Pestana *et al.* [136]).

The general form of the equations for the hydrodynamic coefficients as a function of KC are given by:

$$C_a = C_{a_0} + C_{a_1}\mathrm{KC} \tag{6.2}$$

$$C_d = C_{d_0} + C_{d_1}(\mathrm{KC})^{-1} \tag{6.3}$$

The coefficients obtained experimentally for this manifold are $C_{a_0} = 44.1$, $C_{a_1} = 21.2$, $C_{d_0} = 4.5$, and $C_{d_1} = 1.6$. Constant added mass and drag coefficients are also evaluated in order to compare the results obtained from the KC-dependent model to the results obtained by using constant coefficients. In this case, the constant coefficients are chosen assuming a KC number of unity, such that $\bar{C}_a = 65.3$ and $\bar{C}_d = 6.1$. A summary of the coefficients considered in this

study is presented in Table 6.2.

Table 6.2: Summary of the hydrodynamic coefficients considered for the subsea manifold in this study.

Model	Added mass (C_a)	Drag (C_d)
KC-dependent coefficients	$44.1 + 21.2\text{KC}$	$4.5 + 1.6(\text{KC})^{-1}$
Constant coefficients	65.3	6.1

6.3 The dynamics of deep water subsea lifting operations

Section 6.2 presented the hydrodynamic modelling of the subsea manifold under steady state oscillatory motion in a calm fluid. It is now necessary to construct a model to predict the dynamics of the system that accounts for the KC dependence of the hydrodynamic coefficients (Figure 6.3).

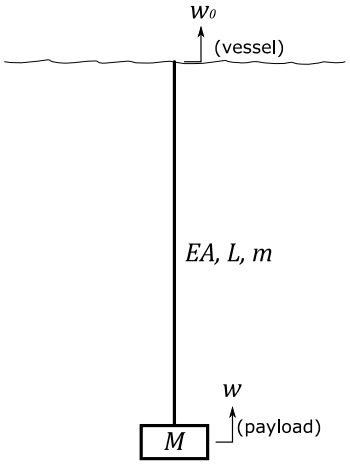

Figure 6.3: Representation of the single degree-of-freedom model for the evaluation of deep water subsea lifting operations.

The first assumption in this direction is to consider only the deep water phase of the lowering operation, hence the influence of the ocean waves on the payload is not considered in this study. This is in agreement with the experimental set-up that considered the object oscillating in a calm fluid.

Next, Driscoll *et al.* [73] showed, by analysing measurements from a real operation, that unidimensional models were sufficient to predict the dynamics of the payload due to the vessel excitation. Also, Tommasini *et al.* [137] showed that single degree-of-freedom and discretized models (e.g. the software Orcaflex) predict similar responses in typical subsea lifting scenarios. Therefore, a single degree-of-freedom model is considered in this study, which is also a common approach in the literature [71,72,137,159,193].

Another recurrent assumption in the literature [71,76,137,203] is to consider the dynamics of the vessel to be independent of the dynamics of the cable-equipment system, due to a large difference in mass. Thus, the vertical displacement of the lifting point is prescribed as an imposed displacement to the top of the cable.

Further, snap loads are not represented in this formulation, as in [74,86,137]. This is in agreement with the recommended practice DNVGL-RP-N103 [192] that requires the cable to be always taut during subsea lifting operations. Scenarios that lead to slack conditions should then be classified as unsafe during the planning of the operation.

Finally, the cable is assumed to have constant unloaded length during the analysis, such that evaluation of the full lowering into deep waters is conducted by running several independent simulations considering different depths for the payload. This is especially important in operations that require constant interruptions of the lowering process, such as in subsea load transfers [194] or when successive slings are added to the lifting line [2].

The equation of motion for this system, considering the assumptions presented above, was obtained by Tommasini *et al.* [137]. In their study, the kinetic and potential energies were calculated for the cable and payload, and the hydrodynamic forces were assumed to be a non-conservative generalized force. Using Lagrange's equation, the equation of motion obtained was:

$$\left(M + \rho V C_a + \frac{1}{3}mL\right)\ddot{w} + \frac{1}{2}\rho A_p C_d |\dot{w}|\dot{w} + \frac{EA}{L}w = \frac{EA}{L}w_0 - \frac{mL}{6}\ddot{w}_0 - \left(M - \rho V + \frac{m_s L}{2}\right)g \tag{6.4}$$

where m is the mass per unit length of the cable, L is the suspended length of the cable, EA is the rigidity of the cable, w is the displacement of the structure, w_0 is the displacement of the lifting point, $\ddot{w}_0$ is the acceleration of the lifting point, m_s is the equivalent submerged mass of the cable, and g is the gravitational acceleration.

Substituting Eqs. (6.2) and (6.3) into Eq. (6.4) and considering $\mathrm{KC} = 2\pi W/D$, the equation of motion becomes:

$$\left(M + \rho V C_{a_0} + \frac{1}{3}mL\right)\ddot{w} + \frac{2\pi\rho V C_{a_1} W}{D}\ddot{w} + \frac{1}{2}\rho A_p C_{d_0}|\dot{w}|\dot{w} + \frac{\rho A_p C_{d_1} D}{4\pi W}|\dot{w}|\dot{w} + \frac{EA}{L}w = \frac{EA}{L}w_0 - \frac{mL}{6}\ddot{w}_0 - \left(M - \rho V + \frac{m_s L}{2}\right)g \tag{6.5}$$

This equation presents two new nonlinear terms in addition to the traditional added mass and

quadratic drag terms. The first one is an amplitude-dependent term proportional to the acceleration and the second term is inversely dependent on the amplitude and proportional to the square of the velocity.

The solution of this equation can be split into static and dynamic parts ($w = w_{\mathrm{st}} + w_{\mathrm{dyn}}$) and the solution of Eq. (6.5) can be obtained by solving the following independent equations:

$$\frac{EA}{L} w_{\mathrm{st}} = -\left(M - \rho V + \frac{m_s L}{2}\right) g \tag{6.6}$$

$$\begin{aligned}\left(M + \rho V C_{a_0} + \frac{1}{3} mL\right) \ddot{w}_{\mathrm{dyn}} + \left(\frac{2\pi \rho V C_{a_1} W}{D}\right) \ddot{w}_{\mathrm{dyn}} + \frac{1}{2} \rho A_p C_{d_0} |\dot{w}_{\mathrm{dyn}}| \dot{w}_{\mathrm{dyn}} \\ + \frac{\rho A_p C_{d_1} D}{4\pi W} |\dot{w}_{\mathrm{dyn}}| \dot{w}_{\mathrm{dyn}} + \frac{EA}{L} w_{\mathrm{dyn}} = \frac{EA}{L} w_0 - \frac{mL}{6} \ddot{w}_0\end{aligned} \tag{6.7}$$

Next, the static force acting on the top of the cable can be directly obtained by the submerged weight of the cable and the payload. Meanwhile, the dynamic force acting on the cable is given by:

$$F_{\mathrm{dyn}} = \frac{EA}{L} \left(w_0 - w_{\mathrm{dyn}}\right) \tag{6.8}$$

The static displacement of the equipment can be directly obtained from Eq. (6.6), but evaluation of the dynamic response is more challenging, since it requires the solution of a nonlinear differential equation. In order to reduce the number of independent variables, Eq. (6.7) can be written in non-dimensional form. So, assuming a harmonic input for the displacement at the top of the cable:

$$w_0 = W_0 \cos(\Omega t) \tag{6.9}$$

and introducing the following dimensionless variables:

$$\tau = \omega_{n0} t \tag{6.10}$$

$$\Lambda = \frac{\Omega}{\omega_{n0}} \tag{6.11}$$

$$y = \frac{w_{\mathrm{dyn}}}{W_0} \tag{6.12}$$

where ω_{n0} is the natural frequency of the system when $\mathrm{KC} \to 0$:

$$\omega_{n0} = \sqrt{\frac{EA}{L\left(M + \rho V C_{a_0} + \frac{1}{3}mL\right)}} \tag{6.13}$$

it is possible to re-write Eq. (6.7) in the non-dimensional form:

$$(1 + \mu Y)y'' + \left(\gamma + \frac{\beta}{Y}\right)|y'|y' + y = (1 + \alpha\Lambda^2)\cos(\Lambda\tau) \tag{6.14}$$

In this case, y' and y'' denote the single and double differentiation of y with respect to τ, respectively, Y is the amplitude of y, and the new parameters of the system are defined as:

$$\alpha = \frac{mL}{6\left(M + \rho V C_{a_0} + \frac{1}{3}mL\right)} \tag{6.15}$$

$$\gamma = \frac{\rho A_p C_{d_0} W_0}{2\left(M + \rho V C_{a_0} + \frac{1}{3}mL\right)} \tag{6.16}$$

$$\mu = \frac{2\pi\rho V C_{a_1} W_0}{D\left(M + \rho V C_{a_0} + \frac{1}{3}mL\right)} \tag{6.17}$$

$$\beta = \frac{\rho A_p C_{d_1} D}{4\pi\left(M + \rho V C_{a_0} + \frac{1}{3}mL\right)} \tag{6.18}$$

The mass ratio (α) and the dimensionless damping (γ) are related to the constant terms of the hydrodynamic coefficients (C_{a_0} and C_{d_0}). On the other hand, the dimensionless amplitude-dependent added mass coefficient (μ) and the dimensionless amplitude-dependent drag coefficient (β) are new parameters introduced in the system, and they are related to the KC-dependent terms of the hydrodynamic coefficients (C_{a_1} and C_{d_1}). Finally, the non-dimensional form of the dynamic force on the cable is given by:

$$f = \frac{F_{\text{dyn}}}{W_o\left(M + \rho V C_{a_0} + \frac{1}{3}mL\right)\Omega^2} \tag{6.19}$$

which can be presented in non-dimensional form as:

$$f = \frac{1}{\Lambda^2}(y_0 - y) \tag{6.20}$$

where $y_0 = \cos(\Lambda\tau)$.

6.4 Solution of the nonlinear equation of motion

After presenting the non-dimensional equation of motion considering amplitude-dependent hydrodynamic coefficients, it is necessary to present the methods to solve this equation. To this end, this study considers two different approaches: an iterative procedure for the time domain integration, presented in Section 6.4.1; and an analytical approach based on the Harmonic Balance Method (HBM), presented in Section 6.4.2.

Aiming to compare the results obtained by using KC-dependent hydrodynamic coefficients, the dynamics of the system with constant hydrodynamic coefficients is obtained directly from time domain integration of Eq. (6.14) considering $\mu = \beta = 0$ and substituting the constant coefficients from Table 6.2 for C_{a_0} and C_{d_0}. A Runge-Kutta solver is used via the Matlab function 'ode45'.

6.4.1 Iterative time domain integration

The equation of motion presented in Eq. (6.14) is nonlinear, including the term $\gamma|y'|y'$ and the amplitude-dependent terms $\mu Y y''$ and $\beta Y^{-1}|y'|y'$. Due to the presence of these two amplitude-dependent terms, time domain integration of Eq. (6.14) is not straightforward, as knowledge of the amplitude of the response is not available a priori. A simple way to deal with this fact is to use an iterative procedure, as presented in Table 6.3, where ϵ is the tolerance for the convergence of the algorithm.

Similarly to the constant coefficient case, time domain integration of Eq. (6.14) has been obtained by using a Runge-Kutta solver, implemented via the 'ode45' function in Matlab.

Table 6.3: Algorithm for the iterative time domain integration of the equation of motion.

1. Set an initial value for Y
2. Solve Eq. (6.14) in the time domain
3. Obtain the steady state amplitude of y: $Y_{\text{new}} = [\max(y) - \min(y)]/2$
4. Check convergence of Y using $|Y_{\text{new}} - Y| < \epsilon Y$
5. If convergence has been achieved, stop; otherwise, return to 2 using $Y = Y_{\text{new}}$

6.4.2 Harmonic Balance Method

The steady state response of Eq. (6.14) can also be obtained by using analytical procedures, which can provide deeper understanding of the dynamics of the system and faster results. In this study, the Harmonic Balance Method [197–199] is used to solve the equation of motion

analytically. The non-dimensional displacement is assumed to be represented by a truncated Fourier series:

$$y = \sum_{k=1}^{N} Y_k \cos(k\Lambda\tau + \phi_k) \tag{6.21}$$

This approximation is substituted into the equation of motion and the solution is obtained by determining the values of the amplitudes and phases of each harmonic component.

6.4.2.1 Solution considering the first harmonic component

A first approximation for the response of the system can be obtained by taking only the first harmonic as the response of the system:

$$y = Y_1 \cos(\Lambda\tau + \phi_1) \tag{6.22}$$

Substituting Eq. (6.22) into Eq. (6.14) leads to:

$$\begin{aligned} -(1+\mu Y_1)Y_1\Lambda^2 \cos(\Lambda\tau+\phi_1) - (\gamma Y_1+\beta)Y_1\Lambda^2 |\sin(\Lambda\tau+\phi_1)| \sin(\Lambda\tau+\phi_1) \\ + Y_1 \cos(\Lambda\tau+\phi_1) = (1+\alpha\Lambda^2)\cos(\Lambda\tau) \end{aligned} \tag{6.23}$$

The quadratic term $|\sin(\Lambda\tau+\phi_1)| \sin(\Lambda\tau+\phi_1)$ can be approximated by a Fourier series keeping only the first term, such that:

$$|\sin(\Lambda\tau+\phi_1)| \sin(\Lambda\tau+\phi_1) \cong \frac{8}{3\pi}\sin(\Lambda\tau+\phi_1) \tag{6.24}$$

Substituting Eq. (6.24) into Eq. (6.23) leads to:

$$\begin{aligned} -(1+\mu Y_1)Y_1\Lambda^2 \cos(\Lambda\tau+\phi_1) - \frac{8}{3\pi}(\gamma Y_1+\beta)Y_1\Lambda^2 \sin(\Lambda\tau+\phi_1) \\ + Y_1 \cos(\Lambda\tau+\phi_1) = (1+\alpha\Lambda^2)\cos(\Lambda\tau) \end{aligned} \tag{6.25}$$

Making the variable substitution $\Lambda\tau + \phi_1 = \Lambda\hat{\tau}$ and expanding the trigonometric function:

$$\begin{aligned} (1-\Lambda^2-\mu Y_1\Lambda^2)Y_1 \cos(\Lambda\hat{\tau}) - \frac{8}{3\pi}(\gamma Y_1+\beta)Y_1\Lambda^2 \sin(\Lambda\hat{\tau}) \\ = (1+\alpha\Lambda^2)\cos(\Lambda\hat{\tau})\cos(\phi_1) + (1+\alpha\Lambda^2)\sin(\Lambda\hat{\tau})\sin(\phi_1) \end{aligned} \tag{6.26}$$

Equating the coefficients of $\cos(\Lambda\hat{\tau})$ and $\sin(\Lambda\hat{\tau})$ on both sides of the Eq. (6.26) results in:

$$(1-\Lambda^2-\mu Y_1\Lambda^2)Y_1=(1+\alpha\Lambda^2)\cos\phi_1 \tag{6.27a}$$

$$-\frac{8}{3\pi}(\gamma Y_1+\beta)\Lambda^2 Y_1=(1+\alpha\Lambda^2)\sin\phi_1 \tag{6.27b}$$

Adding the squares of these two equations leads to the following quartic equation for the amplitude of the non-dimensional displacement:

$$\left[\left(\frac{8\gamma\Lambda^2}{3\pi}\right)^2+(\mu\Lambda^2)^2\right]Y_1^4+\left[2\mu\Lambda^4-2\mu\Lambda^2+\frac{128\gamma\beta\Lambda^4}{9\pi^2}\right]Y_1^3 + \left[(1-\Lambda^2)^2+\left(\frac{8\beta\Lambda}{3\pi}\right)^2\right]Y_1^2-(1+\alpha\Lambda^2)^2=0 \tag{6.28}$$

Further, the phase of the response can be obtained by:

$$\phi_1=\arctan\left[\frac{-(\gamma Y_1+\beta)8\Lambda^2}{3\pi(1-\Lambda^2-\mu Y_1\Lambda^2)}\right] \tag{6.29}$$

The amplitude of the non-dimensional displacement (Y_1) is obtained by solving Eq. (6.28) (via the Matlab function 'roots' in this study). This equation leads to four possible solutions; however, only positive real values are physically significant. The stability of each solution is assessed by substituting it into Eq. (6.14) as an initial condition and checking if the response of the system maintains the calculated response or diverges to a different condition.

The amplitude of the dimensionless dynamic force on the cable can then be obtained from Eq. (6.20) by considering the difference of two sine waves with the same frequency:

$$f_{\max}=\frac{\sqrt{1+Y_1^2-2Y_1\cos\phi_1}}{\Lambda^2} \tag{6.30}$$

Finally, the maximum tension at the top and the maximum and minimum tension at the bottom of the cable can be obtained by combining the static weight of the system and the amplitude of the dynamic force (via Eq. (6.19)):

$$F_{\mathrm{top}_{\max}}=(M-\rho V+m_sL)g+\frac{EAW_0}{L}\sqrt{1+Y_1^2-2Y_1\cos\phi_1} \tag{6.31a}$$

$$F_{\mathrm{bot}_{\max}}=(M-\rho V)g+\frac{EAW_0}{L}\sqrt{1+Y_1^2-2Y_1\cos\phi_1} \tag{6.31b}$$

$$F_{\mathrm{bot}_{\min}}=(M-\rho V)g-\frac{EAW_0}{L}\sqrt{1+Y_1^2-2Y_1\cos\phi_1} \tag{6.31c}$$

The maximum forces must then be compared to the structural limits of the cable and payload and the minimum force should always be positive to comply with the safety requirements during real operations.

6.4.2.2 Solution considering the first and third harmonic components

The quadratic term $|y'|y'$ is an anti-symmetric nonlinear function that introduces odd harmonics in the response of the system when a sinusoidal input is considered. In order to increase the accuracy for the response of the system, and also to be able to represent super-harmonic resonances (as presented in [137]), these higher harmonics can be included in the assumed solution for y.

Considering the first and third harmonics, the non-dimensional displacement is represented by:

$$y = Y_1 \cos(\Lambda\tau + \phi_1) + Y_3 \cos(3\Lambda\tau + \phi_3) \tag{6.32}$$

Substitution of Eq. (6.32) into Eq. (6.14) results in difficulties in representing the quadratic nonlinear term as a Fourier series, as presented in Eq. (6.24). This difficulty can be avoided by approximating the quadratic term by a cubic polynomial:

$$y'|y'| \cong A_1 y' + A_3 {y'}^3 \tag{6.33}$$

As the function $y'|y'|$ does not have smooth derivatives, the coefficients A_i cannot be calculated directly via a Taylor series. Alternatively, these coefficients may be found via a least squares fit of the nonlinear function. Considering the amplitude of the first harmonic as the maximum non-dimensional velocity to make the fit, the coefficients A_i can be obtained by the following minimization problem:

$$\text{min:} \quad \int_0^{\Lambda Y_1} \left({y'}^2 - A_1 y' - A_3 {y'}^3\right)^2 \mathrm{d}y' \tag{6.34}$$

where only the positive non-dimensional velocities are needed in the evaluation of the integral due to the anti-symmetry of $y'|y'|$.

Furthermore, the amplitude of the response of the non-dimensional displacement is assumed to be equal to the amplitude of only the first harmonic term ($Y = Y_1$), relying on the fact that, whilst higher harmonics contribute to the total force on the cable, they have a negligible contribution to the total displacement of the payload. Therefore, the non-dimensional equation of motion becomes:

$$(1+\mu Y_1)y'' + \left(\gamma + \frac{\beta}{Y_1}\right)\left(\frac{5\Lambda Y_1}{16}y' + \frac{35}{48\Lambda Y_1}y'^3\right) + y = (1+\alpha\Lambda^2)\cos(\Lambda\tau) \tag{6.35}$$

Substituting Eq. (6.32) into Eq. (6.35) and applying a similar procedure as presented above for the solution with only one harmonic component, it is possible to obtain a nonlinear algebraic system of equations for the amplitudes and phases of each harmonic component:

$$\begin{aligned} &64(1-\Lambda^2-\mu\Lambda^2Y_1)Y_1 - 105(\gamma Y_1+\beta)\Lambda^2 Y_3\sin(3\phi_1-\phi_3) \\ &\qquad - 64(1+\alpha\Lambda^2)\cos(\phi_1) = 0 \end{aligned} \tag{6.36a}$$

$$\begin{aligned} &55(\gamma Y_1+\beta)\Lambda^2 Y_1^2 + 630(\gamma Y_1+\beta)\Lambda^2 Y_3^2 - 105(\gamma Y_1+\beta)\Lambda^2 Y_1 Y_3\cos(3\phi_1-\phi_3) \\ &\qquad + 64(1+\alpha\Lambda^2)\sin(\phi_1) = 0 \end{aligned} \tag{6.36b}$$

$$192(1-9\Lambda^2-9\mu\Lambda^2Y_1)Y_3 + 35(\gamma Y_1+\beta)\Lambda^2 Y_1\sin(3\phi_1-\phi_3) = 0 \tag{6.36c}$$

$$162Y_1^2Y_3 + 567Y_3^3 - 7Y_1^3\cos(3\phi_1-\phi_3) = 0 \tag{6.36d}$$

This nonlinear system of equations in Y_1, ϕ_1, Y_3 and ϕ_3 is solved numerically by using the Matlab function 'fsolve', which is based on the interior trust region method [201]. The maximum dynamic cable force is then found from Eqs. (6.19) and (6.20).

6.5 Numerical results and discussion

Aiming to evaluate the influence of the variable hydrodynamic coefficients on the dynamics of the lifting system, the subsea manifold presented in Section 6.2 is considered in combination with a 8.25 inch Braid Optimized for Bending (BOB®) 12x12 strand rope [210], as an example, as presented in Table 6.4. The choice of a synthetic rope construction in cases such as this is because of its lower submerged weight in comparison to traditional steel wire cables, thus allowing greater structural capacity to withstand dynamic loads in ultra-deep water operations.

Table 6.4: Geometric data for the cable used in this study [210].

	Variable	Value
Cable (8.25 inch BOB®)	Mass per unit length (m)	36.3 kg/m
	Equivalent submerged mass per unit length (m_s)	6.5 kg/m
	Axial rigidity (EA)	584 MN
	Safe working load	7300 kN

Also, the results presented in the sequence consider a maximum water depth of 2200 m, which is a typical condition in the Pre-Salt fields, in Brazil, and cover most of the worldwide scenarios. Finally, the solutions obtained by the Harmonic Balance Method considering the first harmonic

are referred to as HBM 1, while the results obtained by considering the first and third harmonics are referred to as HBM 1,3.

6.5.1 Overview of the dynamic response of the system

The dynamic response of the system, as a function of the water depth, for the different solution procedures and considering an input amplitude equal to $1.0\,\mathrm{m}$ and input period equal to $0.5\,\mathrm{rad/s}$ is presented in Figure 6.4. The maximum dynamic force in the steady state regime is presented in Figure 6.4(a). The results obtained by the KC-dependent hydrodynamic coefficient models clearly deviate from the results obtained by the constant coefficient model. The peak dynamic load in the system is higher for the KC-dependent models ($1344\,\mathrm{kN}$ for the iterative Runge-Kutta, $1333\,\mathrm{kN}$ for the HBM 1,3, and $1284\,\mathrm{kN}$ for the HBM 1 compared to $1047\,\mathrm{kN}$ for the constant coefficients model) and it occurs in shallower depths ($1020\,\mathrm{m}$ for the variable coefficients compared to $1115\,\mathrm{m}$ for the constant coefficients). On the other hand, the dynamic loads in the system in shallow waters and in the 1:3 super-harmonic resonance zone (around $175\,\mathrm{m}$ depth) are higher for the constant coefficients model in comparison to the variable coefficients models. Further, the results obtained by the different solutions of the variable hydrodynamic coefficients model are in agreement with each other (error of the peak dynamic force compared to the Iterative Runge-Kutta equal to $-0.82\,\%$ for HBM 1,3 and $-4.46\,\%$ for HBM 1), except for HBM 1 in the super-harmonic resonance, since this solution is not able to predict the amplifications of loads in this zone. For comparison, the static force due to the submerged weight of the payload is $1449\,\mathrm{kN}$ and the total submerged weight of the cable in $2200\,\mathrm{m}$ depth is $141\,\mathrm{kN}$. Further, the general behaviour presented above is also observed in Figure 6.4(b) and (c), where the maximum dynamic displacement and the maximum velocity are presented.

Reasons for this behaviour can be addressed by analysing the graphs of the added mass and drag coefficient as a function of the depth, as presented respectively in Figure 6.4(d) and Figure 6.4(e). The added mass coefficient is linearly proportional to the amplitude of the response, so when the system reaches resonance, W (and consequently C_a) reach a maximum. This higher added mass coefficient, increases the effective mass of the system, and thus brings the resonance to shallower depths, as seen previously in Figure 6.4(a).

(a)

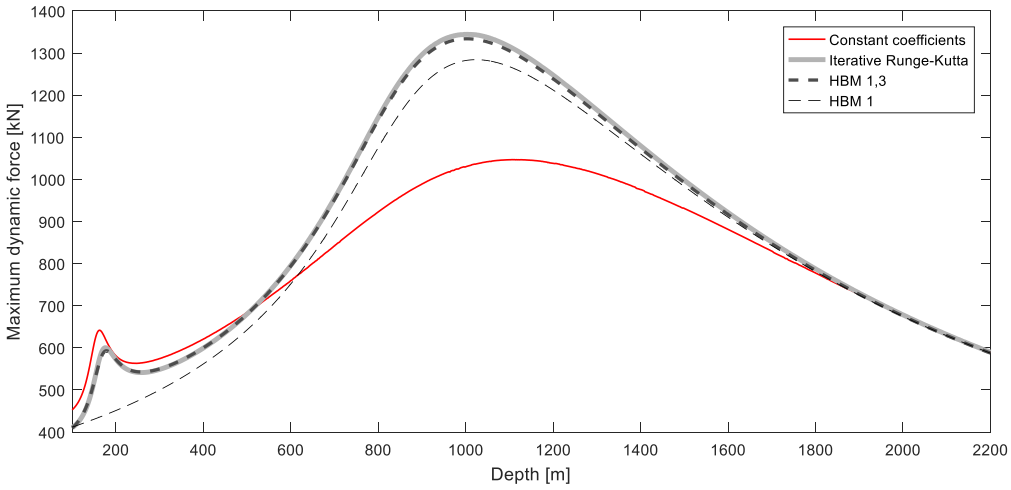

(b)

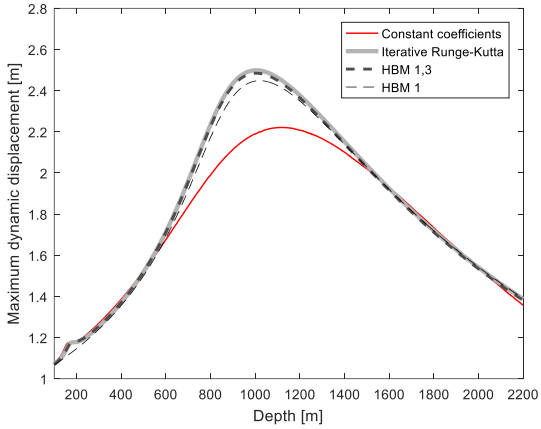

(c)

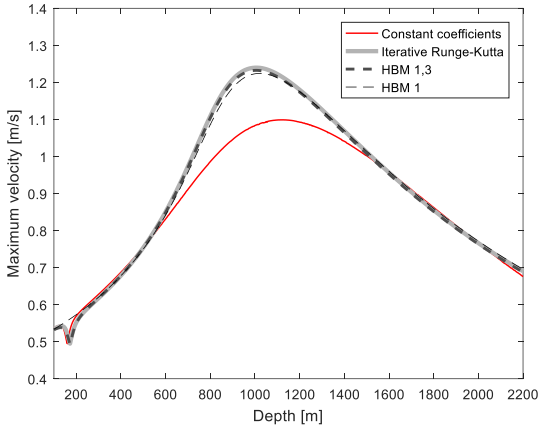

(d)

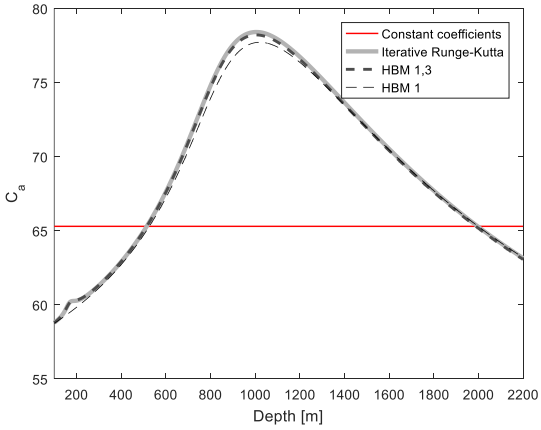

(e)

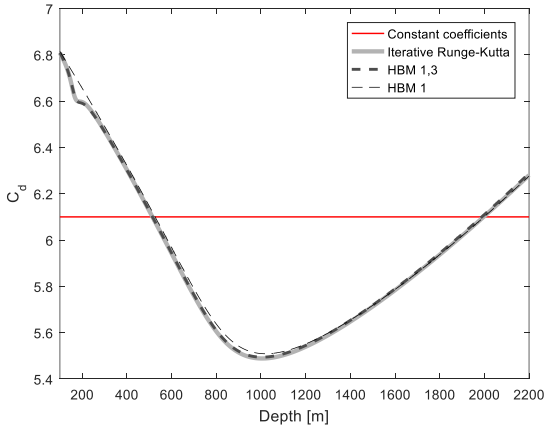

Figure 6.4: Dynamics of the subsea lifting for different solutions considering $W_0 = 1.0$ m and $\Omega = 0.5$ rad/s: (a) maximum dynamic load in the cable, (b) maximum dynamic displacement ($w = W_0 y$), (c) maximum velocity ($\dot{w} = \omega_{n0} W_0 y'$), (d) added mass coefficient, and (e) drag coefficient.

Additionally, as the drag coefficient is inversely proportional to the amplitude of the response, C_d reaches a minimum in the resonance zone. Thus, the damping of the system is reduced and the maximum displacement and dynamic cable force in the resonance zone are higher in comparison to the constant coefficient model, as presented in Figure 6.4(a). This is not the only factor that leads to higher loads for the variable coefficients model. According to Eq. (6.8), the dynamic load on the cable depends on the stiffness and elongation of the cable. So, when the resonance occurs at shallower depth (due to an increase in the added mass), the stiffness of the cable is higher due to the shorter suspended length of cable, leading to higher forces on the cable even for the same displacement. This effect can be observed by comparing the higher deviation between the variable and constant coefficients models in the dynamic force (Figure 6.4(a)) than in the dynamic displacement (Figure 6.4(b)), which is only due to the lower drag coefficient.

Also, the variation of the added mass coefficient not only affects the depth at which the resonance occurs but also creates a slight bending to the left in the dynamic response of the system at the resonance, which is a typical feature of a softening nonlinear system. In contrast to the more common case, where the stiffness is responsible for the nonlinear features of the system, in this problem, it is the inertial term that presents nonlinear behaviour, increasing its value as the amplitude of the response increases.

6.5.2 Influence of the input amplitude and frequency

The influence of the amplitude of the input on the dynamic forces in the cable is presented in Figure 6.5, where values of 0.1, 0.5, 1.0, and 1.5 m are used. The frequency of the input is kept constant at 0.5 rad/s. For clarity of the plots, in this Section, only the results obtained via the iterative Runge-Kutta method are presented for the variable coefficients model, since the solutions obtained by using the harmonic balance method deviate by less than 5 % from the results from the iterative Runge-Kutta method (as presented in Section 6.5.1).

Considering the variable hydrodynamic coefficients models, as the input amplitude increases, the maximum dynamic loads increase relative to the constant coefficients model results and they occur at shallower depths. The increase in the input amplitude increases the amplitude of the dynamic displacement of the payload, which reduces the drag coefficient and increases the added mass coefficient, as described in Section 6.5.1. Also, as presented previously, not only

the reduction of the damping coefficient, but also the increased stiffness of the cable in shallower depths (when the cable is shorter), contribute to the higher dynamic loads when the resonance peak occurs in shallower depths.

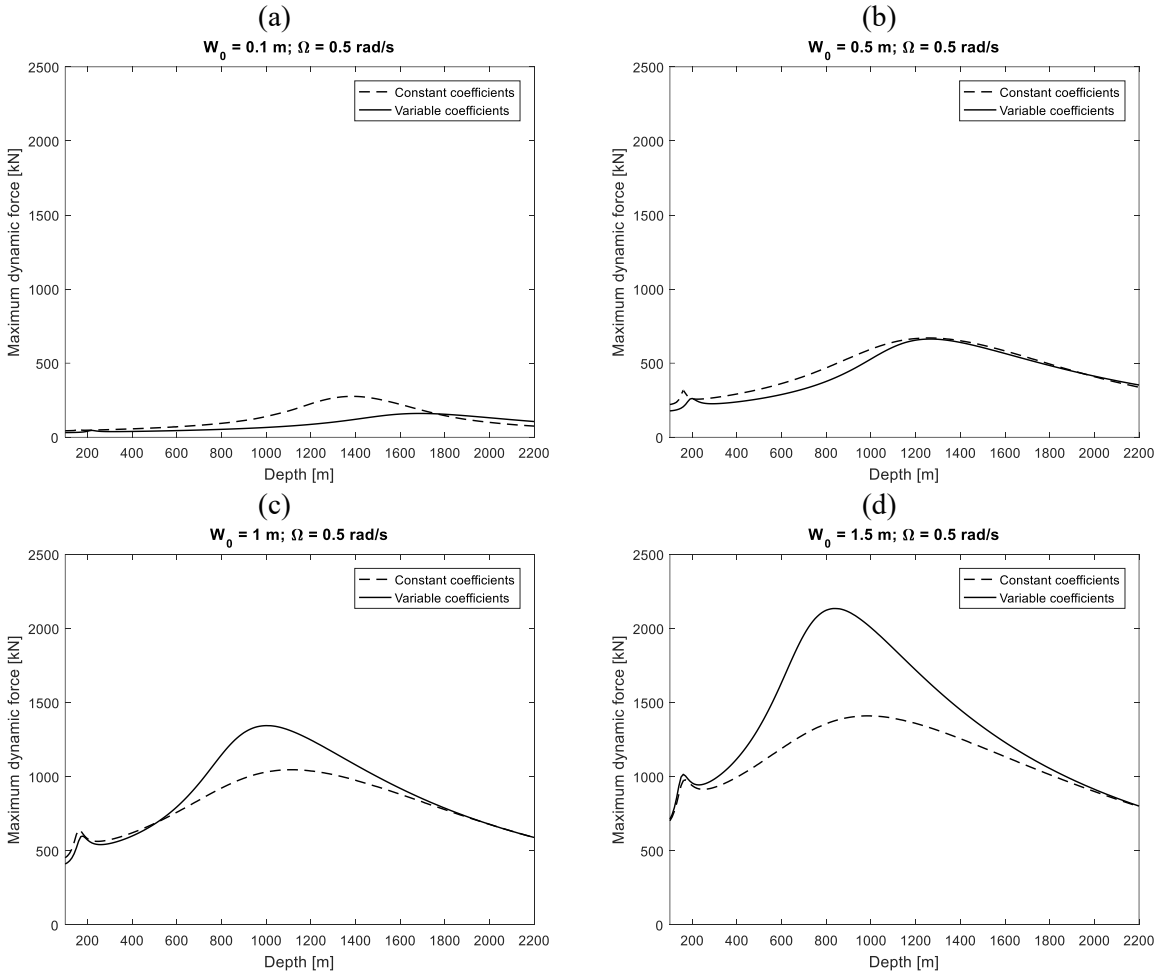

Figure 6.5: Maximum dynamic force in the cable as a function of depth for different input amplitudes. Results obtained considering $\Omega = 0.5$ rad/s and (a) $W_0 = 0.1$ m, (b) $W_0 = 0.5$ m, (c) $W_0 = 1.0$ m, (d) $W_0 = 1.5$ m.

The influence of the frequency of the input is highlighted in Figure 6.6 considering the frequencies 0.4, 0.6, 0.8, and 1.0 rad/s, while the amplitude is equal to 1.0 m. In this case, the increase of the input frequency only brings the resonance to shallower depths in a similar way for both the variable and the constant coefficient models. The ratio of the maximum dynamic force at the resonance for the variable coefficients models and for the constant coefficient model are kept nearly constant when the input frequency is varied.

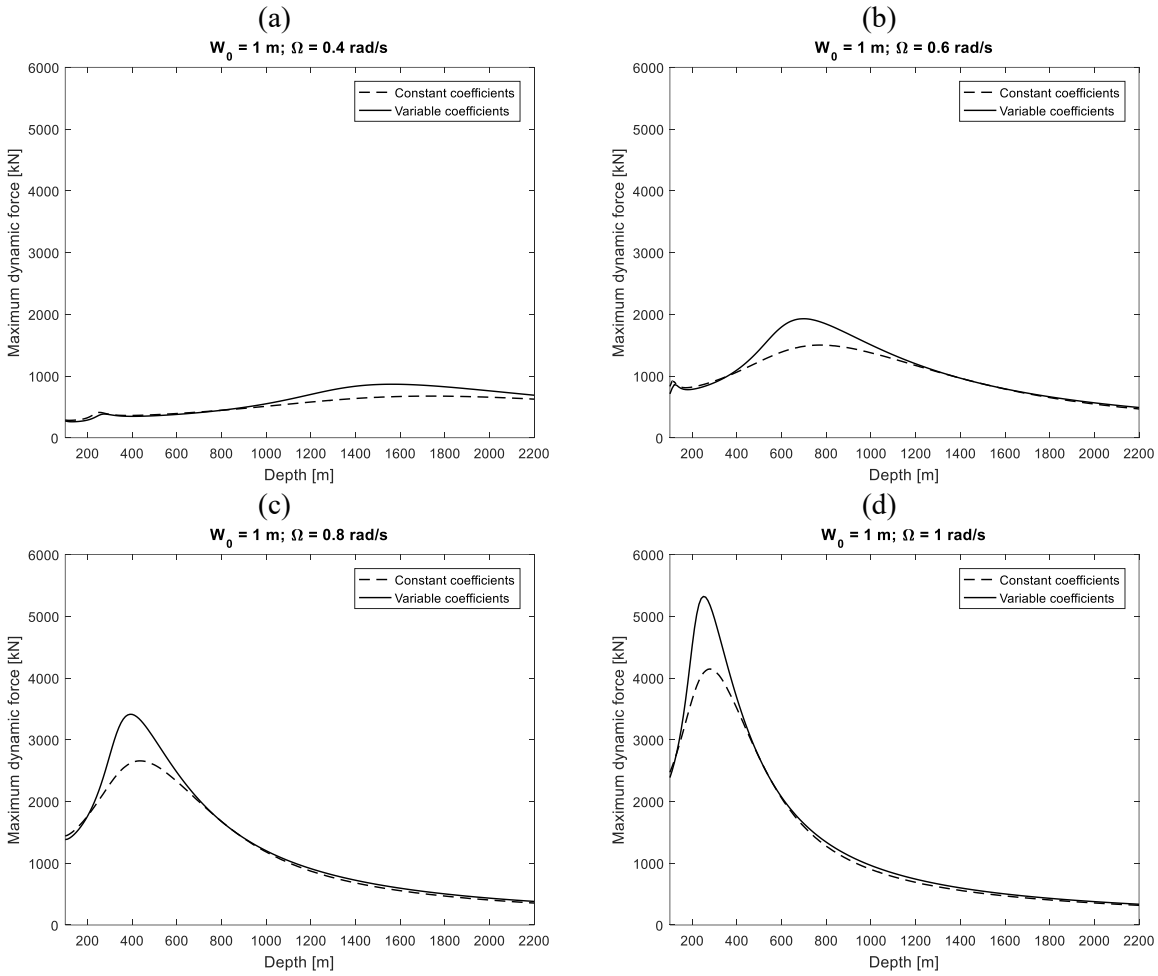

Figure 6.6: Maximum dynamic force in the cable as a function of depth for different input frequencies. Results obtained considering $W_0 = 1.0\,\mathrm{m}$ and (a) $\Omega = 0.4\,\mathrm{rad/s}$, (b) $\Omega = 0.6\,\mathrm{rad/s}$, (c) $\Omega = 0.8\,\mathrm{rad/s}$, (d) $\Omega = 1.0\,\mathrm{rad/s}$.

Another feature of the variable hydrodynamic coefficients model is the prediction of undamped resonance period curves that are dependent on the input, differently from the traditional approach considering constant hydrodynamic coefficients. The undamped resonance period of the cable-equipment system considering the KC-dependent hydrodynamic coefficient is given by:

$$T_{\text{resonance}} = 2\pi \sqrt{\frac{\left(M + \rho V \left(C_{a_0} + \frac{2\pi C_{a_1}}{D} W\right) + \frac{1}{3} mL\right) L}{EA}} \tag{6.37}$$

and is presented in Figure 6.7 considering various input frequencies and amplitudes. In this case, higher input amplitudes lead to higher values of W and thus higher values for the resonance period. The influence of the frequency is presented in the form of a further increase in the values of the resonance period in the depths when the system matches the input frequency. From a different perspective, for a given input frequency, the resonance occurs at shallower

depths when the input amplitude increases, in accordance with Figure 6.5. Furthermore, if the input frequency is higher, the resonance occurs in shallower depths, in accordance with Figure 6.6.

Differently from the constant coefficients model, the curves for the resonance period of the system can only be obtained after actually solving the equation of motion in the variable coefficients case, since the amplitude of the response is necessary in this approach.

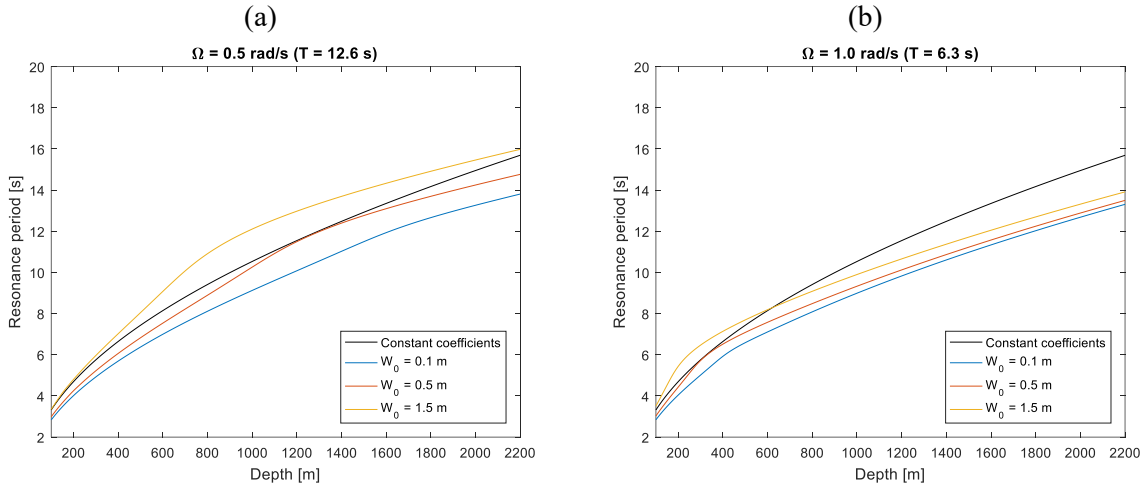

Figure 6.7: Undamped resonance period as a function of the depth considering various input amplitudes and (a) $\Omega = 0.5$ rad/s and (b) $\Omega = 1.0$ rad/s.

6.5.3 Dynamics of the system under general conditions

Sections 6.5.1 and 6.5.2 presented the results for the dynamics of the system in specific conditions for the input. The aim of this section is to extend the results for more general scenarios, so deeper insight about the behaviour of the system can be obtained. To this end, the non-dimensional response of the system is presented as a function of the non-dimensional variables: $\alpha, \beta, \gamma, \mu$, and Λ. However, due to the high number of independent variables, some assumptions are taken to simplify the study.

The first one is to consider the product $\alpha\Lambda^2$ (equal to $mL^2\Omega^2/6EA$) negligible in Eq. (6.14). In the example case, the term $\alpha\Lambda^2$ is less than 0.1 when $L < 2200$ m and $\Omega < 1.4$ rad/s (which is representative of most of scenarios) and, thus, the term $(1 + \alpha\Lambda^2)$ can be approximated to unity in Eq. (6.14). The second assumption is to consider μ as a function of γ, which can be obtained by dividing Eq. (6.17) by Eq. (6.16):

$$\mu = \left(\frac{4\pi V C_{a_1}}{A_p D C_{d_0}}\right)\gamma \tag{6.38}$$

Noting that the term inside the brackets in Eq. (6.38) is constant for a given payload, μ is linearly proportional to γ (i.e. $\mu = 0.9208\gamma$ for the example manifold). Finally, β varies from 0.1547 to 0.1583 when $100 \leq L \leq 2200$ for the example considered. So, a constant value of $\beta = 0.1565$ is taken as a simplification. Based on these assumptions, only Λ and γ are considered as independent variables when evaluating the non-dimensional response of this particular system.

The non-dimensional force as a function of Λ and γ obtained via the iterative Runge-Kutta solution is presented in Figure 6.8. For higher values of γ (i.e. higher input amplitude, according to Eq. (6.16)), the peak value of the non-dimensional force moves to lower values of the frequency ratio, which translates to shallower depths as per Eq. (6.11). This is in agreement with the discussion presented in Section 6.5.2. Further, a ridge is observed for $0.5 < \Lambda < 1.0$ and a saddle occurs at $\Lambda = 0.77$ and $\gamma = 0.18$. This behaviour is due to the combined influence of two effects. The first one is the reduction of the maximum non-dimensional force as γ increases, since γ controls the damping level of the system according to Eq. (6.14). This effect governs the dynamics of the system when $\gamma < 0.1$. On the other hand, the increase of γ brings the resonance to lower Λ, which increases the non-dimensional force as it is inversely proportional to Λ^2, according to Eq. (6.20). This effect governs the dynamics of the system when $\gamma > 0.2$. These opposing effects on the non-dimensional force as γ increases leads to the saddle. Super-harmonic resonance is also evident in Figure 6.8 when $\Lambda \cong 1/3$ and at other integer fractions shown by downward inflexions of the contour lines. These super-harmonic resonances present amplifications in the non-dimensional force that are not preponderant in comparison to the forces obtained in the fundamental resonance of the system, as illustrated also in Figure 6.4.

The non-dimensional force obtained from the constant coefficients model and for the variable coefficients model via the Harmonic Balance Method are presented in Figure 6.9, along with their percentage deviation in comparison to the results from the variable coefficients model using the iterative Runge-Kutta method. The results obtained by the constant coefficient model (Figure 6.9(a-b)) show clear deviations from the results for the variable coefficients model obtained via the iterative Runge-Kutta method, which is highlighted by non-dimensional forces under-predicted by up to 69% when $\Lambda < 1$ or over-predicted by up to 94% when $\Lambda > 1$.

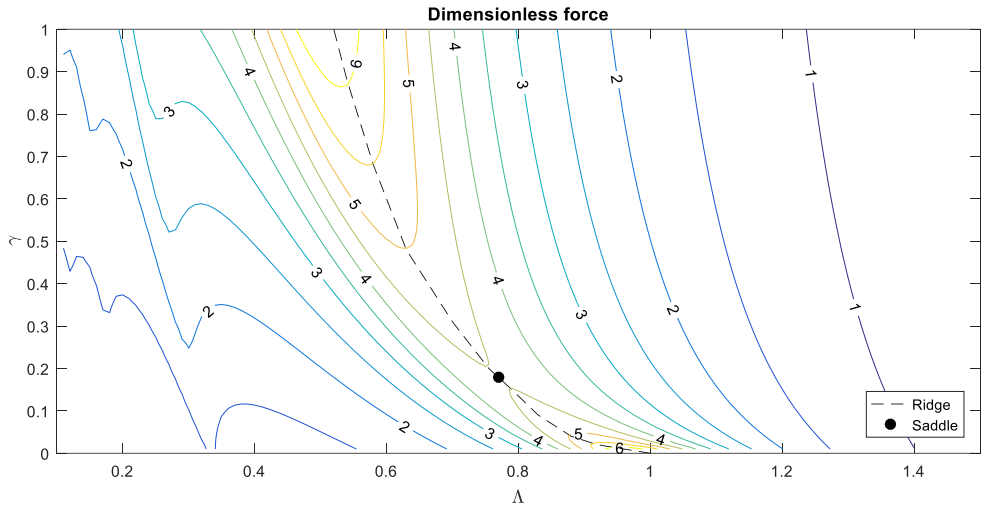

Figure 6.8: Maximum dimensionless force (f) obtained via the iterative Runge-Kutta solution as a function of the dimensionless damping (γ) and frequency ratio (Λ). Assuming $\beta = 0.1565$, $\mu = 0.9208\gamma$ and $\alpha\Lambda^2 = 0$.

The non-dimensional force obtained via HBM 1 (Figure 6.9(c-d)) shows very small errors in comparison to the iterative Runge-Kutta solution, except in the super-harmonic resonance zones ($\Lambda \cong 1/3$) where the force can be up to 27% lower. The results obtained by the HBM 1,3 Figure 6.9(e-f)) improves the results obtained by the HBM 1 by predicting the dynamic amplifications in the 1:3 super-harmonic resonance ($\Lambda \cong 1/3$), but higher super-harmonic resonances are still not represented, which translates in errors of the order of 9% at the 1:5 super-harmonic resonance ($\Lambda \cong 1/5$). Although deviations occur in the super-harmonic resonance zones for the harmonic balance method, the forces in these zones are not preponderant when the system is expected to cross the fundamental resonance zone. In this case, the HBM 1 solution can be used for accurate estimation of the dynamic loads in the system and, due to its analytical form, results are directly obtained with little computational effort. If 1:3 super-harmonic resonances are expected to be important in the definition of the viability of the operation, HBM 1,3 can be considered as an accurate and fast method (up to 50 times faster than the iterative Runge-Kutta method considering 50 periods of simulation and a tolerance of 10^{-3} for Y).

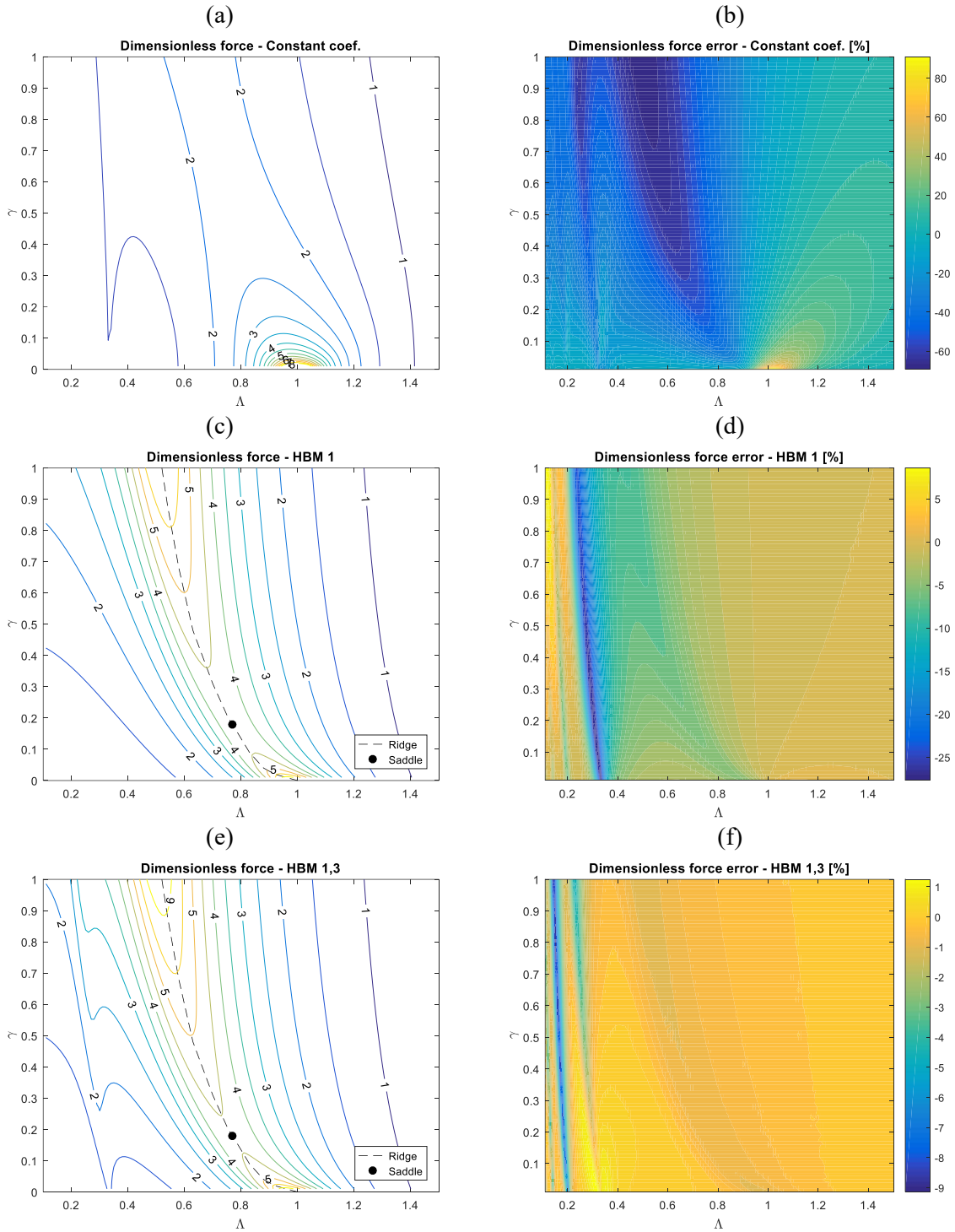

Figure 6.9: Non-dimensional force for different solutions and their percentage deviations compared to the variable coefficients iterative Runge-Kutta solutions. (a-b) Constant coefficient model, (c-d) harmonic balance method considering the first harmonic, and (e-f) harmonic balance method considering the first and third harmonics. Assuming $\beta = 0.1565$, $\mu = 0.9208\gamma$ and $\alpha\Lambda^2 = 0$.

6.5.4 Influence of μ and β on the dynamics of the system

Given the high number of independent variables for the system, some of them were kept constant in the above section and the results presented were only valid for the particular manifold presented in Section 6.2. The aim of this section is then to vary the variables that were kept constant previously in order to understand their influence in the dynamics of the system in different operational scenarios.

The first analysis presents the non-dimensional dynamic force as a function of Λ and γ by considering different values of the dimensionless amplitude-dependent drag coefficient (β) and a constant value of $\mu = 0.9208\gamma$ and $\alpha\Lambda^2 = 0$ (the same as in Section 6.5.3). This study is presented in Figure 6.10, which assumes $\beta = 0.0782$ (50% less compared to Figure 6.8) in Figure 6.10(a) and $\beta = 0.2347$ (50% higher compared to Figure 6.8) in Figure 6.10(b).

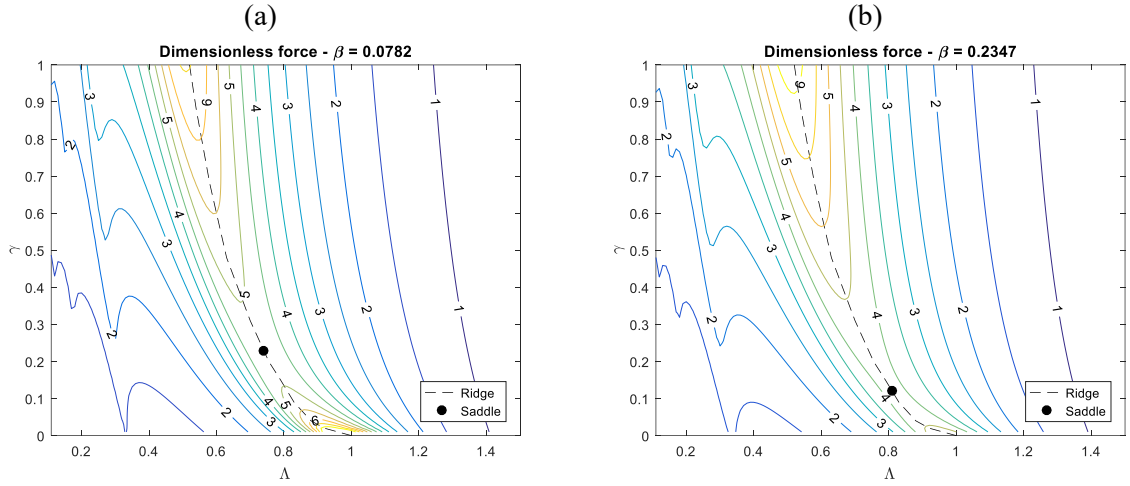

Figure 6.10: Non-dimensional dynamic force obtained by the iterative Runge-Kutta solution. Assuming $\mu = 0.9208\gamma$, $\alpha\Lambda^2 = 0$ and (a) $\beta = 0.0782$, and (b) $\beta = 0.2347$.

The maximum deviation between the results presented in Figure 6.8 and Figure 6.10 is less than 10%, except when $\gamma < 0.1$ and $0.8 < \Lambda < 1.2$, where the dimensionless force is increased by up to 38% in Figure 6.10(a) and reduced by up to 23% in Figure 6.10(b) in comparison to Figure 6.8. This is in agreement with the conclusions presented in Section 6.5.3, where it was shown that the influence of the damping level governed the response of the system near the resonance zone when $\gamma < 0.1$. In addition, the saddle moves to $\gamma = 0.23$ and $\Lambda = 0.74$ in Figure 6.10(a) and to $\gamma = 0.12$ and $\Lambda = 0.81$ in Figure 6.10(b).

The second analysis considers the influence of the dimensionless amplitude-dependent added mass coefficient (μ) on the dimensionless force (Figure 6.11). The results are obtained by assuming $\beta = 0.1565$, $\alpha\Lambda^2 = 0$ (the same as in Section 6.5.3) and (a) $\mu = 0.4604\gamma$ (50% less

compared to Figure 6.8) and (b) $\mu = 1.3812\gamma$ (50% higher compared to Figure 6.8). In this case, reducing the value of μ reduces the values of the dimensionless forces, especially on the ridge, where it can be up to 45% less in comparison to the results observed in Figure 6.8. Also, the ridge is not so steep as in Figure 6.8 and the saddle moves to $\gamma = 0.41$ and $\Lambda = 0.73$. On the other hand, increasing the value of μ tends to bring closer the contour lines to the left of the ridge, which is reflected in a steep increase in the non-dimensional forces when the system starts to cross the resonance zone from lower to higher values of Λ. Furthermore, the saddle moves to $\gamma = 0.09$ and $\Lambda = 0.80$ and the dimensionless force is majorly affected at the resonance zone, where it can be increased by up to 108% in comparison to the results presented in Figure 6.8.

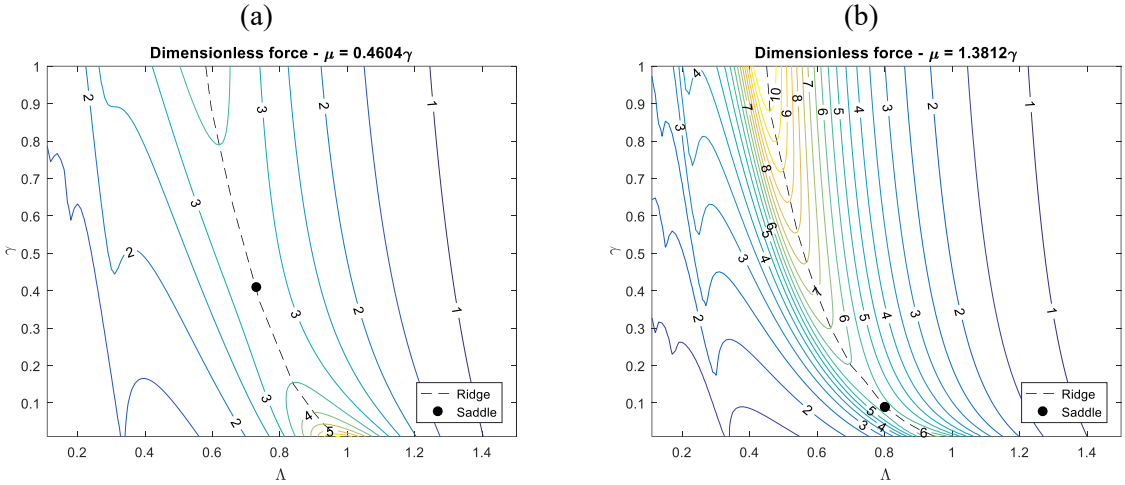

Figure 6.11: Non-dimensional dynamic force obtained by the iterative Runge-Kutta solution. Assuming $\beta = 0.1565$, $\alpha\Lambda^2 = 0$ and (a) $\mu = 0.4604\gamma$, and (b) $\mu = 1.3812\gamma$.

If even larger values of μ are considered, the non-dimensional force presents a fold to the left in the resonance zone, as presented in Figure 6.12. The results in this scenario consider $\beta = 0.1565, \alpha\Lambda^2 = 0, \gamma = 0.3, \mu = 3.6832\gamma$ and are obtained by HBM 1, since the unstable branch of the solution can be directly obtained by the analytical solution of Eq. (6.28), without the need for more sophisticated methods. According to this figure, when $0.38 < \Lambda < 0.41$, the system has three possible solutions: the stable branches A-B and C-D, and the unstable branch B-C. Points A-B-C-D are the solutions of the system at $\Lambda = 0.38$ and $\Lambda = 0.41$, when the discriminant of Eq. (6.28) is null (adding one real solution for the system). The stability of each branch is obtained by substituting the solutions of Eq. (6.28) as initial conditions into Eq. (6.14) and checking if the response of the system maintains the calculated response or diverges to a different condition, depending on the domain of attraction of each stable solution. In this case, if the system slowly progresses forward in the frequency ratio (e.g. during lowering operations),

the non-dimensional force will follow the curve A-B and then jump directly to D. On the other hand, if the system slowly progresses backward in frequency ratio (e.g. during recovering operations), the non-dimensional force will follow curve D-C and then drop directly to A. This is a typical hysteretic behaviour observed in nonlinear systems. Further details on this behaviour might be found in classical nonlinear dynamics literature, such as Nayfeh and Mook [185].

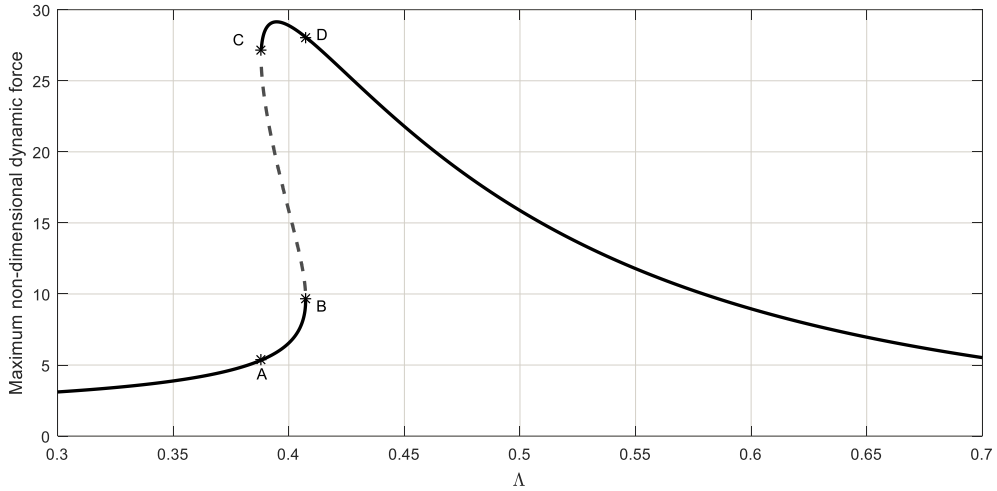

Figure 6.12: Maximum non-dimensional force as a function of the frequency ratio obtained via the HBM 1. Assuming $\beta = 0.1565$, $\alpha\Lambda^2 = 0$, $\gamma = 0.3$ and $\mu = 3.6832\gamma$.

Based on the results presented in Section 6.5, it seems clear the importance of considering variable hydrodynamic coefficients to model the dynamics of subsea lifting operations. The inclusion of the amplitude-dependent coefficients in the equation of motion leads to some phenomena that are not observed when considering constant coefficient models. In particular, variations in the natural frequency and damping of the system as functions of the amplitude of the response of the payload are apparent. This leads to shifts in the magnitude and corresponding depths of the maximum cable loads, and may even lead to multiple solutions in certain scenarios, such as presented in Figure 6.12. These outcomes reinforce the need to accurately predict the hydrodynamic coefficients of subsea structures as a function of the Keulegan-Carpenter number to safely install or recover subsea structures.

Finally, the conclusions obtained in this study were based on a linear law for the added mass coefficient and a reciprocal relation for the drag coefficient as a function of the KC number. In scenarios where the hydrodynamic coefficients follow different trends, deviations in the dynamics of the system might occur. For example, if the added mass decreases with the KC number, the system will act as a hardening nonlinear system and the resonant peak will increase in frequency as amplitude increases. More complex laws for the hydrodynamic coefficients might

need specific studies to understand the full dynamical behaviour of the system. Furthermore, comparison of the proposed models with data from real operations or experiments considering the coupled system (vessel, cable and payload) would be of great value for the analysis of the dynamics of the subsea lifting system. This might be considered in the scope of future works.

6.6 Conclusions

The dynamics of deep water subsea lifting operations considering KC-dependent hydrodynamic coefficients were analysed in this study. Initially, experimental data from the literature for the hydrodynamics coefficients of a typical subsea manifold was presented, indicating a linear trend in the added mass and a shifted reciprocal behaviour in the drag coefficient as a function of the amplitude of oscillation of the body, which was represented by the Keulegan-Carpenter number. Then, the non-dimensional equation of motion for a single degree-of-freedom system representing deep water subsea lifting operations was presented. This equation included two amplitude-dependent terms that, in addition to the traditional quadratic drag term, are responsible for the nonlinear behaviour of the system.

The solution of the nonlinear equation of motion was obtained by two different approaches. The first approach was based on an iterative time domain integration, while the second relied on an analytical technique known as the Harmonic Balance Method. The results obtained for the model with variable hydrodynamic coefficients were then compared with the results found for an equivalent model with constant coefficients.

The first example presented the maximum dynamic force on the cable as a function of the depth. It was shown that the model with variable coefficients predicted a shift in the magnitude and depth where the peak forces occurred, which were due to the variation of the damping and natural frequency of the system as a function of the amplitude of oscillation of the payload. In this case, for a higher amplitude of oscillation of the payload, the drag decreased and the added mass (and natural period) increased, resulting in resonances at shallower depths with higher magnitude. Additionally, it was found that the reduction of the damping and the higher stiffness (due to shorter suspended length of cable) of the system led to increased loads in the resonance zone, when the resonance occurred at shallower depths.

The general behaviour of the system was assessed by analysing the non-dimensional force on the cable as a function of the frequency ratio and non-dimensional damping coefficient. It was

noted that the natural resonance zone occurred at lower frequency ratio when the non-dimensional damping was increased, creating a ridge in the dimensionless force map. Furthermore, the magnitude of the dimensionless force in the ridge was found to be influenced in two opposing ways as the dimensionless damping coefficient was increased, which led to the presence of a saddle point in the dimensionless force map. Variations of the nonlinear damping and added mass coefficients could change the location and magnitude of the dimensionless force in the ridge and saddle. Additionally, a fold of the map could occur, leading to multiple solutions in certain zones.

Further, the accuracy of the Harmonic Balance Method solution and of the constant coefficient model in comparison to the iterative time domain integration method was presented. It was found that the use of the constant coefficient model could lead to overestimation of the dimensionless force by up to 94% when the frequency ratio was greater than unity or underestimated by up to 69% when the frequency ratio was lower than unity. The Harmonic Balance Method presented negligible error in comparison to the iterative time domain integration, except in the super-harmonic resonance zones, where maximum errors reached 27% when considering only the first harmonic component, or 9% when considering both the first and third harmonic components. However, the Harmonic Balance Method, particularly considering only the first harmonic, requires much less computation effort than the iterative time domain integration due to its analytical form, which represents a significant advantage of this method when super-harmonic resonances are not the critical zones of the operation.

These results have demonstrated the importance of using amplitude-dependent hydrodynamic coefficients to safely plan and execute deep water subsea lifting operations, since several phenomena introduced by this nonlinear behaviour are not represented by constant coefficient models.

7. CONCLUSION

This Section presents the ultimate contributions of this thesis as well as suggestions for future studies.

Chapter 2 presented a comprehensive literature review about offshore lifting operations, covering the historical perspective; the dynamic models considered for the lifting in air, lowering through the wave zone, lowering through deep waters and landing; the control methodologies to alleviate the dynamic loads or reduce motions of the payload; and the hydrodynamic modelling of oscillating bodies. It was shown that lifting operations were firstly focused on oil and gas applications, progressing to offshore renewable energy scenarios during the past decade. In addition, few studies addressing important aspects of the operation, such as variable length cables, non-stationary response, super-harmonic resonances and variable hydrodynamic coefficients, were found in the literature, motivating the research presented in this doctoral thesis.

Chapter 3 presented a study on the dynamics of deep water subsea lifting operations considering a variable length cable, aiming to cover the objective n.1 of this thesis, as presented in Section 1.2.3. The results showed that the proposed model was accurate in comparison with an Orcaflex model through all the depths evaluated, even at zones where super-harmonic response occurred. Furthermore, the results showed that the increase of the lowering speed tended to reduce the static force on the system, while the increase on the retrieval speed led to an increase of the static force. Regarding the dynamic forces, a transition point was noticed when the frequency ratio was about 0.75. After this point, the maximum dynamic force was reduced for increasing payout speeds and tented to occur at shallower depths. Before the transition point, the forces increased if the payout speed increased. Also, the maximum dynamic force could even occur before this point depending on the payout speed and drag coefficient considered. Finally, the operational weather window and, consequently, the availability of the vessel were directly influenced by the payout speed considered for the operation. Depending on the scenario and payout speed, the availability of the vessel could be increased or decreased due to the combined effect of the variation on the static and dynamic forces, and the exposure time of the system under the influence of irregular waves. This was a key point, since the use of traditional models that consider only fixed length scenarios could not always lead to safe or cost effective operations.

Chapter 4 described two methodologies to predict the design loads in deep water subsea lifting operations that were modelled using variable length cables. The variable length formulation led to a non-stationary response for the system, as the standard deviation of the dynamic forces increased in the resonance zone. The first method, called direct method, was based on running several independent random simulations and calculating the statistics of the response at each time step. The second method, called weighted least squares method, used few random responses to calculate a normalizing function that could eliminate the non-stationarity of the signal. Three random simulations were found to be sufficient to achieve reasonable accuracy with the weighted least squares method in comparison with the direct method. As a limitation of the least squares method, the normalizing function could only predict one resonance peak during the time series, which could affect the accuracy of the method in scenarios where multiple resonances are present. Finally, both methods were compared for the prediction of the operational weather window, which resulted in an agreement of viability of the operation in 95 % of the sea states analysed. It was then argued that, due to the speed of the weighted least squares method, it could be used in the preliminary assessment of real operations, where multiple operational procedures are analysed. After selecting one procedure, the direct method could be used to provide more reliable results for the weather window to be considered in the real operation.

Chapter 5 presented a study about super-harmonic resonances in deep water subsea lifting operations. The equation of motion described in Chapter 3 was re-written in non-dimensional format for a constant length scenario and solved via the Harmonic Balance Method. It was shown that amplifications of the response of the system occurred when the input frequency was an integer multiple of natural frequency of the system. This was due to the quadratic drag term acting on the payload and, therefore, could not be reproduced in traditional equivalent energy dissipation models. Solutions were obtained considering the first, first and third, and first, third and fifth harmonic components in the response of the system. It was shown that inclusion of the third harmonic enabled the representation of the 1:3 super-harmonic resonance and inclusion of the fifth harmonic enabled the representation of the 1:5 super-harmonic resonance. Higher harmonics could also be added to the solution to represent higher super-harmonic resonances, but they were considered of minor importance as they occur at water depths where influence of the wave dynamics must be included in the analysis and the proposed model is not valid. In addition, in the super-harmonic resonance zones, the higher frequency harmonic terms showed an increase of their amplitudes, and their phases became equal to the phase of the first

harmonic term, increasing the dynamic loads on the cable. For the example considered, an increase of only 4% in the maximum displacement of the payload led to 35% increase of the maximum dynamic force on the cable. Lastly, the operational weather window for the example scenario was presented, comparing the response of an equivalent energy dissipation model to the results obtained via the nonlinear equation of motion. It was shown that super-harmonic resonance might restrict the weather window and that the Harmonic Balance Method could be used as a reliable and fast method to analyse the system.

Finally, Chapter 6 describes the dynamics of the deep water subsea lifting operation considering amplitude-dependent hydrodynamic coefficients. The nonlinear non-dimensional equation of motion presented in Chapter 5 was expanded to include the KC-dependent terms and, once again, the solution was obtained via the Harmonic Balance Method. An iterative procedure was also presented to deal with the amplitude-dependent equation of motion. Comparing to the results obtained using constant coefficient models, the proposed model predicted a shift in the magnitude and depth where the peak forces occurred, which were due to the variation of the damping and natural frequency of the system as a function of the amplitude of oscillation of the payload. In this case, for a higher amplitude of oscillation of the payload, the drag decreased and the added mass (and natural period) increased, resulting in resonances at shallower depths with higher magnitude. Additionally, it was found that the reduction of the damping and the higher stiffness (due to shorter suspended length of cable) of the system led to increased loads in the resonance zone, when the resonance occurred at shallower depths. It was also found that increasing the KC-dependent added mass coefficient could lead to a fold on the dimensionless force map and, consequently, multiple solutions for the system.

7.1 Summary of contributions

- (Chapter 2) Comprehensive literature review on offshore lifting operations, covering the historical perspective, dynamic models, control methods and hydrodynamic modelling;
- (Chapter 3) Development of a variable length single degree-of-freedom model to analyse the dynamics of deep water subsea lifting operations;
- (Chapter 3) Description of the accuracy of single degree-of-freedom model when the superior modes of vibrations of the system were not excited by the input terms;
- (Chapter 3) Description of the influence of the winch speed on the dynamics of deep

water subsea lifting operations, via modification of the static and dynamic forces on the system and time of exposure to random waves;

- (Chapter 3) Description of the possibility of increasing the availability of the vessel by selecting an appropriate lowering/lifting speed;
- (Chapter 3) Description of the possibility of non-conservative results when analysing continuous lowering/lifting operations by constant length models;
- (Chapter 4) Development of two methods to predict the design loads on deep water subsea lifting operations modelled using variable length cables;
- (Chapter 4) Description of the convergence limits of the direct method and of the weighted least squares method to predict the statistics of the non-stationary response;
- (Chapter 5) Presentation of a non-dimensional nonlinear equation of motion for the dynamics of the system assuming constant length cable;
- (Chapter 5) Solution of the nonlinear equation of motion via the Harmonic Balance Method considering the first, third and fifth harmonic components;
- (Chapter 5) Description of the super-harmonic resonance as an outcome of the quadratic drag force acting on the payload;
- (Chapter 5) Description of the dynamics of the system in super-harmonic resonance, via the increase of the amplitude of higher harmonic terms, whose phase became equal to the phase of the first harmonic;
- (Chapter 5) Description of the limitations of using equivalent energy dissipation models or assuming maximum loads on the system at the deepest condition when the system does not crosses the fundamental resonance;
- (Chapter 6) Development of a nonlinear non-dimensional equation of motion considering amplitude-dependent hydrodynamic coefficients;
- (Chapter 6) Solution of the equation of motion via the Harmonic Balance Method and via an iterative time domain integration;
- (Chapter 6) Description of the variation of the magnitude and depth where the peak forces occurred in the variable hydrodynamic coefficients model, via the variation of damping and natural frequency of the system as a function of the amplitude of oscillation of the payload;
- (Chapter 6) Description of the possibility of multiple solutions due to the KC-dependent added mass coefficient;

– (Chapter 6) Description of the limitations of using constant coefficient models to analyse deep water subsea lifting operations

7.2 Suggestions for future studies

Building on the models presented in this thesis, several studies might be conducted to consolidate the knowledge on the dynamics of deep water subsea lifting operations. The following topics are listed as suggestions.

7.2.1 Optimization of the lowering/lifting velocity profile

The dynamic model presented in Chapter 3 for the analysis of the dynamics of the operation considering a variable length cable showed that the availability of the vessel could be maximized by selecting an appropriate lowering or recovering speed for the operation. The study, however, only considered constant velocities throughout the operation. Further improvements might be possible by developing an optimization method that builds an optimum velocity profile for the operation. A reasonable approach could be the minimization of the operation time, using the structural limits (i.e. loads must be below the structural limits and snap loads must be avoided) as constraints for the optimization algorithm.

7.2.2 Improved function to represent non-stationary response

The normalizing function used to remove the non-stationarity of the signal in Chapter 4 were only able to account for one peak of resonance. However, in real operations, multiple peaks might be possible due to bi-modal sea states, vessel resonances or super-harmonic resonances of the cable-payload system. In order to take these phenomena into account, improved normalizing functions, that are able to represent multiple amplification peaks might be of interest. In addition, other phases of the operation (such as the wave zone crossing or the landing on the seabed) can lead to non-stationary responses for the system, particularly due to impact loads. Modelling of these phenomena might also be important for the accurate determination of the operational weather window.

7.2.3 Variable length models considering KC-dependent hydrodynamic coefficients

In Section 6, the KC-dependent model was used to show that several nonlinear phenomena could arise during the lifting procedure. Especially, the maximum loads and the depth where

they occur could be different in comparison to constant hydrodynamic coefficient models, which could affect the planning of the operation. However, this model was only applicable to the constant length scenario. In order to improve the modelling of the dynamics of the system also in the variable length scenario, it is still necessary to build a dynamic model that takes into account both the variable hydrodynamic coefficients and the variable length assumptions. A possible approach to this problem would be to consider the variation of the hydrodynamic coefficients directly into the time domain integration by checking the amplitude of the oscillation on previous time steps. In addition, attention should be given to the impact of the lowering/lifting speed on the determination of the hydrodynamic coefficients.

7.2.4 Modelling the dynamics of the operation considering snap loads

An assumption used throughout this thesis was to consider the cable to be always taut during the operation. This is agreement with the guidance of the recommended practice DNVGL-RP-N103. However, this is not always possible to be achieved during the operation, particularly when the payload is light (i.e. less than 10 tonnes) or when it has a high projected area in comparison to its weight (i.e. area (m^2) divided by weight (tonnes) is more than one). Therefore, in order to accurately predict the dynamics of the system in these scenarios, it is necessary to include the modelling of snap loads throughout the simulation. These scenarios will typically need a discretized representation of the cable, as wave propagation will play an important role on the dynamics of the system. In this sense, the use of the finite element method is considered an appropriate tool for the modelling of the system; while reduce order modelling techniques might be used as a compromise solution, preserving the accuracy without increasing excessively the computational effort.

7.2.5 Advanced hydrodynamic modelling

In Section 6, it was shown that KC-dependent hydrodynamic coefficients, based on Morison's equation, were key for the accurate modelling of the operation. Although an analytical solution has been presented for this problem, when the assumptions considered to build the single degree-of-freedom system are not applicable, the computationally expensive iterative procedure (described in Section 6.4.1) would be necessary to solve the problem.

In order to obtain a more general representation of the hydrodynamic forces on the system and avoid the need for iterative solutions, coupling a CFD (Computational Fluid Dynamics) solver

to the cable-payload system would be of great interest for the modelling of the operation. This could also enable the understanding of other phenomena that could be important for the dynamics of the system, such as vortex shedding. Furthermore, due to the high computational cost of CFD, reduced order techniques for fluid dynamics could be envisaged to speed up the simulations. This study could also be used as a basis for predicting simplified relations (such as Morison's equation) to represent the hydrodynamics forces on the subsea lifting scenario, considering only the actual or past dynamical state of the system.

7.2.6 Experimental and field measurements

The models presented in this thesis where mainly theoretical, building on consolidated assumptions used throughout past decades in the offshore lifting literature. In order to increase the knowledge on the dynamics of the system, experimental and field measurements are suggested for the future. In the laboratory perspective, coupled vessel-cable-payload systems could be envisaged to study the dynamics of the system under variable length scenarios, super-harmonic resonances and to assess the influence of the amplitude of the oscillation on the hydrodynamic forces. On the other hand, field measurements could be used to explore the influence of random seas on the system and as an overall validation for the dynamic models presented in this thesis.

References

[1] D. Rowan, R. V. Ahilan, Experience with deepwater installations, Advances in Underwater Technology. 19 (1989) 91–104.

[2] F.E. Roveri, M.C. de Oliveira, M.J. Moretti, Installation of a production manifold in 2000 ft water depth offshore Brazil, in: Offshore Technology Conference, 1996: pp. 763–773.

[3] R. Nelson, J. Soliah, T. Caldwell, D. Morrison, J. Pritchard, Heave Compensated landing system - A novel tool for subsea intervention, in: Offshore Technology Conference, 1997: pp. 145–154.

[4] S.J. Rowe, B. Mackenzie, R. Snell, Deepwater Installation of Subsea Hardware, in: Proceedings of the 10th Offshore Symposium of the Society of Naval Architects and Naval Engineers, 2001: pp. 1–9.

[5] R.G. Standing, B. Mackenzie, R.O. Snell, Enhancing the Technology for Deepwater Installation of Subsea Hardware, in: Offshore Technology Conference, 2002: p. OTC 14180.

[6] J. Beckman, Joint industry project addresses heavy lift constraints, Offshore. (2005).

[7] S. Torben, P. Ingeberg, O. Bunes, P. Teigen, Fiber Rope Deployment System and Rope Management Process, in: The Eighteenth (2008) International Offshore and Polar Engineering Conference, 2008: pp. 34–41.

[8] P. Ingeberg, S. Torben, O. Bunes, S. Bull, Development of a fiber rope based deployment system for deep water application, in: The Sixteenth (2006) International Offshore and Polar Engineering Conference, 2006: pp. 126–133.

[9] S.R. Torben, Fiber Rope Deployment System For Ultra Deep Water Installations, in: Offshore Technology Conference, 2007: p. OTC 18932.

[10] S. Torben, P. Ingeberg, Field pilot of subsea equipment installation in deep water using fibre rope in two-fall arrangement, in: Offshore Technology Conference, 2011: p. OTC 21204.

[11] T. Job, L. Costa, B. Seawald, U.A. de Lima, The Current and Future State in Manifold

Installation at Petrobras: A Proposal for the Best Cost-Effectiveness in the Brazilian Pre-Salt, in: Rio Oil & Gas Expo and Conference, 2018: p. IBP1875_18.

[12] M.B. Cerqueira, F.E. Roveri, J.A.N. Ferreira, P.F.K. Stock, E.L. Labanca, M.L. Kuppens, Método pendular de instalação de equipamentos submarinos, Boletim Técnico Da Produção de Petróleo. 1 (2012) 327–339.

[13] L.T. Costa, U.A. De Lima, Installation of manifolds - a sucess story, in: Offfshore Technology Conference, 2017: p. OTC 27967.

[14] A.M. Wang, S. Zhu, X. Zhu, J. Xu, M. He, C. Zhang, Pendulous installation method and its installation analysis for a deepwater manifold in south china sea, in: The Twenty-Third (2013) International Offshore and Polar Engineering, 2013: pp. 774–784.

[15] T. Risoey, H. Mork, H. Johnsgard, J. Gramnaes, The pencil buoy method - a subsurface transportation and installation method, in: Offshore Technology Conference, 2007: p. OTC 19040.

[16] H. Mork, J. Lunde, A Cost-Effective and Safe Method for Transportation and Installation of Subsea Structures — The Pencil Buoy Method, in: SPE Offshore Europe Oil and Gas Conference and Exhibition, 2007: p. SPE 108608.

[17] A. Joensen, D. Paul, A Low Tech , Low Risk System for the Installation of Large Structures in Deep Water, in: SPE Offshore Europe Oil and Gas Conference and Exhibition, 2011: p. SPE 145461.

[18] Y. Cao, X. Hu, S. Zhang, S. Xu, J. Lee, J. Yu, Design of a novel installation device for a subsea production system, Applied Ocean Research. 59 (2016) 24–37.

[19] P.C. de Mello, F. Rateiro, A.L.C. Fujarra, A.T. Oshiro, C.R. Neves, M.F. dos Santos, E.A. Tannuri, Experimental Set-Up for Analysis of Subsea Equipment Installation, in: Proceedings of the 30th International Conference on Ocean, Offshore and Arctic Engineering, 2011: pp. OMAE2011-49946.

[20] F. Rateiro, C.H. Fucato, E.A. Tannuri, C.R. Neves, M.F. Santos, Numerical Analysis of a Novel Method for Subsea Equipment Installation, in: Proceedings of the 30th International Conference on Offshore Mechanics and Arctic Engineering, 2011: pp. OMAE2011-49948.

[21] A.L.C. Fujarra, E.A. Tannuri, I.Q. Masetti, H. Igreja, Experimental and numerical

evaluation of the installation of subsea equipment for risers support, in: Proceedings of the ASME 27th International Conference on Offshore Mechanics and Arctic Engineering, 2008: pp. OMAE2008-57472.

[22] J. Velema, J. Bokhorst, Lift installation of a subsea oil tank storage: a 60.000 MT pendulum, in: Proceedings of the ASME 2015 34th International Conference on Ocean, Offshore and Arctic Engineering, 2015: pp. OMAE2015-42191.

[23] A. Sarkar, O.T. Gudmestad, Study on a new method for installing a monopile and a fully integrated offshore wind turbine structure, Marine Structures. 33 (2013) 160–187.

[24] W. Guachamin Acero, Z. Gao, T. Moan, Numerical study of a novel procedure for installing the tower and Rotor Nacelle Assembly of offshore wind turbines based on the inverted pendulum principle, Journal of Marine Science and Application. 16 (2017) 243–260.

[25] W. Guachamin-Acero, Z. Jiang, L. Li, Numerical study of a concept for major repair and replacement of offshore wind turbine blades, Wind Energy. 23 (2020) 1673–1692.

[26] D. Ahn, S.C. Shin, S.Y. Kim, H. Kharoufi, H.C. Kim, Comparative evaluation of different offshore wind turbine installation vessels for Korean west–south wind farm, International Journal of Naval Architecture and Ocean Engineering. 9 (2017) 45–54.

[27] J. Paterson, F. D'Amico, P.R. Thies, R.E. Kurt, G. Harrison, Offshore wind installation vessels – A comparative assessment for UK offshore rounds 1 and 2, Ocean Engineering. 148 (2018) 637–649.

[28] R. Lacal-Arántegui, J.M. Yusta, J.A. Domínguez-Navarro, Offshore wind installation: Analysing the evidence behind improvements in installation time, Renewable and Sustainable Energy Reviews. 92 (2018) 133–145.

[29] I. Frazer, D. Perinet, O. Vennemann, Technology Required for the Installation of Production Facilities in 10,000 ft of Water, in: Offshore Technology Conference, 2005.

[30] A. Wang, Y. Yang, S. Zhu, H. Li, J. Xu, M. He, Latest Progress In Deepwater Installation Technologies, in: The Twenty-Second (2012) International Offshore and Polar Engineering Conference, 2012: pp. 1079–1090.

[31] G. Mcpherson, Developments in Deepwater Installation Systems, in: Offshore Technology Conference, 2015: p. OTC-26059.

[32] M.D. Esteban, B. Couñago, J.S. López-Gutiérrez, V. Negro, F. Vellisco, Gravity based support structures for offshore wind turbine generators: Review of the installation process, Ocean Engineering. 110 (2015) 281–291.

[33] A.F. Haselsteiner, J.H. Ohlendorf, S. Oelker, L. Ströer, K.D. Thoben, K. Wiedemann, E. De Ridder, S. Lehmann, Lifting Wind Turbine Components from a Floating Vessel: A Review on Current Solutions and Open Problems, Journal of Offshore Mechanics and Arctic Engineering. 141 (2019) 1–12.

[34] Z. Jiang, Installation of offshore wind turbines: A technical review, Renewable and Sustainable Energy Reviews. 139 (2021) 110576.

[35] T.E. Schellin, T. Jiang, S.D. Sharma, Crane ship response to wave groups, Journal of Offshore Mechanics and Arctic Engineering. 113 (1991) 211–218.

[36] J.A. Witz, Parametric excitation of crane loads in moderate sea states, Ocean Engineering. 22 (1995) 411–420.

[37] G.F. Clauss, M. Vannahme, An experimental study of the nonlinear dynamics of floating cranes, in: Proceedings of the 9th International Offshore Polar Engineering Conference, 1999: p. ISOPE-99-JSC-343.

[38] K. Ellermann, E. Kreuzer, M. Markiewicz, Nonlinear dynamics of floating cranes, Nonlinear Dynamics. 27 (2002) 107–183.

[39] K. Ellermann, E. Kreuzer, Nonlinear dynamics in the motion of floating cranes, Multibody System Dynamics. 9 (2003) 377–387.

[40] R. Van Der Wal, H. Cozijn, C. Dunlop, Model Tests and Computer Simulations for Njord FPU Gas Module Installation, in: Marine Operations Specialty Symposium MOSS 2008, 2008: pp. 1–20.

[41] J.H. Cha, M. Il Roh, K.Y. Lee, Dynamic response simulation of a heavy cargo suspended by a floating crane based on multibody system dynamics, Ocean Engineering. 37 (2010) 1273–1291.

[42] K.Y. Lee, J.H. Cha, K.P. Park, Dynamic response of al floating crane in waves by considering the nonlinear effect of hydrostatic force, Ship Technology Research. 57 (2010) 62–71.

[43] K.-P. Park, J.-H. Cha, K.-Y. Lee, Dynamic factor analysis considering elastic boom

effects in heavy lifting operations, Ocean Engineering. 38 (2011) 1100–1113.

[44] J.W. Hong, M. Il Roh, S.H. Ham, S. Ha, Dynamic simulation of subsea equipment installation using an offshore support vessel based on flexible multibody system dynamics, Journal of Marine Science and Technology. 24 (2016) 807–821.

[45] S.H. Ham, M. Il Roh, H. Lee, S. Ha, Multibody dynamic analysis of a heavy load suspended by a floating crane with constraint-based wire rope, Ocean Engineering. 109 (2015) 145–160.

[46] Y.J. Ha, B.W. Nam, S.Y. Hong, D.W. Jung, H.J. Kim, Experimental and numerical study on mating operation of a topside module by a floating crane vessel in waves, Ocean Engineering. 154 (2018) 375–388.

[47] Mateusz Graczyk, P.C. Sandvik, Study of landing and lift-off operation for wind turbine components on a ship deck, in: Proceedings of the ASME 2012 31st International Conference on Ocean, Offshore and Arctic Engineering, 2012: pp. OMAE2012-84273.

[48] N. Ku, M. Il Roh, Dynamic response simulation of an offshore wind turbine suspended by a floating crane, Ships and Offshore Structures. 10 (2015) 621–634.

[49] Z. Ming, Z. Peng, Z. Changming, Dynamic response analysis of offshore wind turbine installation suspended by a floating crane, Proceedings of the Institution of Mechanical Engineers, Part C: Journal of Mechanical Engineering Science. 231 (2017) 2650–2663.

[50] W.G. Acero, Z. Gao, T. Moan, Methodology for Assessment of the Allowable Sea States During Installation of an Offshore Wind Turbine Transition Piece Structure Onto a Monopile Foundation, Journal of Offshore Mechanics and Arctic Engineering. 139 (2017) 1–16.

[51] Z. Ren, Z. Jiang, R. Skjetne, Z. Gao, Development and application of a simulator for offshore wind turbine blades installation, Ocean Engineering. 166 (2018) 380–395.

[52] Y. Zhao, Z. Cheng, P. Christian, Z. Gao, An integrated dynamic analysis method for simulating installation of single blades for wind turbines, Ocean Engineering. 152 (2018) 72–88.

[53] Z. Jiang, Z. Gao, Z. Ren, Y. Li, L. Duan, A parametric study on the final blade installation process for monopile wind turbines under rough environmental conditions, Engineering Structures. 172 (2018) 1042–1056.

[54] A.S. Verma, Z. Jiang, N.P. Vedvik, Z. Gao, Z. Ren, Impact assessment of a wind turbine blade root during an offshore mating process, Engineering Structures. 180 (2019) 205–222.

[55] Y. Zhao, Z. Cheng, Z. Gao, P. Christian, Numerical study on the feasibility of o ff shore single blade installation by fl oating crane vessels, Marine Structures. 64 (2019) 442–462.

[56] Z. Jiang, The impact of a passive tuned mass damper on offshore single-blade installation, Journal of Wind Engineering and Industrial Aerodynamics. 176 (2018) 65–77.

[57] A.S. Verma, Z. Jiang, Z. Gao, N.P. Vedvik, Effects of a passive tuned mass damper on blade root impacts during the offshore mating process, Marine Structures. 72 (2020) 102778.

[58] I. Kopsov, P. Sandvik, Analysis of subsea structure installation, in: The Fifth (1995) International Offshore and Polar Engineering Conference, 1995: pp. 193–199.

[59] L. Li, Z. Gao, T. Moan, H. Ormberg, Analysis of lifting operation of a monopile for an offshore wind turbine considering vessel shielding effects, Marine Structures. 39 (2014) 287–314.

[60] L. Li, Z. Gao, T. Moan, Response analysis of a nonstationary lowering operation for an offshore wind turbine monopile substructure, Journal of Offshore Mechanics and Arctic Engineering. 137 (2015) 05192.

[61] L. Li, C. Parra, X. Zhu, M. Chen, Splash zone lowering analysis of a large subsea spool piece, Marine Structures. 70 (2020) 102664.

[62] T. Næss, J. Havn, F. Solaas, On the importance of slamming during installation of structures with large suction anchors, Ocean Engineering. 89 (2014) 99–112.

[63] M.A. Hannan, W. Bai, Nonlinear hydrodynamic responses of submerged moving payload in vicinity of a crane barge in waves, Marine Structures. 41 (2015) 154–179.

[64] M.A. Hannan, W. Bai, Analysis of nonlinear dynamics of fully submerged payload hanging from offshore crane vessel, Ocean Engineering. 128 (2016) 132–146.

[65] D.H. Jeong, M. Il Roh, S.H. Ham, Lifting simulation of an offshore supply vessel considering various operating conditions, Advances in Mechanical Engineering. 8

(2016) 1–13.

[66] W. Raman-Nair, S.N. Chin, T. Sayeed, Deployment and retrieval of a cylinder from a moored rectangular barge, Applied Ocean Research. 98 (2020) 102112.

[67] Arthur D. Little Inc., Stress analysis of ship-suspended heavily loaded cables for deep underater emplacements, Department of the Navy, Report 1370863. (1963).

[68] P. Holmes, Mechanics of raising and lowering heavy loads in the deep ocean: cable and payload dynamics, Report R433, U. S. Naval Civil Engineering Laboratory. (1966).

[69] W.D. Iwan, Dynamic response of suspended underwater systems, The Journal of the Acoustical Society of America. 51 (1972) 1668–1696.

[70] J.S. Chung, A.K. Whitney, Axial Stretching Oscillation of an 18,000-Ft Vertical Pipe in the Ocean., Journal of Energy Resources Technology, Transactions of the ASME. 105 (1983) 195–200.

[71] J.M. Niedzwecki, S.K. Thampi, Snap loading of marine cable systems, Applied Ocean Research. 13 (1991) 210–219.

[72] S. Huang, Stability analysis of the heave motion of marine cable-body systems, Ocean Engineering. 26 (1999) 531–546.

[73] F.R. Driscoll, R.G. Lueck, M. Nahon, The motion of a deep sea remotely operated vehible system - Part 1: motion observations, Ocean Engineering. 27 (2000) 57–76.

[74] F.R. Driscoll, R.G. Lueck, M. Nahon, The motion of a deep sea remotely operated vehible system - Part 2: analytical model, Ocean Engineering. 27 (2000) 29–56.

[75] R.G. Lueck, F.R. Driscoll, M. Nahon, A wavelet for predicting the time domain response of vertically tethered systems, Ocean Engineering. 27 (2000) 1441–1453.

[76] F.R. Driscoll, R.G. Lueck, M. Nahon, Development and validation of a lumped-mass dynamics model of a deep-sea ROV system, Applied Ocean Research. 22 (2000) 169–182.

[77] L. Huang, J. Zhang, X. Yu, R.E. Randall, B. Wilde, Numerical Simulation on Dynamics of Suction Piles during Lowering Operations, in: The Twenty-First (2011) International Offshore and Polar Engineering Conference, 2011.

[78] B.W. Nam, N.W. Kim, S.Y. Hong, Experimental and numerical study on coupled motion

responses of a floating crane vessel and a lifted subsea manifold in deep water, International Journal of Naval Architecture and Ocean Engineering. 9 (2017) 552–567.

[79] F.R. Driscoll, M. Nahon, R.G. Lueck, A comparison of ship–mounted and cage–mounted passive heave compensation systems, Journal of Offshore Mechanics and Arctic Engineering. 122 (2000) 214–221.

[80] W. Quan, Y. Liu, A. Zhang, X. Zhao, X. Li, The nonlinear finite element modeling and performance analysis of the passive heave compensation system for the deep-sea tethered ROVs, Ocean Engineering. 127 (2016) 246–257.

[81] E.D. de Araújo Neto, B.M. Jacovazzo, F.N. Correa, B.P. Jacob, Numerical evaluation of a subsea equipment installation method designed to avoid resonant responses, Applied Ocean Research. 88 (2019) 288–305.

[82] P. Wang, R. Fung, M. Lee, Finite element analysis of a three-dimensional underwater cable with time-dependent length, Journal of Sound and Vibration. 209 (1998) 223–249.

[83] X. Hu, S. Liu, Numerical simulation of deepwater deployment for offshore structures with deploying cables, Journal of Central South University. 22 (2015) 922–930.

[84] Y. Hu, J. Cao, B. Yao, Z. Zeng, L. Lian, Dynamic behaviors of a marine riser with variable length during the installation of a subsea production tree, Journal of Marine Science and Technology. 23 (2017) 378–388.

[85] P. Gao, K. Yan, M. Ni, X. Fu, Z. Liu, A Dynamic Model for Continuous Lowering Analysis of Deep-Sea Equipment, Based on the Lumped-Mass Method, Applied Sciences. 10 (2020) 3177.

[86] W. Quan, Q. Chang, Variable-Length Cable Dynamics of Payout and Reel-in with a Vertically Tethered Underwater Drill Rig, IEEE Access. 8 (2020) 66625–66637.

[87] C.P. Pesce, The application of Lagrange equations to mechanical systems with mass explicitly dependent on position, Journal of Applied Mechanics, Transactions ASME. 70 (2003) 751–756.

[88] C. Pesce, E. Tannuri, L. Casetta, The Lagrange equations for systems with mass varying explicitly with position: some applications to offshore engineering, Journal of the Brazilian Society of Mechanical Sciences and Engineering. XXVIII (2006) 496–504.

[89] L. Cveticanin, Dynamics of Bodies with Time-Variable Mass, Springer, 2016.

[90] D. Morrison, C. Cermelli, Deployment of subsea equipment in ultradeep water, in: Proceedings of the 22nd International Conference on Offshore Mechanics and Arctic Engineering, 2003: pp. OMAE2003-37190.

[91] J. Ireland, G. Macfarlane, Y. Drobyshevski, Investigation into the sensitivity of the dynamic hook load during subsea deployment of a suction can, in: Proceedings of the 26th International Conference on Offshore Mechanics and Arctic Engineering, 2007: pp. OMAE2007-29244.

[92] T. Jacobsen, B.J. Leira, Numerical and experimental studies of submerged towing of a subsea template, Ocean Engineering. 42 (2012) 147–154.

[93] M. Richter, F. Zeil, D. Walser, K. Schneider, O. Sawodny, Modeling offshore ropes for deepwater lifting applications, in: Proceedings of the 2016 IEEE International Conference on Advanced Intelligent Mechatronics, 2016: pp. 1222–1227.

[94] H.S. Kang, C.H.H. Tang, L.K. Quen, A. Steven, X. Yu, Prediction on parametric resonance of offshore crane cable for lowering subsea structures, in: Proceedings of the 6th International Conference on Underwater System Technology: Theory and Applications, 2016: pp. 165–170.

[95] H.S. Kang, C.H.H. Tang, L.K. Quen, A. Steven, X. Yu, Parametric resonance avoidance of offshore crane cable in subsea lowering operation through A* Heuristic planner, Indian Journal of Geo-Marine Sciences. 46 (2017) 2422–2433.

[96] Z. Chen, T. Zhao, J. Jiao, D. Mao, Simulation and motion analysis of deepwater manifold lifting, Journal of Marine Science and Technology. 25 (2017) 696–704.

[97] X. Li, J. Cui, M. Zhao, T. Ge, Dynamic analysis of an underwater suspension system in ocean currents with method of averaging, Indian Journal of Geo-Marine Sciences. 46 (2017) 2220–2227.

[98] X. Zhang, M. Duan, D. Mao, Y. Yu, J. Yu, Y. Wang, A mathematical model of virtual simulation for deepwater installation of subsea production facilities, Ships and Offshore Structures. 12 (2017) 182–195.

[99] Y. Wang, H. Tuo, L. Li, Y. Zhao, H. Qin, C. An, Dynamic simulation of installation of the subsea cluster manifold by drilling pipe in deep water based on OrcaFlex, Journal of Petroleum Science and Engineering. 163 (2018) 67–78.

[100] Y. Zhao, Y. Wang, L. Li, C. Yang, Y. Du, H. Chen, M. Duan, Numerical simulation of subsea cluster manifold installation by the sheave method, in: Proceedings of the International Conference on Offshore Mechanics and Arctic Engineering, 2018: pp. OMAE2018-77336.

[101] H. Qin, J. Liu, W. Xiao, B. Wang, Quasistatic Nonlinear Analysis of a Drill Pipe in Subsea Xmas Tree Installation, Mathematical Problems in Engineering. (2019) 4241363.

[102] W. Xiao, H. Qin, J. Liu, Q. Liu, J. Cui, F. Wang, Natural Frequencies and Mode Shapes of Drill Pipe in Subsea Xmas Tree Installation, Mathematical Problems in Engineering. (2020) 5634194.

[103] B.V.E. How, S.S. Ge, Y.S. Choo, Dynamic load positioning for subsea installation via adaptive neural control, IEEE Journal of Oceanic Engineering. 35 (2010) 366–375.

[104] B.V.E. How, S.S. Ge, Y.S. Choo, Control of coupled vessel, crane, cable, and payload dynamics for subsea installation operations, IEEE Transactions on Control Systems Technology. 19 (2011) 208–220.

[105] R. Domenici Pereira Simões, J.O. de Aquino Limaverde Filho, E. Pereira Barroso Neto, E. Libório Feitosa Fortaleza, Analytical solution to motion planning and modal-based tracking control for dynamic positioning of subsea equipment, Ocean Engineering. 164 (2018) 712–721.

[106] J.K. Woodacre, R.J. Bauer, R.A. Irani, A review of vertical motion heave compensation systems, Ocean Engineering. 104 (2015) 140–154.

[107] R.J. Henry, Z.N. Masoud, A.H. Nayfeh, D.T. Mook, Cargo pendulation reduction on ship-mounted cranes via boom-luff angle actuation, Journal of Vibration and Control. 7 (2001) 1253–1264.

[108] Z.N. Masoud, A.H. Nayfeh, D.T. Mook, Cargo pendulation reduction of ship-mounted cranes, Nonlinear Dynamics. 35 (2004) 299–311.

[109] N.K. Ku, J.H. Cha, M. Il Roh, K.Y. Lee, A tagline proportional-derivative control method for the anti-swing motion of a heavy load suspended by a floating crane in waves, Proceedings of the Institution of Mechanical Engineers Part M: Journal of Engineering for the Maritime Environment. 227 (2013) 357–366.

[110] Z. Ren, Z. Jiang, Z. Gao, R. Skjetne, Active tugger line force control for single blade

installation, Wind Energy. 21 (2018) 1344–1358.

[111] T.A. Johansen, T.I. Fossen, S.I. Sagatun, F.G. Nielsen, Wave Synchronizing Crane Control during Water Entry in Offshore Moonpool Operations - Experimental Results, Modeling, Identification and Control. 25 (2004) 29–44.

[112] B. Skaare, O. Egeland, Parallel force/position crane control in marine operations, IEEE Journal of Oceanic Engineering. 31 (2006) 599–613.

[113] S. Messineo, F. Celani, O. Egeland, Crane feedback control in offshore moonpool operations, Control Engineering Practice. 16 (2008) 356–364.

[114] S. Messineo, A. Serrani, Offshore crane control based on adaptive external models, Automatica. 45 (2009) 2546–2556.

[115] M. Böhm, M. Krstic, S. Küchler, O. Sawodny, Modeling and boundary control of a hanging cable immersed in water, Journal of Dynamic Systems, Measurement and Control. 136 (2014) 011006.

[116] W. Quan, Y. Liu, Z. Zhang, X. Li, C. Liu, Scale model test of a semi-active heave compensation system for deep-sea tethered ROVs, Ocean Engineering. 126 (2016) 353–363.

[117] M. Li, P. Gao, J. Zhang, J. Gu, Y. Zhang, Study on the system design and control method of a semi-active heave compensation system, Ships and Offshore Structures. 13 (2018) 43–55.

[118] J.R. Morison, J.W. Johnson, S.A. Schaaf, The Force Exerted by Surface Waves on Piles, Journal of Petroleum Technology. 2 (1950) 149–154.

[119] G.H. Keulegan, L.H. Carpenter, Forces on cylinders and plates in an oscillating fluid, Journal of Research of the National Bureau of Standards. 60 (1958) 423–440.

[120] T. Sarpkaya, Wave forces on offshore structures, Cambridge University Press, 2010.

[121] K. Hu, S. Fu, L. Ma, L. Song, Nonlinear Hydrodynamics of a Floating Cylinder in Oscillatory Flow Alone and Combined with a Current, Journal of Waterway, Port, Coastal, and Ocean Engineering. 143 (2017) 04016015.

[122] Z. Gao, M. Efthymiou, L. Cheng, T. Zhou, M. Minguez, W. Zhao, Hydrodynamic damping of a circular cylinder at low KC: Experiments and an associated model, Marine Structures. 72 (2020) 102777.

[123] C. Ren, L. Lu, L. Cheng, T. Chen, Hydrodynamic damping of an oscillating cylinder at small Keulegan-Carpenter numbers, Journal of Fluid Mechanics. 913 (2021).

[124] B. Molin, Hydrodynamic modeling of perforated structures, Applied Ocean Research. 33 (2011) 1–11.

[125] S. Ann, O.M. Faltinsen, An experimental and numerical study of heave added mass and damping of horizontally submerged and perforated rectangular plates, Journal of Fluids and Structures. 39 (2013) 87–101.

[126] J. Li, S. Liu, M. Zhao, B. Teng, Experimental investigation of the hydrodynamic characteristics of heave plates using forced oscillation, Ocean Engineering. 66 (2013) 82–91.

[127] C.A. Garrido-Mendoza, K.P. Thiagarajan, A. Souto-Iglesias, A. Colagrossi, B. Bouscasse, Computation of flow features and hydrodynamic coefficients around heave plates oscillating near a seabed, Journal of Fluids and Structures. 59 (2015) 406–431.

[128] X. Tian, L. Tao, X. Li, J. Yang, Hydrodynamic coefficients of oscillating flat plates at 0.15 less than KC less than 3.15, Journal of Marine Science and Technology. 22 (2016) 101–113.

[129] F. Mentzoni, T. Kristiansen, Numerical modeling of perforated plates in oscillating flow, Applied Ocean Research. 84 (2019) 1–11.

[130] F. Mentzoni, T. Kristiansen, Two-dimensional experimental and numerical investigations of perforated plates in oscillating flow, orbital flow and incident waves, Applied Ocean Research. 97 (2020) 102078.

[131] F. Mentzoni, T. Kristiansen, Two-dimensional experimental and numerical investigations of parallel perforated plates in oscillating and orbital flows, Applied Ocean Research. 97 (2020) 102042.

[132] A.C. Fernandes, F.P.S. Mineiro, Assessment of hydrodynamic properties of bodies with complex shapes, Applied Ocean Research. 29 (2007) 155–166.

[133] J. Pablo, J. Avila, J. Cezar, Experimental evaluation of the hydrodynamic coefficients of a ROV through Morison ' s equation, Ocean Engineering. 38 (2011) 2162–2170.

[134] F. Solaas, P.C. Sandvik, Hydrodynamic coefficients of suction anchors during installation operations, in: Proceedings of the 36th International Conference on Offshore

Mechanics and Arctic Engineering, 2017: pp. OMAE2017-62447.

[135] Y. Du, M. Zheng, X. Liang, Y. Wang, Z. Chai, H. Jo, Experimental and numerical investigation of hydrodynamic coefficients of subsea manifolds, Ships and Offshore Structures. (2020) 1–13.

[136] R.G. Pestana, D.F.C. Silva, C.N. Gomes, L.O. Carvalho, V. Vileti, P.T.T. Esperança, M. Kim, Subsea manifold installation: Operational windows estimation based on hydrodynamic model testing, Ocean Engineering. 219 (2021) 108364.

[137] R.B. Tommasini, L. de O. Carvalho, R. Pavanello, A dynamic model to evaluate the influence of the laying or retrieval speed on the installation and recovery of subsea equipment, Applied Ocean Research. 77 (2018) 34–44.

[138] F.E. Roveri, P.F.K. Stock, J.A.N. Ferreira, R.D. Machado, M.B. de Cerqueira, E.L. Labanca, Estrutura Auxiliar de Içamento e Transporte e Método Pendular de Instalação de Equipamentos Submarinos Utilizando Dita Estrutura, Patent PI 05502113-8, Brazil, 2015.

[139] J.M.T.G. Lima, M.L. Kuppens, P.F. da Silveira, P.F.K. Stock, Development of Subsea Facilities in the Roncador Field (P-52), in: Offshore Technology Conference, 2008: p. OTC 19274.

[140] S. Huang, D. Vassalos, A numerical method for predicting snap loading of marine cables, Applied Ocean Research. 15 (1993) 235–242.

[141] A.A. Tjavaras, Q. Zhu, Y. Liu, M.S. Triantafyllou, D.K.P. Yue, The Mechanics of Highly-Extensible Cables, Journal of Sound and Vibration. 213 (1998) 709–737.

[142] B. Buckham, F.R. Driscoll, M. Nahon, Development of a Finite Element Cable Model for Use in Low-Tension Dynamics Simulation, Journal of Applied Mechanics. 71 (2004) 476–485.

[143] T. Bunnik, B. Buchner, A. Veldman, The Use of a Volume of Fluid (VOF) Method Coupled to a Time Domain Motion Simulation to Calculate the Motions of Subsea Structure lifted Through The Splash Zone, in: 25th International Conference on Offshore Mechanics and Arctic Engineering, 2006: pp. OMAE2006-92447.

[144] Y. Park, W. Kim, B.-W. Nam, CFD simulation of hydrodynamic forces acting on subsea manifold templates at wave zone, in: The Twenty-Third (2013) International Offshore

and Polar Engineering, 2013: pp. 654–661.

[145] D. Jia, M. Agrawal, Fluid-Structure Interaction: Lowering Subsea Structure / Equipment in Splash Zone During Installation, in: Offshore Technology Conference, 2014: p. OTC-25233.

[146] DNV-RP-H103, Modelling and Analysis of Marine Operations, DNV Recommended Practice. (2014).

[147] J.W. Leonard, S.R. Karnoski, Simulation of tension controlled cable deployment, Applied Ocean Research. 12 (1990) 34–42.

[148] M.A. Vaz, M.H. Patel, Three-dimensional behaviour of elastic marine cables in sheared currents, Applied Ocean Research. 22 (2000) 45–53.

[149] J. Prpić-Oršić, R. Nabergoj, Nonlinear dynamics of an elastic cable during laying operations in rough sea, Applied Ocean Research. 27 (2005) 255–264.

[150] N. Yang, D. Jeng, X.L. Zhou, Tension Analysis of Submarine Cables During Laying Operations, The Open Civil Engineering Journal. 7 (2013) 282–291.

[151] Y. Terumichi, M. Ohtsuka, M. Yoshizawa, Y. Fukawa, Y. Tsujioka, Nonstationary vibrations of a string with time-varying length and a mass-spring system attached at the lower end, Nonlinear Dynamics. 12 (1997) 39–55.

[152] K.A.F. Moustafa, E.H. Gad, A.M.A. El-Moneer, M.I.S. Ismail, Modelling and control of overhead cranes with flexible variable-length cable by finite element method, Transactions of the Institute of Measurement & Control. 27 (2005) 1–20.

[153] J. Du, H. Bao, C. Cui, D. Yang, Dynamic analysis of cable-driven parallel manipulators with time-varying cable lengths, Finite Elements in Analysis and Design. 48 (2012) 1392–1399.

[154] Orcina, Orcaflex 10.2b documentation, (2017).

[155] S.S. Rao, Mechanical Vibrations, 5th ed., Prentice Hall, 2010.

[156] O.M. Faltinsen, Sea loads on ships and offshore structures, 1st ed., Cambridge University Press, 1993.

[157] T. Belytschko, W.K. Liu, B. Moran, K.I. Elkhodary, Nonlinear Finite Elements For Continua And Structures, 2nd ed., John Wiley and Sons, 2014.

[158] DNV-OS-H101, Marine Operations, General, Offshore Standard. (2011).

[159] R.B. Tommasini, R. Pavanello, L. de O. Carvalho, Prediction of design loads for deep water subsea lifting operations based on non-stationary time response, Marine Structures. 74 (2020) 102818.

[160] J.I. Gobat, M.A. Grosenbaugh, Time-domain numerical simulation of ocean cable structures, Ocean Engineering. 33 (2006) 1373–1400.

[161] W. Hsu, K.P. Thiagarajan, L. Manuel, Extreme mooring tensions due to snap loads on a fl oating offshore wind turbine system, Marine Structures. 55 (2017) 182–199.

[162] J. Palm, C. Eskilsson, L. Bergdahl, An hp-adaptive discontinuous Galerkin method for modelling snap loads in mooring cables, Ocean Engineering. 144 (2017) 266–276.

[163] R.B. Gordon, G. Grytoyr, M. Dhaigude, Modeling suction pile loweing through the splash zone, in: Proceedings of the ASME 32nd International Conference on Ocean, Offshore and Arctic Engineering, 2013: pp. OMAE2013-10136.

[164] A. Sarkar, O.T. Gudmestad, Splash zone lifting analysis of subsea structures, in: Proceedings of the 29th International Conference on Ocean, Offshore and Arctic Engineering, 2011: pp. 303–312.

[165] J. Xu, M. Miao, S. Zheng, Modeling and analysis of rope flexibility in deep sea lifting operations, in: Proceedings of 2018 IEEE International Conference on Mechatronics and Automation, ICMA 2018, 2018: pp. 767–772.

[166] F.E. Roveri, M.B. Cerqueira, R.D. Machado, The utilization of the pendulous motion for deploying subsea hardware in ultra-deep water, in: Proceedings of the 17th Conference of Deep Offshore Technology, 2005.

[167] H.-S. Choi, D.K. Kim, S. Kim, E.-J. Cheon, K.-S. Kim, Subsea equipment decommissioning using fiber rope, in: Proceedings of the MATEC Web of Conferences, 2018.

[168] D.C. Montgomery, Introduction to Time Series Analysis and Forecasting, 2nd ed., John Wiley and Sons, 2015.

[169] E. Vanem, Non-stationary extreme value models to account for trends and shifts in the extreme wave climate due to climate change, Applied Ocean Research. 52 (2015) 201–211.

[170] L. Wang, J. Li, Estimation of extreme wind speed in SCS and NWP by a non-stationary model, Theoretical and Applied Mechanics Letters. 6 (2016) 131–138.

[171] M. Jones, D. Randell, K. Ewans, P. Jonathan, Statistics of extreme ocean environments: Non-stationary inference for directionality and other covariate effects, Ocean Engineering. 119 (2016) 30–46.

[172] D.P. Peace, D.P. Tuturea, N. Ellis, J.C. Chiwis, Dynamic analysis of the Hutton TLP mating operation, in: Offfshore Technology Conference, 1985: p. OTC 5048.

[173] J. Hamilton, F. Ramzan, Dynamic analysis of offshore heavy lifts, in: The First International Offshore and Polar Engineering Conference, 1991: p. ISOPE-I-91-004.

[174] I. Fylling, On the statistics of impact velocities and hit positions related to collisions and mating operations for offshore structures, in: Proceedings of the BOSS 94 Behaviour of Offshore Structures, 1994: pp. 297–306.

[175] P.C. Sandvik, Estimation of extreme response from operations involving transients, in: Proceedings of the Second Marine Operations Specialty Symposium, 2012: pp. 6–8.

[176] W. Guachamin, Z. Gao, T. Moan, Assessment of the dynamic responses and allowable sea states for a novel o ff shore wind turbine installation concept based on the inverted pendulum principle, Energy Procedia. 94 (2016) 61–71.

[177] W. Guachamin-acero, L. Li, Methodology for assessment of operational limits including uncertainties in wave spectral energy distribution for safe execution of marine operations, Ocean Engineering. 165 (2018) 184–193.

[178] W.G. Acero, L. Li, Z. Gao, T. Moan, Methodology for assessment of the operational limits and operability of marine operations, Ocean Engineering. 125 (2016) 308–327.

[179] R.B. Tommasini, R. Pavanello, L. de O. Carvalho, A Study on the Validity of a One Degree of Freedom Model for Deepwater Subsea Lifts, in: Proceedings of the ASME 2019 38th International Conference on Ocean, Offshore and Arctic Engineering, 2019: p. OMAE 2019 96047.

[180] S.K. Chakrabarti, Hydrodynamics of Offshore Structures, WIT Press, 1987.

[181] W.I.G. Acero, Assessment of marine operations for offshore wind turbine installation with emphasis on response-based operational limits, PhD thesis. Norwegian University of Science and Technology, 2016.

[182] S. Coles, An Introduction to Statistical Modeling of Extreme Values, Springer, 2001.

[183] R.H. Byrd, J.C. Gilbert, J. Nocedal, A trust region method based on interior point techniques for nonlinear programming, Mathematical Programming. 89 (2000) 149–185.

[184] R.B. Tommasini, T.L. Hill, J.H.G. Macdonald, R. Pavanello, L. de O. Carvalho, The dynamics of deep water subsea lifting operations in superharmonic resonance via the harmonic balance method, Marine Structures. (n.d.).

[185] A.H. Nayfeh, D.T. Mook, Nonlinear Oscillations, John Wiley and Sons, 1995.

[186] L. Hou, Y. Chen, Z. Lu, Bifurcation analysis for 2:1 and 3:1 super-harmonic resonances of an aircraft cracked rotor system due to maneuver load, Nonlinear Dynamics. 81 (2015) 531–547.

[187] R. Masana, M.F. Daqaq, Energy harvesting in the super-harmonic frequency region of a twin-well oscillator, Journal of Applied Physics. 111 (2012) 044501.

[188] C.Y. Liaw, N.J. Shankar, K.S. Chua, Subharmonic motions and wave force-structure interaction, Marine Structures. 5 (1992) 281–295.

[189] L. Liu, B. Zhou, Y. Tang, Study on the nonlinear dynamical behavior of deepsea Spar platform by numerical simulation and model experiment, Journal of Vibration and Control. 20 (2014) 1528–1537.

[190] O. Gottlieb, S.C.S. Yim, Nonlinear dynamics of a coupled surge-heave small-body ocean mooring system, Ocean Engineering. 24 (1997) 479–495.

[191] O. Gottlieb, S.C.S. Yim, Drag induced instabilities and chaos in mooring systems, Ocean Engineering. 20 (1993) 569–599.

[192] DNVGL-RP-N103, Modelling and analysis of marine operations, DNVGL Recommended Practice. (2017).

[193] M.A. Jordan, J.L. Bustamante, Numerical stability analysis and control of umbilical-ROV systems in one-degree-of-freedom taut-slack condition, Nonlinear Dynamics. 49 (2007) 163–191.

[194] L.T. Costa, U.A. de Lima, Installation of Manifolds - A Success Story, in: Offshore Technology Conference, 2017: p. OTC-27967-MS.

[195] A.H. Nayfeh, Perturbation Methods, John Wiley and Sons, 2008.

[196] R. Masiani, D. Capecchi, F. Vestroni, Resonant and coupled response of hysteretic two-degree-of-freedom systems using harmonic balance method, Non-Linear Mechanics. 37 (2002) 1421–1434.

[197] T.C. Kim, T.E. Rook, R. Singh, Super- and sub-harmonic response calculations for a torsional system with clearance nonlinearity using the harmonic balance method, Journal of Sound and Vibration. 281 (2005) 965–993.

[198] L. Li, Y. Du, Design of Nonlinear Tuned Mass Damper by Using the Harmonic Balance Method, Journal of Engineering Mechanics. 146 (2020) 04020056.

[199] L. Chen, B. Basu, S.R.K. Nielsen, Nonlinear periodic response analysis of mooring cables using harmonic balance method, Journal of Sound and Vibration. 438 (2019) 402–418.

[200] D.C. Montgomery, Applied Statistics and Probability for Engineers, 3rd ed., John Wiley and Sons, 2003.

[201] T.F. Coleman, Y. Li, An interior trust region approach for nonlinear minimization subject to bounds, SIAM Journal on Optimization. 6 (1996) 418–445.

[202] R.B. Tommasini, T.L. Hill, J.H.G. Macdonald, R. Pavanello, L. de O. Carvalho, Nonlinear dynamics of deep water subsea lifting operations considering KC-dependent hydrodynamic coefficients, Ocean Engineering. 233 (2021) 109172.

[203] W. Quan, Q. Chang, Q. Zhang, J. Gong, Dynamics calculation for variable-length underwater cable with geometrically nonlinear motion, Ocean Engineering. 212 (2020) 107695.

[204] V. Venugopal, K.S. Varyani, P.C. Westlake, Drag and inertia coefficients for horizontally submerged rectangular cylinders in waves and currents, Proceedings of the Institution of Mechanical Engineers Part M: Journal of Engineering for the Maritime Environment. 223 (2009) 121–136.

[205] J.P.J. Avila, J.C. Adamowski, Experimental evaluation of the hydrodynamic coefficients of a ROV through Morison's equation, Ocean Engineering. 38 (2011) 2162–2170.

[206] F. Mentzoni, M. Abrahamsen-Prsic, T. Kristiansen, Hydrodynamic Coefficients of Simplified Subsea Structures, in: Proceedings of the 37th International Conference on Offshore Mechanics and Arctic Engineering, 2018: pp. OMAE2018-78315.

[207] S. Holmes, W. Calver II, M. Tognarelli, Y. Constantinides, M. Russo, Determining the Hydrodynamic Coefficients of a BOP, in: Proceedings of the 35th International Conference on Offshore Mechanics and Arctic Engineering, 2016: pp. OMAE2016-54932.

[208] O. Oritsland, A summary of subsea module hydrodynamic data, Marine Operations Part III.2. Report No. 70. Report MT5 (1989).

[209] S. An, O.M. Faltinsen, An experimental and numerical study of heave added mass and damping of horizontally submerged and perforated rectangular plates, Journal of Fluids and Structures. 39 (2013) 87–101.

[210] Cortland, Braid Optimized for Bending (BOB®) 12x12 Strand Tech Sheet, (n.d.). https://www.cortlandcompany.com/resources-literature/downloads/braid-optimized-bending-bob-12x12-strand-tech-sheet (accessed August 24, 2020).